ผลงานของ Asst. Prof. Dr.Boris Golman

SURANAREE UNIVERSITY OF TECHNOLOGY

INSTITUTE OF ENGINEERING

SCHOOL OF CHEMICAL ENGINEERING

LECTURE NOTES

Advanced

Powder Technology

ASST.PROF., DR. BORIS GOLMAN

2012

Contents

Part I.

Properties of Particulate Solids

1. Particle size distribution

1.1. Description of the size of a single particle

A particle size is some measure of the spatial extent of a particle. The particle size can be characterized using various definitions which are divided into three groups: equivalent sphere diameters, equivalent circle diameters and statistical diameters. In the first group, the size of the particle is taken as the diameter of a sphere having the same property as particle under consideration, as shown in Table 1 [1, 2].

Table 1: Definitions of particle size based on the equivalent sphere diameters.

Symbol	Diameter	Definition	Formula
		Equivalent Sphere Diameter	
d_v	Volume	Diameter of a sphere having the same volume as the particle	$V = \frac{\pi}{6} d_v^3$
d_s	Surface	Diameter of a sphere having the same external surface as the particle	$S = \pi d_s^2$
d_{sv}	Surface-volume (Sauter)	Diameter of a sphere having the same ratio of external surface area to volume as the particle	$d_{sv} = (d_v^3/d_s^2)$
d_d	Drag	Diameter of a sphere having the same resistance to motion as the particle in a fluid of the same viscosity (η) and at the same velocity (u)	$F_D = 3\pi d_d \eta u$
d_f	Free-falling	Diameter of a sphere having the same free-falling speed as a particle of the same density in a fluid of the same density and at the same viscosity	
d_{St}	Stokes	Free-falling diameter in the laminar flow region	$d_{St} = \sqrt{d_v^3/d_d}$

Consider a cubic particle with the side length of 1 mm, as shown in Fig. 1. The volume of this particle is $V_{\text{cube}} = 1\ \text{mm}^3$ and the surface is $S_{\text{cube}} = (1 \times 1) \times 6 = 6\ \text{mm}^2$. Then, the equivalent volume diameter is the diameter of a spherical particle having the same volume as the cubic one, i.e. $V_{\text{sphere}} = V_{\text{cube}} = 1\ \text{mm}^3$. As the volume of the sphere is $V_{\text{sphere}} = \pi d_v^3/6 = 1\ \text{mm}^3$, the equivalent volume diameter is $d_v = \sqrt[3]{6/\pi} = 1.241$ mm.

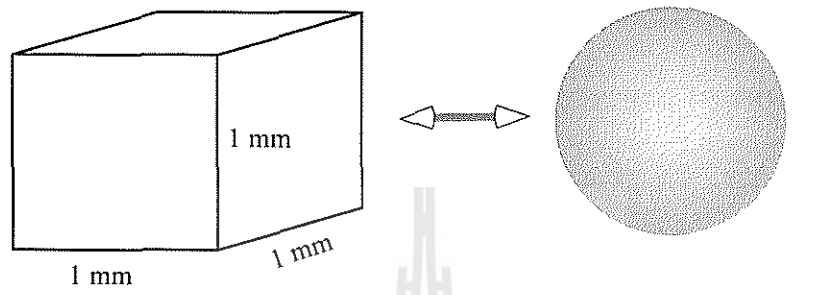

Cubic particle

Equivalent spherical particle

$V_{\text{cube}} = 1\ \text{mm}^3$

$S_{\text{cube}} = 6\ \text{mm}^2$

$(S/V)_{\text{cube}} = 6\ \text{mm}^{-1}$

$V_{\text{sphere}} = \pi d_v^3/6\ \text{mm}^3$

$S_{\text{sphere}} = \pi d_s^2\ \text{mm}^2$

$(S/V)_{\text{sphere}} = (6/d_{sv})\ \text{mm}^{-1}$

Figure 1: Illustration of equivalent sphere diameters.

Similarly, the equivalent surface diameter is defined as the diameter of a spherical particle having the same external surface as the cubic one, i.e. $S_{\text{sphere}} = \pi d_s^2 = S_{\text{cube}} = 6\ \text{mm}^2$. Therefore, the equivalent surface diameter is $d_s = \sqrt{6/\pi} = 1.382$ mm.

The equivalent surface-volume (Sauter) diameter is defined as the diameter of a spherical particle having the same surface to volume ratio as the cubic one, i.e. $(S/V)_{\text{sphere}} = \pi d_{sv}^2/\pi d_{sv}^3/6 = (S/V)_{\text{cube}} = 6\ \text{mm}^{-1}$. Then, $6/d_{sv} = 6$ and the equivalent surface-volume diameter is $d_{sv} = 1$ mm.

In the second group of particle size definitions, the size of the particle is taken as the diameter of a circle having the same property as particle under consideration, as shown in Table 2. To illustrate the definition of equivalent circle diameter, consider a square particle with the side length of 1 mm, as illustrated in Fig. 2. The surface of this particle is $S_{\text{square}} = 1\ \text{mm}^2$ and the perimeter is $P_{\text{square}} = 4$ mm.

The equivalent circle diameter is defined as the diameter of a circle having the same projected area as the square particle, i.e. $S_{\text{circle}} = \pi d_a^2 = S_{\text{square}} = 1\ \text{mm}^2$. Therefore, the equivalent circle diameter is $d_a = \sqrt{1/\pi} = 0.565$ mm. Similarly, the equivalent perimeter diameter is defined

as the diameter of a circle having the same perimeter as the square particle, i.e. $P_{\text{circle}} = \pi d_c = P_{\text{square}} = 4$ mm. Then, the equivalent perimeter diameter is $d_c = 4/\pi = 1.273$ mm.

Table 2: Definitions of particle size based on the equivalent circle diameters.

Symbol	Diameter	Definition	Formula
		Equivalent Circle Diameter	
d_a	Projected area	Diameter of a circle having the same projected area as the particle in stable orientation	$S = \pi d_a^2$
d_p	Projected area	Diameter of a circle having the same projected area as the particle in random orientation	$S = \pi d_p^2$
d_c	Perimeter	Diameter of a circle having the same perimeter as the projected outline of the particle	$P = \pi d_c$
		Sieve Diameter	
d_A	Sieve	Width of the minimum square aperture through which the particle will pass	

The third group of particle size distributions combines the so called statistical definitions of particle size, as shown in Table 3. In this case, the size of particle is measured in many particle orientations and then averaged to yield a mean value, as illustrated in Fig. 3.

Table 3: Definitions of particle size based on the statistical diameters

Symbol	Diameter	Definition	Formula
		Statistical Diameters	
d_F	Feret	The distance between pairs of parallel tangents to the projected outline of the particle in some fixed direction	
d_M	Martin	Chord length, parallel to some fixed direction, which divides the particle projected outline into two equal areas	
d_R	Unrolled	Chord length through the centroid of the particle outline	

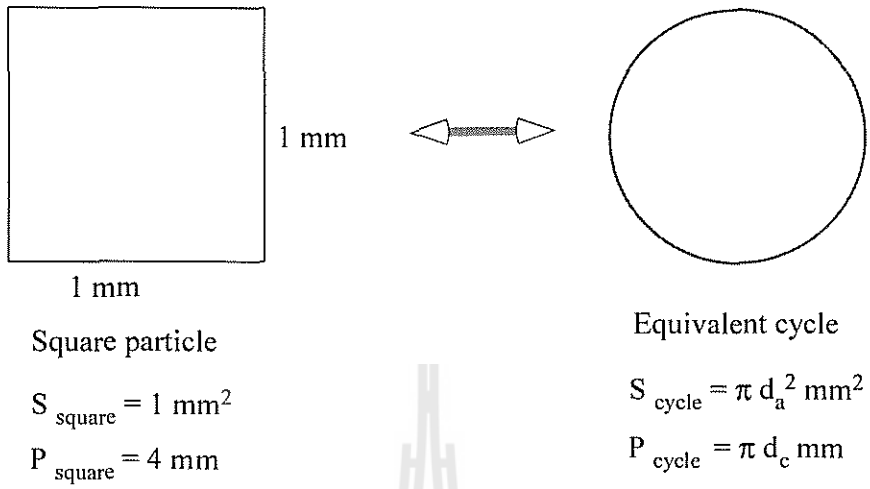

Figure 2: Illustration of equivalent cycle diameters.

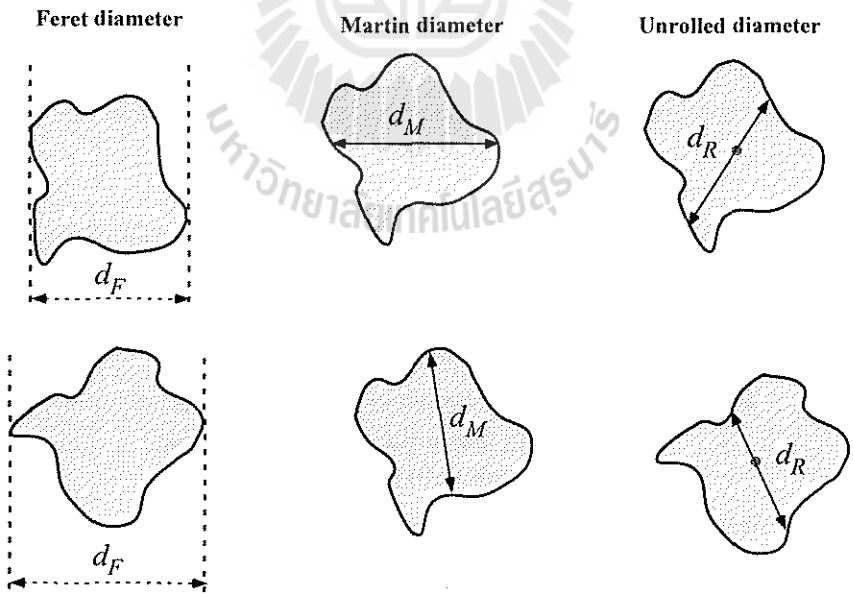

Figure 3: Illustration of statistical diameters.

1.2. Average sizes

The average size is used to represent the central tendency of a population of particles.

The ***mode***, x_m, is the most commonly occurring value in distribution. It is the value at which the frequency is a maximum, as shown in Fig. 4.

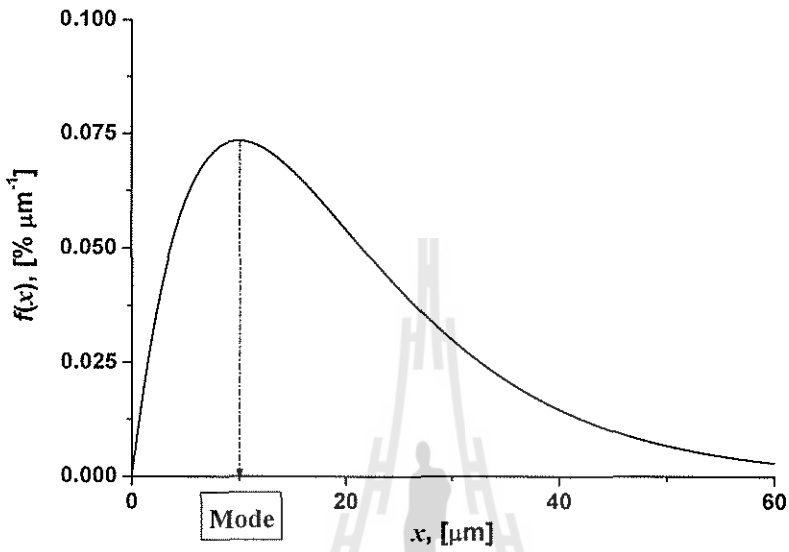

Figure 4: Illustration of a mode of particle size distribution.

The ***median***, x_{50}, is the size which divides the distribution into two equal parts. It is the 50% size on the cumulative distribution curve, as illustrated in Fig. 5.

The ***mean***, $\overline{x}$, is the center of gravity of the distribution. Many different means can be defined for a given size distribution.

Mean particle sizes defined according to the moment-ratio system are derived from ratios between two moments of a particle size distribution. The j sample moment M'_j of a random sample containing N elements from a population of particle sizes, x, is defined as

$$M'_j = \frac{\sum_i n_i x_{m_i}^j}{N}, \tag{1.1}$$

where x_{m_i} is the midpoint of the i interval, n_i is the number of particles in the i size bin and $N = \sum_i n_i$.

The arithmetic sample mean M'_1 of the particle size x is defined as $\overline{x}$, $\overline{x} = M'_1 = \frac{\sum_i n_i x_{m_i}}{N}$.

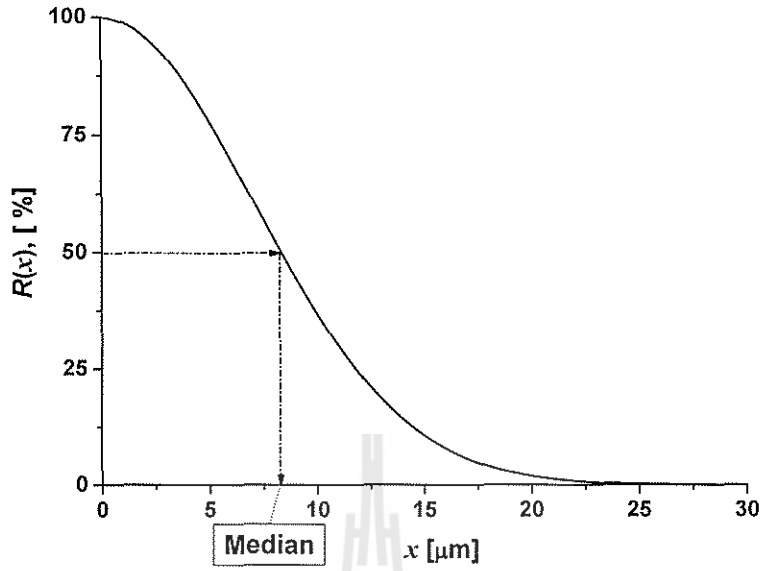

Figure 5: Illustration of a median of particle size distribution.

The j sample moment about the mean $\overline{x}$ is

$$M_j = \frac{\sum_i n_i (x_{m_i} - \overline{x})^j}{N}, \tag{1.2}$$

The mean size $\overline{x}_{p,q}$ of a sample of particle sizes is defined as $\frac{1}{p-q}$ power of the ratio of the p and q moments of the distribution of the particle sizes

$$\overline{x}_{p,q} = \left[\frac{\sum_{i=1}^{m} f_r(x_{m_i}) x_{m_i}^{p-r}}{\sum_{i=1}^{m} f_r(x_{m_i}) x_{m_i}^{q-r}} \right]^{\frac{1}{p-q}} \quad \text{if } p \neq q, \tag{1.3}$$

and

$$\overline{x}_{p,p} = \exp \left[\frac{\sum_{i=1}^{m} f_r(x_{m_i}) x_{m_i}^{p-r} \ln x_{m_i}}{\sum_{i=1}^{m} f_r(x_{m_i}) x_{m_i}^{p-r}} \right] \quad \text{if } p = q, \tag{1.4}$$

where $f_r(x_{m_i})$ is the particle quantity in the i bin, $r = 0, 1, 2, 3$ represents the type of quantity, i.e. number ($r = 0$), diameter ($r = 1$), surface ($r = 2$), volume or mass ($r = 3$), respectively, and m is the number of bins. The sum $p + q$ is called the order of the mean size.

Relationships between mean sizes:

- Differences between mean sizes decrease according as the uniformity of the particle sizes x increases
- Relationship useful for relating several mean particle diameters:

$$[\overline{x}_{p,q}]^{p-q} = \frac{\overline{x}_{p,0}^{p}}{\overline{x}_{q,0}^{q}} \tag{1.5}$$

- The symmetry relationship:

$$\overline{x}_{p,q} = \overline{x}_{q,p} \tag{1.6}$$

The nomenclature of main particle sizes is summarized in Table 4.

Table 4: Nomenclature for mean particle sizes $\overline{x}_{p,q}$.

Notation	Nomenclature
$\overline{x}_{-3,0}$	harmonic mean volume diameter
$\overline{x}_{-2,1}$	diameter-weighted harmonic mean volume diameter
$\overline{x}_{-1,2}$	surface-weighted harmonic mean volume diameter
$\overline{x}_{-2,0}$	harmonic mean surface diameter
$\overline{x}_{-1,1}$	diameter-weighted harmonic mean surface diameter
$\overline{x}_{-1,0}$	harmonic mean diameter
$\overline{x}_{0,0}$	geometric mean diameter
$\overline{x}_{1,1}$	diameter-weighted geometric mean diameter
$\overline{x}_{2,2}$	surface-weighted geometric mean diameter
$\overline{x}_{3,3}$	volume-weighted geometric mean diameter
$\overline{x}_{1,0}$	arithmetic mean diameter
$\overline{x}_{2,1}$	diameter-weighted mean diameter
$\overline{x}_{3,2}$	surface-weighted mean diameter
$\overline{x}_{4,3}$	volume-weighted mean diameter
$\overline{x}_{2,0}$	mean surface diameter
$\overline{x}_{3,1}$	diameter-weighted mean surface diameter
$\overline{x}_{4,2}$	surface-weighted mean surface diameter
$\overline{x}_{5,3}$	volume-weighted mean surface diameter
$\overline{x}_{3,0}$	mean volume diameter
$\overline{x}_{4,1}$	diameter-weighted mean volume diameter
$\overline{x}_{5,2}$	surface-weighted mean volume diameter
$\overline{x}_{6,3}$	volume-weighted mean volume diameter

Estimation of mean particle sizes is illustrated in Table 5 by using an example of a microscopic measurement of a sample of fine quartz. Calculated mean particle sizes are summarized below:

$\overline{x}_{0,0} = 4.75$, $\overline{x}_{1,0} = 5.15$, $\overline{x}_{2,0} = 5.55$, $\overline{x}_{3,0} = 5.95$, $\overline{x}_{3,2} = 6.84$, $\overline{x}_{3,3} = 7.26$, $\overline{x}_{4,3} = 7.64$.

Table 5: Estimation of mean particle sizes of a microscopic measurement of a sample of fine quartz.

Bin No.,	Size range		Midpoint,	Quantity,	$f_r \cdot x_{m_i}$	$f_r \cdot x_{m_i}^2$	$f_r \cdot x_{m_i}^3$	$f_r \cdot x_{m_i}^4$	$\ln x_{m_i}$	$f_r \cdot \ln x_{m_i}$	$f_r \cdot x_{m_i}^3 \cdot \ln x_{m_i}$
i [-]	initial [μm]	end [μm]	x_{m_i} [μm]	f_r [-]							
1	1.5	2.5	2	10	20	40	80	160	0.69	6.9	55.5
2	2.5	3.5	3	35	105	315	945	2835	1.10	38.5	1038.2
3	3.5	4.5	4	43	172	688	2752	11008	1.39	59.6	3815.1
4	4.5	5.5	5	44	220	1100	5500	27500	1.61	70.8	8851.9
5	5.5	6.5	6	22	132	792	4752	28512	1.79	39.4	8514.4
6	6.5	7.5	7	18	126	882	6174	43218	1.95	35.0	12014.0
7	7.5	8.5	8	12	96	768	6144	49152	2.08	25.0	12776.1
8	8.5	9.5	9	7	63	567	5103	45927	2.20	15.4	11212.4
9	9.5	10.5	10	4	40	400	4000	40000	2.30	9.2	9210.3
10	10.5	11.5	11	5	55	605	6655	73205	2.40	12.0	15958.0
Total:				200	1029	6157	42105	321517		311.8	83446.0

1.3. Particle size distributions

A population of particles is defined by a particle size distribution (PSD). PSD is used to describe the size and frequency of particles in the population.

Common terms used in representation of size distributions:

$f(x)$	frequency distribution function of size variable x or fractional density distribution
$dF = f(x)dx$	fraction of the distribution found in the size range x to $x + dx$, where F is the cumulative distribution function
$D(x)$	cumulative undersize distribution function
$R(x)$	cumulative oversize distribution function
(x_{min}, x_{max})	range of independent variable over which the distribution is defined and normalized

The frequency function $f(x)$ is normalized such that

$$\int_{x_{min}}^{x_{max}} f(x)dx = 1 \tag{1.7}$$

The cumulative undersize distribution function is defined as a fraction of the total amount of particles with size less than x

$$D(x) = \int_{x_{min}}^{x} f(x)dx \tag{1.8}$$

The cumulative oversize distribution function is defined as a fraction of the total amount of particles with size larger than x

$$R(x) = \int_{x}^{x_{max}} f(x)dx \tag{1.9}$$

The relationship between the cumulative oversize and undersize functions is as follows

$$R(x) = 1 - D(x) \tag{1.10}$$

The frequency function is related to the cumulative functions as

$$f(x) = \frac{dD}{dx} = -\frac{dR}{dx} \tag{1.11}$$

Therefore, the frequency function for any size x can be obtained as a slope of the cumulative distribution function.

Tabular and graphical presentation of size distribution data.

A step-by-step guide to the tabular and graphical presentation of size distribution data [3]

1. Divide the entire size range into a series of successive particle size intervals (bins) where interval limits are $x_{min}, x_1, \cdots, x_{i-1}, x_i, x_{i+1}, \cdots, x_{max}$.

   The intervals should be contiguous and cover the entire range, i.e. the first bin is $[x_{min}, x_1]$, the second bin is $[x_1, x_2]$, the i bin is $[x_{i-1}, x_i]$ and the last bin is $[x_{N_b-1}, x_{N_b}]$, where N_b is the number of bins.

   The upper size limit of each interval coincides with the lower limit of the next interval.

   The intervals can be uniform and nonuniform.

2. Measure each particle and add it to the corresponding bin.

   If the size of a particle is exactly equal to the interval limit, add this particle to the higher interval.

3. Count particles in each interval, n_i, and the total number of particles, $N_T = \sum_{i=1}^{N_b} n_i$.

4. Calculate the mean of each interval, x_{m_i}.

   If the interval width is large, the geometric mean is used as the mean of the interval, i.e. $x_{m_i} = \sqrt{x_{i-1} \cdot x_i}$. For narrow interval, the arithmetic mean can be used, $x_{m_i} = (1/2)(x_{i-1} + x_i)$.

5. Calculate the relative frequency of each size interval, h_i, by dividing each interval count by the total number of particles, $h_i = n_i/N_T$.

   The relative frequency is calculated in order to standardize for sample size (total number of particles).

6. Calculate the frequency distribution function, f_i, by dividing the relative frequency by the interval width, $f_i = h_i/(x_i - x_{i-1})$.

   The frequency size distribution is normalized by the interval width making it possible to compare distribution data measured with different devices.

   Plot the frequency distribution as a discrete or continuous function. The discrete frequency function can be plotted as a histogram shown in Fig. (??tab:1-3)), where the width of each rectangular represents the size interval and the height represents the relative frequency. The area under each rectangular is equal to the fraction of particles in that size interval, $f_i \cdot \Delta x = h_i$, where $\Delta x = x_i - x_{i-1}$. The total area is equal to one, $\sum h_i = \sum f_i \cdot \Delta x_i = 1$.

The continuous frequency distribution function can be plotted as a curve connecting values of frequency distribution at the mean of interval, as shown in Fig. (??fig:PSD3)). For the continuous distribution, the fraction of particles in size interval $[x_{i-1}, x_i]$, h_i, is represented by the integral under the distribution curve between these limits, $h_i = \int_{x_{i-1}}^{x_i} f(x)dx$. The total area is $\int_{x_{min}}^{x_{max}} f(x)dx = 1$.

The frequency distribution is plotted with $f(\%/\mu\text{m})$ as an ordinate and the size as an abscissa in linear case. For logarithmic scale, The ordinate is $f(\%/\log \mu\text{m})$ in order to normalize the area under the curve to 100.

7. Calculate the undersize, D, and oversize, R, distribution function.

   The undersize cumulative distribution function for i bin is calculated by summing the relatives frequencies starting from the first bin up to i bin, $D_i = \sum_{j=1}^{i} h_j \cdot 100\%$. The oversize cumulative distribution for i bin is $R_i = 100 - D_i$.

Example 1.

The equivalent circle diameter of particles, d_a, were measured by an image analysis and were used as representation of particle sizes. The size axis, x, was divided into 11 bins of equal width of 1 μm and each particle was measured and added to the corresponding bin. The number of particles in each bin was calculated and the results were summarized in the Table 6. The arithmetic mean value of the bin boundaries is used as a bin midpoint x_{m_i}. The histogram of the particle size data is shown in Fig. 6.

Table 6: Particle size data for bins of equal width.

Bin No.,	Size range		Bin midpoint size,	Number of particles in a bin,
i [-]	initial [μm]	end [μm]	x_i [μm]	n_i [-]
1	0	1	0.5	0
2	1	2	1.5	7
3	2	3	2.5	29
4	3	4	3.5	55
5	4	5	4.5	91
6	5	6	5.5	99
7	6	7	6.5	88
8	7	8	7.5	73
9	8	9	8.5	44
10	9	10	9.5	14
11	10	11	10.5	0
				$N_T = 500$

Usually, it is better to distribute the histogram bins geometrically other than linearly for presentation of PSD, so that each subsequent histogram bin is a constant factor larger than

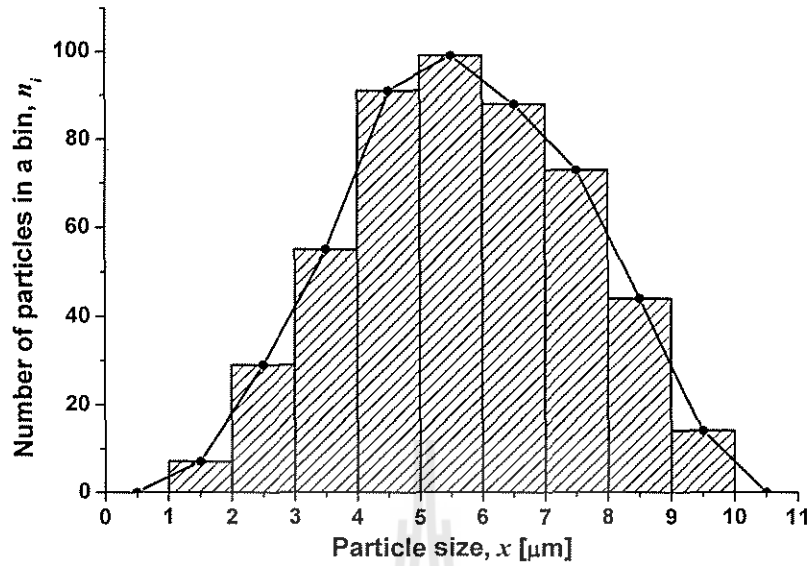

Figure 6: Histogram representation of particle size data for bins of equal width.

the previous one. This has two advantages:

1. The bin resolution is constant across the whole histogram. The resolution is defined as a bin width divided by a bin midpoint size x_{m_i}. Suppose we have a linear set of bins of limit 1 μm, 2 μm, 3 μm, etc. The resolution of the bin in the range of 1 $\sim$ 2 μm is (width/midpoint) = 1 $\mu m/1.5$ $\mu m = 0.67$, while the resolution of the 15 $\sim$ 16 μm bin is 1 $\mu m/15.5$ $\mu m = 0.065$. Consequently there is less detail in the small size end of the size distribution than at the large size end. However, a geometric representation has the same resolution for each bin, so the detail is uniformly distributed over the representation.

2. The geometric representation provides the maximum amount of detail for a given number of bins.

The commercial instrument usually presents data using bins whose limits advance by the $\sqrt{2}$ or $\sqrt[4]{2}$ per bin. Bin limits on $\sqrt{2}$ progression starting at 1 μm would be 1, 1.4, 2, 2.8, 4, 5.6, 8, 11.3, 16 μm. However, now we no longer have constant bin widths, so the shape of the distribution becomes dependent on the particular bin sizes chosen. To illustrate this, we replace the two bins labeled 3 $\sim$ 4 μm and 4 $\sim$ 5 μm with a single bin, 3 $\sim$ 5 μm. The original bins contain 55 and 91 particles, so the new wider bin would contain 146 particles as illustrated in Table 7. The graph of this data is shown in Fig. 7. Someone inspecting this graph could suggest that there was an unusually large amount of material in this size bin, which is untrue because the width of this bin is double of other bins. To overcome this difficulty we need to plot the

fraction or percentage of material per unit of bin width on y-axis.Table 8 and Fig. 8 illustrate the correct form of the frequency distribution.

Table 7: Calculation of frequency distributions for bins of nonequal width.

Bin No., i [-]	Size range		Bin midpoint size, x_{m_i} [μm]	Number of particles in a bin, n_i [-]
	initial [μm]	end [μm]		
1	0	1	0.5	0
2	1	2	1.5	7
3	2	3	2.5	29
4	3	5	4.0	146
5	5	6	5.5	99
6	6	7	6.5	88
7	7	8	7.5	73
8	8	9	8.5	44
9	9	10	9.5	14
10	10	11	10.5	0
				$N_T = 500$

Table 8: Tabular presentation of frequency distribution function.

Bin No., i [-]	Size range initial [μm]	Size range end [μm]	Bin mid. size, x_{m_i} [μm]	Number of part. in a bin n_i[−]	Rel. freq., n_i/N [%]	% per μm $\frac{n_i/N}{\text{(end-init.)}}$ $\left[\frac{\%}{\mu m}\right]$
1	0	1	0.5	0	0	0
2	1	2	1.5	7	1.4	1.4
3	2	3	2.5	29	5.8	5.8
4	3	5	4.0	146	29.2	14.6
5	5	6	5.5	99	19.8	19.8
6	6	7	6.5	88	17.6	17.6
7	7	8	7.5	73	14.6	14.6
8	8	9	8.5	44	8.8	8.8
9	9	10	9.5	14	2.8	2.8
10	10	11	10.5	0	0	0
					100	

To plot correctly the cumulative distribution we can represent particle size data similar to Table 9. Cumulative distributions plotted using these data are shown in Fig. 9.

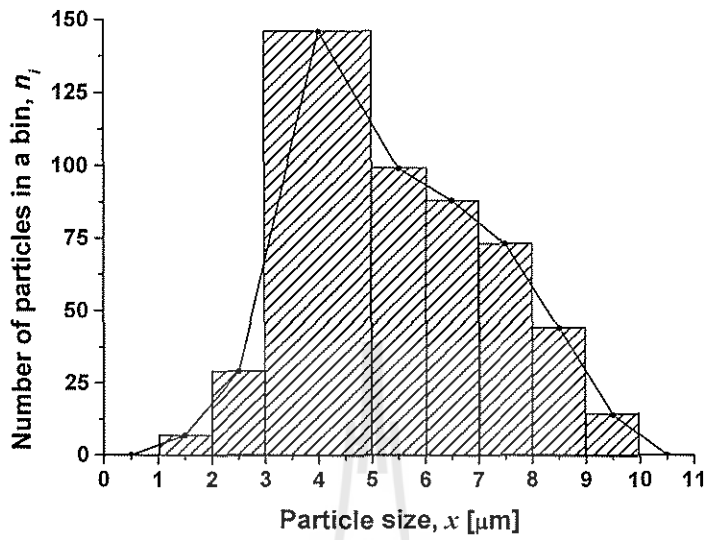

Figure 7: Histogram representation of particle size data for bins of nonequal width.

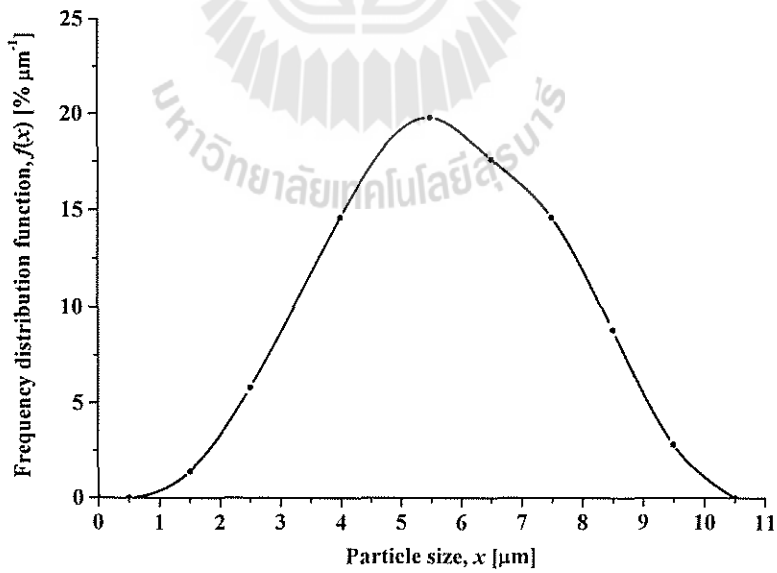

Figure 8: Frequency distribution function.

Table 9: Tabular presentation of cumulative distribution function.

Bin No.,	Size range		Bin mid. size,	Relat. freq.,	Cumulative undersize
i [-]	initial [μm]	end [μm]	x_{m_i} [μm]	n_i/N [%]	D [%]
1	0	1	0.5	0	0
2	1	2	1.5	1.4	1.4
3	2	3	2.5	5.8	7.2
4	3	5	4.0	29.2	36.4
5	5	6	5.5	19.8	56.2
6	6	7	6.5	17.6	73.8
7	7	8	7.5	14.6	88.4
8	8	9	8.5	8.8	97.2
9	9	10	9.5	2.8	100
10	10	11	10.5	0	100
				100%	

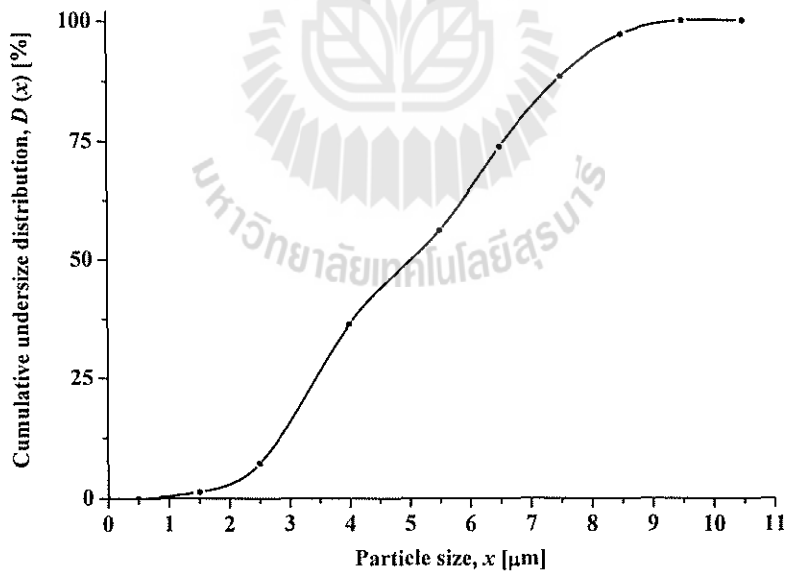

Figure 9: Cumulative undersize distribution function.

The frequency of the particular value of a particle size x can be expressed in terms of the number of particles, the diameters, surfaces or volumes of the particles. The corresponding frequency distributions are called number, diameter, surface, or volume distributions.

- The number distribution, f_n, is the distribution by number of particles as a function of their sizes.
- The diameter distribution, f_l, is the distribution by diameter of particles as a function of their sizes.
- The surface distribution, f_s, is the distribution by surface of particles as a function of their sizes.
- The volume distribution, f_v, is the distribution by volume of particles as a function of their sizes.

The weight distribution, f_{w} is the distribution by weight of particles as a function of their sizes. It is similar to the volume distribution, assuming that the particle density does not depend on the particle size.

Conversion between different distributions

Assume that we need to convert the number distribution to the weight distribution. One spherical particle of diameter x has a mass of m_p, $m_p = \rho_s \left(\frac{\pi x^3}{6}\right)$. Here ρ_s is the particle density. In the size ratio, $(x, x + dx)$ there are dN particles. According to the definition of the number distribution,

$$dN = f_n(x)dx \cdot N_T$$

The mass of particles in the same size range is

$$dW = \rho_s \left(\frac{\pi x^3}{6}\right) \cdot f_n(x)dx \cdot N_T$$

Also, by definition of the weight distribution,

$$dW = f_{\mathrm{w}}(x)dx \cdot W_T$$

Combining two equations for dW results in

$$f_{\mathrm{w}}(x)dx = \frac{\rho_s \left(\frac{\pi x^3}{6}\right) \cdot f_n(x)dx \cdot N_T}{W_T}$$

The total amount of particles is

$$W_T = \int_{x_{min}}^{x_{max}} dW = \int_{x_{min}}^{x_{max}} \rho_s \left(\frac{\pi x^3}{6}\right) \cdot f_n(x)dx \cdot N_T = \rho_s \left(\frac{\pi}{6}\right) \cdot N_T \int_{x_{min}}^{x_{max}} x^3 f_n(x)dx$$

Therefore,

$$f_w(x)dx = \frac{\rho_s \left(\frac{\pi x^3}{6}\right) \cdot f_n(x)dx \cdot N_T}{\rho_s \left(\frac{\pi}{6}\right) \cdot N_T \int_{x_{min}}^{x_{max}} x^3 f_n(x)dx} = \frac{x^3 f_n(x)dx}{\int_{x_{min}}^{x_{max}} x^3 f_n(x)dx}$$

The ***general formula for conversion of distributions*** is

$$f_\beta dx = \frac{x^{\beta-\alpha} f_\alpha(x)dx}{\int_{x_{min}}^{x_{max}} x^{\beta-\alpha} f_\alpha(x)dx} \tag{1.12}$$

α, β	Description
0	number
1	length
2	surface
3	weight, volume
-1	surface per volume

1.4. Standard forms of distribution functions

1.4.1. Arithmetic normal distribution

The arithmetic normal frequency distribution is defined as [4]

$$f(x) = \frac{1}{\sigma\sqrt{2\pi}} \exp\left(-\frac{1}{2}\left(\frac{x - x_m}{\sigma}\right)^2\right) \tag{1.13}$$

where x_m is the arithmetic mean of the distribution and σ is the standard deviation. This function is symmetrical about the mean, as shown in Figs. 10 and 11.

The distribution is normalized on interval x in $(-\infty, +\infty)$, i.e.

$$\int_{-\infty}^{+\infty} f(x)dx = 1 \tag{1.14}$$

The normal distribution is used seldom for the description of particle size distributions, because these distributions are typically very asymmetric as they are shifted to the lower value of particle size range. Also the normal distribution is extended to the negative values of the size coordinate x.

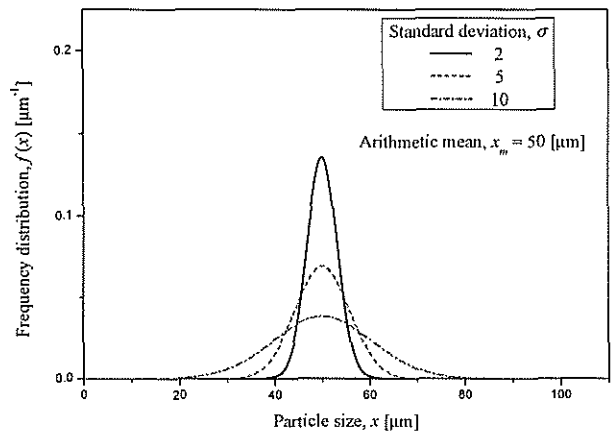

Figure 10: Illustration of arithmetic normal distribution for various standard deviations.

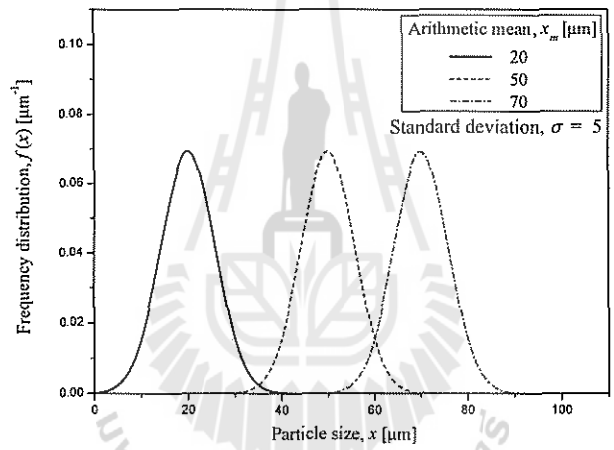

Figure 11: Illustration of arithmetic normal distribution for various arithmetic means.

Introduce a new variable z, $z = \dfrac{x - x_m}{\sqrt{2}\sigma}$. Then, the derivative of z is equal to $dz = \dfrac{dx}{\sqrt{2}\sigma}$ and dx is $dz\sqrt{2}\sigma$. Substitution of z into Eq. (1.13) and the resulting equation together with dx into Eq. (1.14) yields

$$\int_{-\infty}^{+\infty} \frac{1}{\sigma\sqrt{2\pi}} \exp\left(-z^2\right)\sqrt{2}\sigma dz = \frac{1}{\sqrt{\pi}} \int_{-\infty}^{+\infty} \exp\left(-z^2\right) dz = \frac{1}{\sqrt{\pi}} \left[\frac{\sqrt{\pi}}{2} \cdot \mathrm{erf}(z)\right]_{-\infty}^{+\infty} = \frac{1}{2}(\mathrm{erf}(+\infty) - (\mathrm{erf}(-\infty)) = \frac{1}{2}(1 - (-1)) = 1, \tag{1.15}$$

where $\text{erf}(z)$ is an error function defined as

$$\text{erf}(z) = \frac{2}{\sqrt{\pi}} \int_0^z \exp\left(-z^2\right) dz;$$
$$\text{erf}(-x) = -\text{erf}(x),\ \text{erf}(+\infty) = 1\,, \text{erf}(-\infty) = -1.$$

The cumulative distribution D is given by

$$D = \int_{-\infty}^{x} f(x)dx \tag{1.16}$$

The cumulative distribution in terms of z is

$$D(z) = \frac{1}{2}(1 + \text{erf}(z)) \tag{1.17}$$

because

$$D(z) = \frac{1}{\sqrt{\pi}} \int_{-\infty}^{z} \exp\left(-z^2\right) dz = \frac{1}{\sqrt{\pi}} \left[\frac{\sqrt{\pi}}{2} \cdot \text{erf}(z)\right]_{-\infty}^{z} = \frac{1}{2}(\text{erf}(z) - \text{erf}(-\infty))$$
$$= \frac{1}{2}(\text{erf}(z) - (-1)) = \frac{1}{2}(1 + \text{erf}(z)).$$

Eq. (1.17) can be rearranged as

$$2D - 1 = \text{erf}(z) = \text{erf}\left(\frac{x - x_m}{\sqrt{2}\sigma}\right)$$

Taking the inverse error function of the left and right sides of the above equation results in

$$\frac{x - x_m}{\sqrt{2}\sigma} = \text{erf}^{-1}(2D - 1)$$

Expressing explicitly x gives

$$x = \sqrt{2}\sigma \cdot \text{erf}^{-1}(2D - 1) + x_m \tag{1.18}$$

This equation can be written in a linear form as

$$Y = aX + b \tag{1.19}$$

where $X = \text{erf}^{-1}(2D - 1)$ and $Y = x$. The slope is $a = \sqrt{2}\sigma$ and the intercept is $b = x_m$.

Figure 12 illustrates the linear form of the normal distribution function.

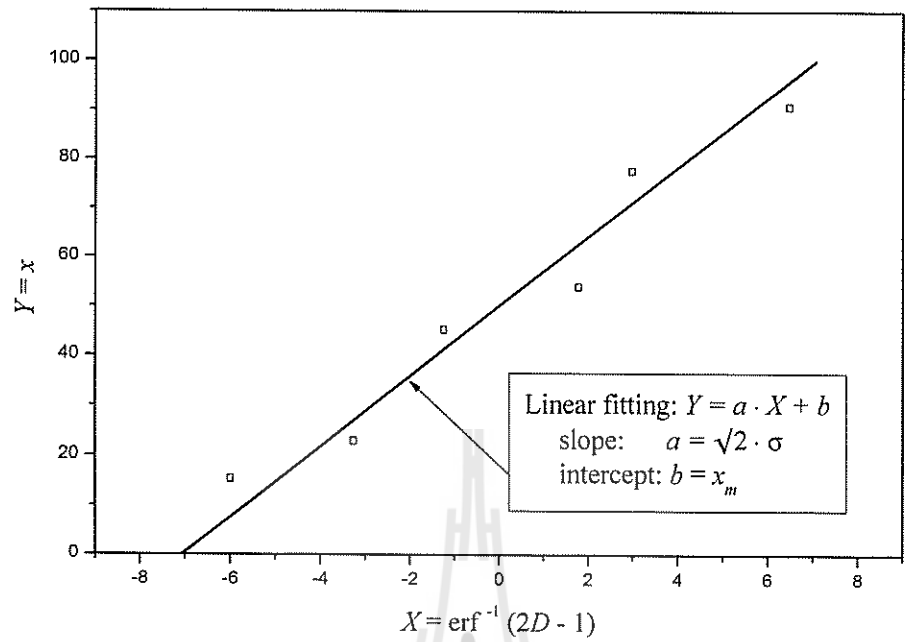

Figure 12: Linear form of arithmetic normal distribution.

Properties of normal distribution function are summarized in Table 10.

1.4.2. Log-normal distribution

The log-normal distribution is simply a normal distribution in terms of $\ln(x)$

$$f(\ln x) = \frac{1}{\sqrt{2\pi}\ln\sigma_g}\exp\left(-\frac{1}{2}\left(\frac{\ln x - \ln x_g}{\ln\sigma_g}\right)^2\right), \tag{1.20}$$

where x_g is the geometric mean of the distribution, i.e. the arithmetic mean of logarithms, and σ_g is the geometric standard deviation, i.e. the standard deviation of logarithms. Figure 13 illustrates the log-normal distribution in terms of $\ln(x)$.

The log-normal distribution in terms of x is

$$\boxed{f(x) = \frac{1}{x\sqrt{2\pi}\ln\sigma_g}\exp\left(-\frac{1}{2}\left(\frac{\ln x - \ln x_g}{\ln\sigma_g}\right)^2\right)} \tag{1.21}$$

Figure 14 illustrates log-normal distribution in terms of x.

The fact that the mean x_g is the a geometric one can be illustrated by considering the mean

Table 10: Properties of normal distribution function.

Frequency distribution	$f(x) = \frac{1}{\sigma\sqrt{2\pi}} \exp\left(-\frac{1}{2}\left(\frac{x - x_m}{\sigma}\right)^2\right)$
Domain, x	$(-\infty, \infty)$
Cumulative distribution	$D(z) = \frac{1}{2}(1 + \text{erf}(z))$
Dimensionless size, z	$z = \frac{x - x_m}{\sqrt{2}\sigma}$
Linear form	$Y = aX + b,$ where $X = \text{erf}^{-1}(2D - 1), Y = x, a = \sqrt{2}\sigma, b = x_m$
Mean size, $\overline{x}$	x_m
Mode size, x_m	x_m
Median size, x_{50}	x_m
Standard deviation, σ	$\sigma = x_{84} - x_{50} = x_{50} - x_{16} = (x_{84} - x_{16})/2$
Coefficient of variation	σ/x_m
Moments	$m_0 = 1, m_1 = x_m, m_2 = x_m^2 + \sigma^2$ $m_3 = x_m^3 + 2\sigma^2 x_m, m_4 = x_m^4 + 6\sigma^2 x_m^2 + 3\sigma^4$

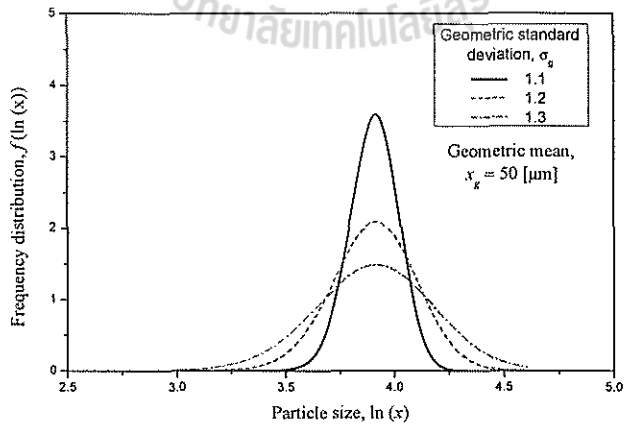

Figure 13: Illustration of log-normal distribution with respect to logarithm of particle size.

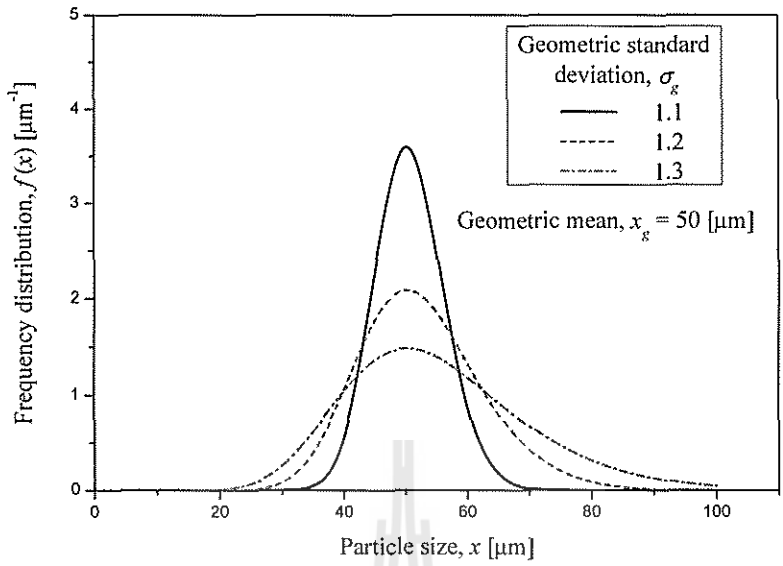

Figure 14: Illustration of log-normal distribution for various standard deviations.

of just two numbers in distribution, x_1 and x_2,

$$\ln x_g = \frac{\ln x_1 + \ln x_2}{2} = \ln (x_1 \cdot x_2)^{1/2}$$

or

$$x_g = (x_1 \cdot x_2)^{1/2}$$

The log-normal distribution is normalized over the range $\ln x$ in $(-\infty, +\infty)$ or over the range x in $(0, +\infty)$.

Figures 14 and 15 illustrates effects of variation of geometric standard deviation and geometric mean on log-normal frequency distribution.

Introduce a new variable z', $\boxed{z' = \frac{\ln x - \ln x_g}{\sqrt{2}\ln \sigma_g}}$. Then, $\ln x$ is $\sqrt{2}\ln \sigma_g z' + \ln x_g$ and $d(\ln x) = \sqrt{2}\ln \sigma_g d(z')$. Taking into account that $f(\ln x) = dD/d(\ln x)$ and substituting $d(\ln x)$ and $\ln x$ into Eq. (1.20) results in

$$\frac{dD}{\sqrt{2}\ln \sigma_g d(z')} = \frac{1}{\sqrt{2\pi}\ln \sigma_g} \exp\left(-\frac{1}{2}\left(\frac{\sqrt{2}\ln \sigma_g z' + \ln x_g - \ln x_g}{\ln \sigma_g}\right)^2\right) = \frac{1}{\sqrt{2\pi}\ln \sigma_g} \exp(-z'^2)$$

Therefore,

$$\frac{dD}{d(z')} = \frac{1}{\sqrt{\pi}} \exp(-z'^2)$$

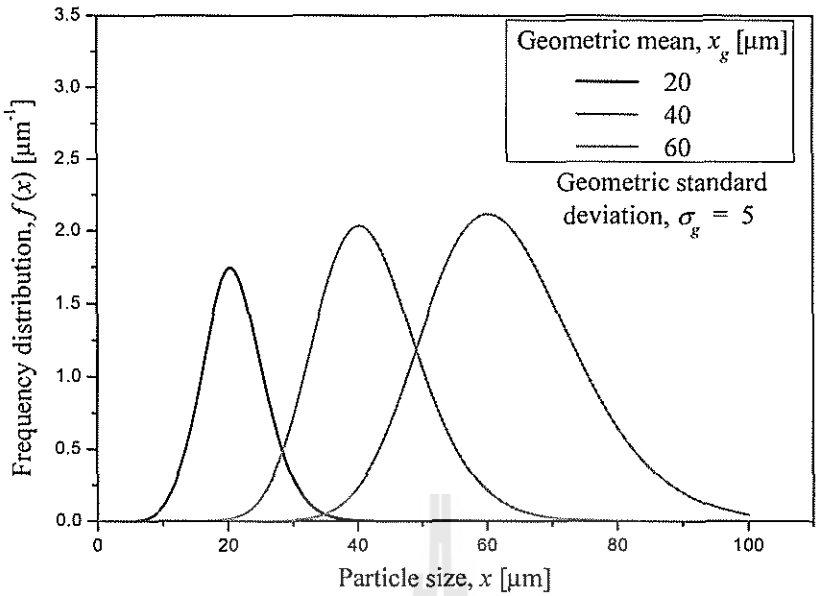

Figure 15: Illustration of log-normal distribution for various arithmetic means.

The cumulative undersize distribution can be obtained by integration of above equation

$$\int_0^D dD = \frac{1}{\sqrt{\pi}} \int_{-\infty}^{z'} \exp(-z'^2) dz'$$

and using the definition of error function as

$$\boxed{D(z') = \frac{1}{2}(1 + \text{erf}(z'))} \tag{1.22}$$

Eq. (1.22) can be rearranged as

$$2D - 1 = \text{erf}(z') = \text{erf}\left(\frac{\ln x - \ln x_g}{\sqrt{2}\ln \sigma_g}\right)$$

Taking the inverse error function of the left and right sides of the above equation results in

$$\frac{\ln x - \ln x_g}{\sqrt{2}\ln \sigma_g} = \text{erf}^{-1}(2D - 1)$$

Expressing explicitly $\ln x$ gives

$$\ln x = \sqrt{2}\ln \sigma_g \cdot \text{erf}^{-1}(2D - 1) + \ln x_g \tag{1.23}$$

This equation can be written in a linear form as

$$Y = aX + b \tag{1.24}$$

where $X = \text{erf}^{-1}(2D - 1)$ and $Y = \ln x$. The slope is $a = \sqrt{2}\ln\sigma_g$ and the intercept is $b = \ln x_g$.

Figure 16 illustrates the linear form of the log-normal distribution function.

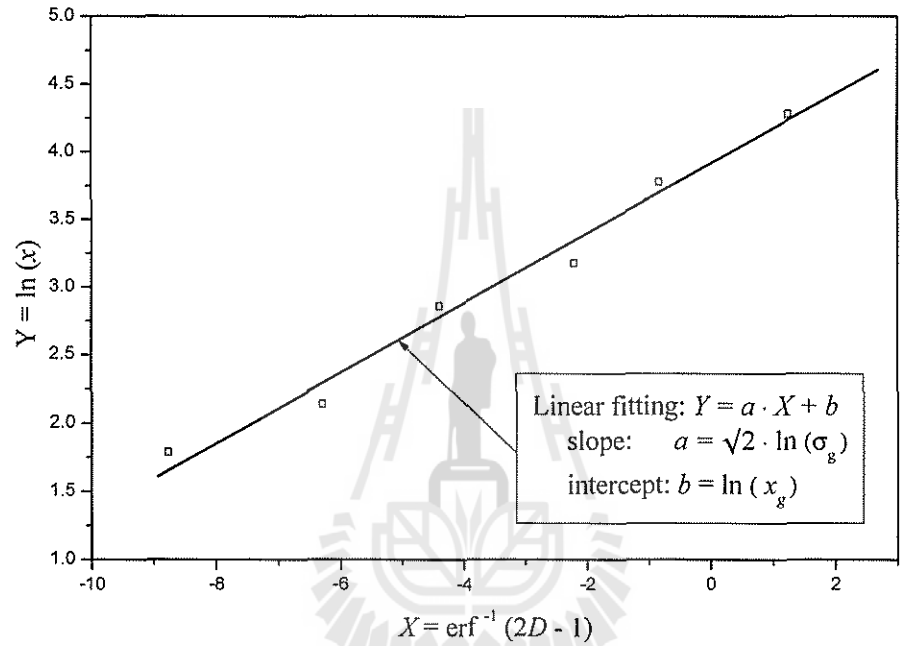

Figure 16: Linear form of log-normal distribution.

Properties of log-normal distribution function

The ***mean*** is defined as

$$\overline{x} = \int_0^\infty f(x) \cdot x dx \tag{1.25}$$

Introducing $f(x)$ by Eq. (1.21) into Eq. (1.25) gives

$$\overline{x} = \frac{1}{\sqrt{2\pi}\ln\sigma_g} \int_0^\infty \exp\left(-\frac{1}{2}\left(\frac{\ln x - \ln x_g}{\ln\sigma_g}\right)^2\right) dx \tag{1.26}$$

Assuming $y = \ln x$ or $x = e^y$ and replacing the derivatives dx in Eq. (1.26) by $dx = e^y dy$

results in

$$\begin{aligned}\overline{x} &= \frac{1}{\sqrt{2\pi}\ln\sigma_g}\int_{-\infty}^{+\infty}\exp\left(-\frac{1}{2}\left(\frac{y-\ln x_g}{\ln\sigma_g}\right)^2\right)e^y dy \\ &= \frac{1}{\sqrt{2\pi}\ln\sigma_g}\int_{-\infty}^{+\infty}\exp\left(-\frac{1}{2}\left(\frac{y-\ln x_g}{\ln\sigma_g}\right)^2 + y\right)dy\end{aligned} \tag{1.27}$$

The limits of integration in Eq. (1.26) become $x = 0 \rightarrow y = -\infty$ and $x = +\infty \rightarrow y = +\infty$.

The exponent $-\dfrac{(y-\ln x_g)^2}{2\ln^2\sigma_g} + y$ is represented as $-\dfrac{(y-a)^2}{2\ln^2\sigma_g} + b$, where a and b are constants to be derived.

Therefore,

$$\frac{-(y^2 + \ln^2 x_g - 2y\ln x_g) + y\cdot 2\ln^2\sigma_g}{2\ln^2\sigma_g} = \frac{-(y^2 + a^2 - 2ay) + b\cdot 2\ln^2\sigma_g}{2\ln^2\sigma_g}$$

or

$$-\ln^2 x_g + 2y\ln x_g + y\cdot 2\ln^2\sigma_g = -a^2 + 2ay + b\cdot 2\ln^2\sigma_g$$

The above equation is satisfied if $a = \ln x_g + \ln^2\sigma_g$ and $b = \ln x_g + \ln^2\sigma_g/2$:

$$\begin{aligned}\text{L.H.S.} &= -\ln^2 x_g + 2y\ln x_g + 2y\ln^2\sigma_g \\ \text{R.H.S.} &= -a^2 + 2ay + 2b\ln^2\sigma_g\end{aligned}$$

Expanding the terms in R.H.S

$$\begin{aligned}a^2 &= (\ln x_g + \ln^2\sigma_g)^2 = \ln^2 x_g + 2\ln x_g\ln^2\sigma_g + \ln^4\sigma_g \\ 2ay &= 2(\ln x_g + \ln^2\sigma_g)y = 2\ln x_g y + 2\ln^2\sigma_g y \\ 2b\ln^2\sigma_g &= 2(\ln x_g + \frac{\ln^2\sigma_g}{2})\ln^2\sigma_g = 2\ln x_g\ln^2\sigma_g + \ln^4\sigma_g\end{aligned}$$

and substituting them into R.H.S gives

$$\begin{aligned}\text{R.H.S.} &= -\ln^2 x_g - 2\ln x_g\ln^2\sigma_g - \ln^4\sigma_g + 2\ln x_g y + 2\ln^2\sigma_g y + 2\ln x_g\ln^2\sigma_g + \ln^4\sigma_g \\ &= -\ln^2 x_g + 2y\ln x_g + 2y\ln^2\sigma_g\end{aligned}$$

or L.H.S. = R.H.S.

Therefore,

$$\frac{-(y-\ln x_g)^2}{2\ln^2\sigma_g} + y = -\frac{(y-(\ln x_g + \ln^2\sigma_g))^2}{2\ln^2\sigma_g} + \left(\ln x_g + \frac{\ln^2\sigma_g}{2}\right)$$

and Eq. (1.27) becomes

$$\overline{x} = \frac{1}{\sqrt{2\pi}\ln\sigma_g}\int_{-\infty}^{+\infty}\exp\left(-\frac{\left(y-(\ln x_g+\ln^2\sigma_g)\right)^2}{2\ln^2\sigma_g}\right)\cdot\exp\left(\ln x_g+\frac{\ln^2\sigma_g}{2}\right)dy \qquad (1.28)$$

Moving the constant outside integral yields

$$\overline{x} = \exp\left(\ln x_g+\frac{\ln^2\sigma_g}{2}\right)\cdot\left\{\frac{1}{\sqrt{2\pi}\ln\sigma_g}\int_{-\infty}^{+\infty}\exp\left(-\frac{\left(y-(\ln x_g+\ln^2\sigma_g)\right)^2}{2\ln^2\sigma_g}\right)dy\right\} \qquad (1.29)$$

The integral in the parenthesis is the arithmetic normal distribution of variable y with the mean $\ln x_g+\ln^2\sigma_g$ and the standard deviation $\ln\sigma_g$. This integral is equal to one similar to Eq. (1.14).

Therefore,

$$\overline{x} = \exp\left(\ln x_g+\frac{\ln^2\sigma_g}{2}\right)$$

Finally, the mean of the log-normal distribution function is

$$\overline{x} = x_g\cdot\exp\left(\frac{1}{2}\ln^2\sigma_g\right) \qquad (1.30)$$

To derive an expression for a ***mode*** size, the following equation should be solved for $x = x_m$

$$\frac{df(x)}{dx} = 0 \qquad (1.31)$$

The differentiation of Eq. (1.21) with respect to x gives

$$\begin{aligned}\frac{df}{dx} = &\frac{d}{dx}\left\{\frac{1}{x\sqrt{2\pi}\ln\sigma_g}\right\}\cdot\exp\left(-\frac{1}{2}\left(\frac{\ln x-\ln x_g}{\ln\sigma_g}\right)^2\right)+\\ &\frac{d}{dx}\left\{\exp\left(-\frac{1}{2}\left(\frac{\ln x-\ln x_g}{\ln\sigma_g}\right)^2\right)\right\}\cdot\frac{1}{x\sqrt{2\pi}\ln\sigma_g}\end{aligned} \qquad (1.32)$$

Derivatives in Eq. (1.32) can be written separately as

$$\frac{d}{dx}\left\{\frac{1}{x\sqrt{2\pi}\ln\sigma_g}\right\} = -\frac{1}{x^2\sqrt{2\pi}\ln\sigma_g}$$

$$\frac{d}{dx}\left\{\exp\left(-\frac{1}{2}\left(\frac{\ln x-\ln x_g}{\ln\sigma_g}\right)^2\right)\right\} =$$

$$\frac{d}{dx}\left\{-\frac{1}{2}\left(\frac{\ln x-\ln x_g}{\ln\sigma_g}\right)^2\right\}\cdot\exp\left(-\frac{1}{2}\left(\frac{\ln x-\ln x_g}{\ln\sigma_g}\right)^2\right)$$

$$\frac{d}{dx}\left\{-\frac{1}{2}\left(\frac{\ln x-\ln x_g}{\ln\sigma_g}\right)^2\right\}=-\frac{1}{2(\ln\sigma_g)^2}\cdot\frac{d}{dx}(\ln x-\ln x_g)^2$$
$$=-\frac{1}{2(\ln\sigma_g)^2}\cdot\frac{d}{dx}((\ln x)^2-2\ln x\ln x_g+(\ln x_g)^2)$$
$$=-\frac{1}{2(\ln\sigma_g)^2}\cdot\left(\frac{d}{dx}(\ln x)^2-2\ln x_g\frac{d}{dx}(\ln x)\right)$$
$$=-\frac{1}{2(\ln\sigma_g)^2}\cdot\left(\frac{2\ln x}{x}-2\ln x_g\frac{1}{x}\right)$$
$$=-\frac{1}{x(\ln\sigma_g)^2}\cdot(\ln x-\ln x_g)$$

Substituting derivatives back into Eq. (1.32) yields

$$\frac{df}{dx}=-\frac{1}{x^2\sqrt{2\pi}\ln\sigma_g}\cdot\exp\left(-\frac{1}{2}\left(\frac{\ln x-\ln x_g}{\ln\sigma_g}\right)^2\right)+$$
$$\left(-\frac{\ln x-\ln x_g}{x(\ln\sigma_g)^2}\right)\cdot\exp\left(-\frac{1}{2}\left(\frac{\ln x-\ln x_g}{\ln\sigma_g}\right)^2\right)\cdot\frac{1}{x\sqrt{2\pi}\ln\sigma_g} \qquad (1.33)$$
$$=-\frac{1}{x^2\sqrt{2\pi}\ln\sigma_g}\cdot\exp\left(-\frac{1}{2}\left(\frac{\ln x-\ln x_g}{\ln\sigma_g}\right)^2\right)\left[1+\frac{\ln x-\ln x_g}{(\ln\sigma_g)^2}\right]$$

Solving Eq. (1.33) for $x=x_m$ yields

$$1+\frac{\ln x_m-\ln x_g}{\ln^2\sigma_g}=0 \quad \text{or} \quad -\ln^2\sigma_g=\ln\left(\frac{x_m}{x_g}\right) \quad \text{and} \quad \frac{x_m}{x_g}=\exp\left(-\ln^2\sigma_g\right)$$

Finally, the mode of log-normal distribution is

$$x_m=x_g\cdot\exp\left(-\ln^2\sigma_g\right) \qquad (1.34)$$

To derive an expression for the ***median*** size, the following equation should be solved for $x=x_{50}$

$$D(z')=\frac{1}{2}\left(1+\text{erf}(z')\right)=0.5, \text{where } z'=\frac{\ln x_{50}-\ln x_g}{\sqrt{2}\ln\sigma_g}$$

Taking into account that $\text{erf}(x)=0$ for $x=0$, the median size could be found from

$$z'=\frac{\ln x_{50}-\ln x_g}{\sqrt{2}\ln\sigma_g}=0 \quad \text{or} \quad \ln x_{50}-\ln x_g=0$$

Finally, the median size of the log-normal distribution is equal to the geometric mean

$$x_{50}=x_g \qquad (1.35)$$

Properties of log-normal distribution function are summarized in Table 11.

Table 11: Properties of log-normal distribution function.

Frequency distribution	$f(x) = \dfrac{1}{x\sqrt{2\pi}\ln\sigma_g}\exp\left(-\dfrac{1}{2}\left(\dfrac{\ln x - \ln x_g}{\ln\sigma_g}\right)^2\right)$
Domain, x	$(0, +\infty)$
Cumulative distribution	$D(z') = \dfrac{1}{2}(1 + \mathrm{erf}(z'))$
Dimensionless size, z'	$z' = \dfrac{\ln x - \ln x_g}{\sqrt{2}\ln\sigma_g}$
Linear form	$Y = aX + b,$
	where $X = \mathrm{erf}^{-1}(2D-1)$, $Y = \ln x$, $a = \sqrt{2}\ln\sigma_g$, $b = \ln x_g$
Mean size, $\overline{x}$	$x_g \exp\left(\dfrac{1}{2}\ln^2\sigma_g\right)$
Mode size, x_m	$x_g \exp\left(-\ln^2\sigma_g\right)$
Median size, x_{50}	x_g
Standard deviation, σ_g	$\sigma_g = x_{84}/x_{50} = x_{50}/x_{16} = \sqrt{(x_{84}/x_{16})}$
Coefficient of variation	$\sqrt{\exp\left(\ln^2\sigma_g\right) - 1}$
Moments	$m_j = x_g^j \exp\left(\dfrac{1}{2}j^2\ln^2\sigma_g\right)$

1.4.3. Rosin-Rammler distribution

In 1933 Rosin and Rammler (J. Inst. Fuel 7, 29, 1933) introduced an empirical distribution for description of particle sizes, which they obtained from the data describing the crushing of coal and other materials. In 1939 Weibull (Weibull W., J. Applied Mechanics, 18, 293, 1951) applied the same distribution to describe the life length of materials under fatigue and fracture loads.

The cumulative oversize distribution is

$$R(x) = 100 \cdot \exp\left\{-\left(\frac{x}{x_e}\right)^n\right\}, \tag{1.36}$$

where $x_e > 0$ is the scale parameter and $n > 0$ is the shape parameter. The scale parameter is the characteristic value of the distribution and the shape parameter controls the width of the frequency distribution of sizes with the higher value corresponding to the narrower distribution, as shown in Figs. 17 and 18.

Rearranging Eq. (1.36) as

$$\frac{100}{R} = \exp\left\{\left(\frac{x}{x_e}\right)^n\right\},$$

and taking natural logarithm from the left and right sides of above equation gives

$$\ln\left(\frac{100}{R}\right) = \left(\frac{x}{x_e}\right)^n \tag{1.37}$$

Taking again logarithm from Eq. (1.37) results in

$$\ln\left(\ln\left(\frac{100}{R}\right)\right) = n \cdot \ln x - n \cdot \ln x_e \tag{1.38}$$

Eq. (1.38) is a linear equation of the form

$$Y = a \cdot X + b, \tag{1.39}$$

where $Y = \ln\left(\ln\left(\frac{100}{R}\right)\right)$ and $X = \ln x$. The slope is $a = n$ and the intercept is $b = -n \cdot \ln x_e$, as illustrated in Fig. 19.

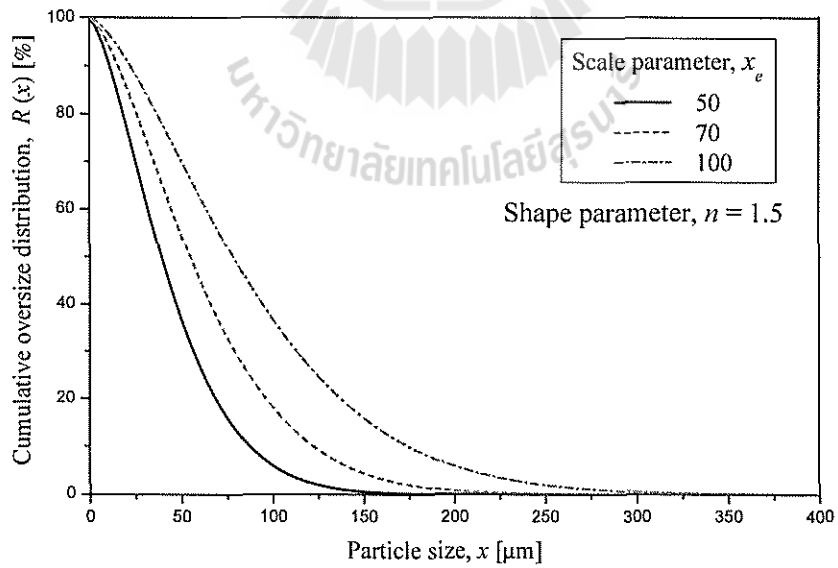

Figure 17: Illustration of Rosin-Rammler distribution for various scale parameters.

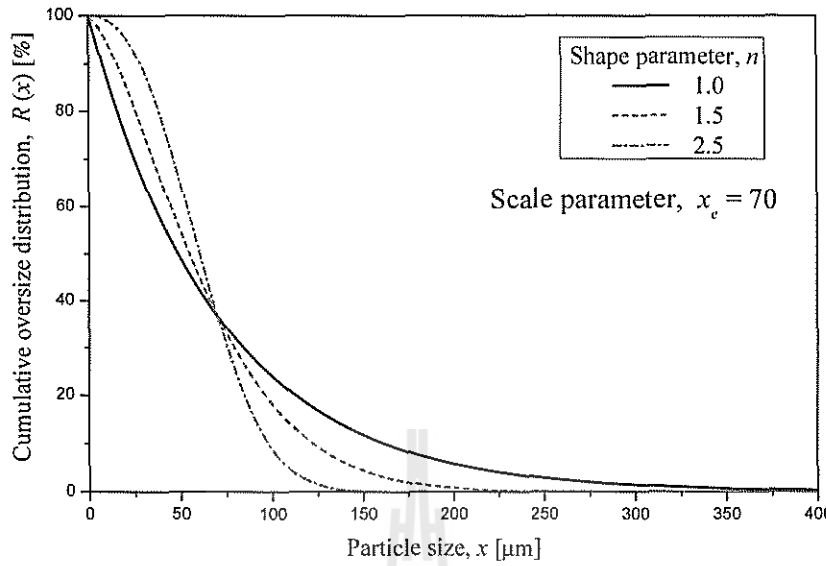

Figure 18: Illustration of Rosin-Rammler distribution for various shape parameters.

An alternative form of Rosin-Rammler distribution is

$$R(x) = 100 \times 10^{-ax^b}, \tag{1.40}$$

where a and b are parameters.

Taking the logarithm of Eq. (1.40) results in

$$2 - \log_{10} R = ax^b \tag{1.41}$$

Rearranging Eq. (1.41) and taking logarithm again yields

$$\log_{10}(2 - \log_{10} R) = \log_{10} a + b \cdot \log_{10} x \tag{1.42}$$

Eq. (1.38) is a linear equation of the form

$$Y = a_1 \cdot X + b_1, \tag{1.43}$$

where $Y = \log_{10}(2 - \log_{10} R)$ and $X = \log_{10} x$. The slope is $a_1 = b$ and the intercept is $b_1 = \log_{10} a$.

Properties of Rosin-Rammler distribution function

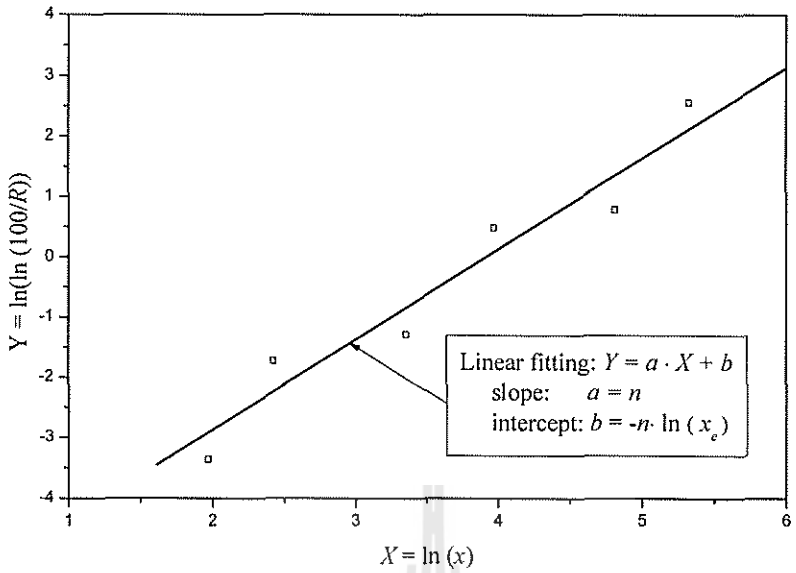

Figure 19: Linear form of Rosin-Rammler distribution.

The ***mode*** size is derived by solving the following equation

$$\left.\frac{df(x)}{dx}\right|_{x=x_m} = 0 \tag{1.44}$$

Taking the derivative of the frequency distribution defined as

$$f(x) = \frac{n}{x_e}\left(\frac{x}{x_e}\right)^{n-1} \exp\left\{-\left(\frac{x}{x_e}\right)^n\right\}$$

results in

$$\begin{aligned}\frac{df(x)}{dx} =& (n-1)\frac{n}{x_e^n}x^{n-2}\exp\left\{-\left(\frac{x}{x_e}\right)^n\right\} + \frac{n}{x_e^n}x^{n-1}\left(-\left(\frac{1}{x_e}\right)^n nx^{n-1}\right)\exp\left\{-\left(\frac{x}{x_e}\right)^n\right\} \\ =& \exp\left\{-\left(\frac{x}{x_e}\right)^n\right\}\left(\frac{(n-1)n}{x_e^n}x^{n-2} - \frac{n^2}{x_e^{2n}}x^{2n-2}\right)\end{aligned}$$

From Eq. (1.44) it follows that

$$\frac{(n-1)n}{x_e^n}x^{n-2} - \frac{n^2}{x_e^{2n}}x_m^{2n-2} = 0$$

Therefore,

$$\frac{n-1}{n}x_e^n = x_m^n$$

Finally, the mode of the Rosin-Rammler distribution is

$$x_m = x_e \left(1 - \frac{1}{n}\right)^{(1/n)} \tag{1.45}$$

The ***median*** size is derived from equation $R(x_{50}) = 50$. Rearranging Eq. (1.36) as

$$\frac{100}{50} = 2 = \exp\left[\left(\frac{x_{50}}{x_e}\right)^n\right]$$

and taking logarithm results in

$$\ln 2 = \left(\frac{x_{50}}{x_e}\right)^n$$

Finally, the median of the Rosin-Rammler distribution is

$$x_{50} = x_e(\ln 2)^{(1/n)} \tag{1.46}$$

Properties of Rosin and Rammler distribution function are summarized in Table 12.

1.4.4. Beta distribution

A modified beta distribution is defined as [5]

$$f(x) = \frac{\Gamma(m(a+1)+2)}{\Gamma(am+1)\Gamma(m+1)} x^{am}(1-x)^m \tag{1.47}$$

or

$$f(x) = \frac{x^{am}(1-x)^m}{\int_0^1 x^{am}(1-x)^m dx} \tag{1.48}$$

where x is the normalized size $x = (x - x_{min})/(x_{max} - x_{min})$ such as $0 \leq x \leq 1$.

The characteristic parameters of this distribution are

$$\text{mode: } x_m = \frac{a}{a+1}$$

$$\text{mean: } \overline{x} = \frac{am+1}{(a+1)m+2}$$

$$\text{variance: } \sigma^2 = \frac{(am+1)(m+1)}{((a+1)m+2)^2((a+1)m+3)}$$

1.5. Methods of particle size measurement

Methods used for measurement of particle size distribution can be classified as follows [6, 7]:

1. Direct dimensional measurement

Table 12: Properties of Rosin-Rammler distribution function.

Frequency distribution	$f(x) = ab \ln 10 x^{b-1} 10^{2-ax^b}$
Domain, x	$(0, +\infty)$
Cumulative distribution	$R(x) = 100 \cdot \exp\left\{-\left(\frac{x}{x_e}\right)^n\right\}$
Dimensionless size, z	$z = \left(\frac{x}{x_e}\right)^n$
Linear form	$Y = aX + b,$ where $X = \ln x, Y = \ln\left(\ln\left(\frac{100}{R}\right)\right), a = n, b = -n \cdot \ln x_e$
Mean size, $\overline{x}$	$x_e \Gamma\left(1 + \frac{1}{n}\right)$
Mode size, x_m	$\left(\frac{n}{x_e}\right)^{-1/n}$
Median size, x_{50}	$x_e (\ln 2)^{1/n}$
Coefficient of variation	$\sqrt{\left(\Gamma\left[\frac{n+2}{n}\right] / \Gamma^2\left[\frac{n+2}{n}\right] - 1\right)}$
Moments	$m_j = \left(\frac{1}{x_e}\right)^{(j/n)} \Gamma\left[\frac{n+j}{n}\right]$

Here, Γ is the gamma function of x defined as $\Gamma(n) = \int_0^\infty t^{n-1} e^{-t} dt, \quad n > 0.$

- Sieving
- Microscopy

2. Transport measurements
   - Sedimentation
3. Rapid physical response measurements
   - Electrical sensing zone
   - Light scattering and diffraction
   - Photon correlation spectroscopy
4. Surface area and porosity
   - Permeatry

- Gas adsorption

1.5.1. Sieving

The main features of the sieving method are summarized in Table 13.

Table 13: Features of sieving method.

Principle	Passage of particles through sieve
Size range	from 5μm to 125mm
Type of diameter	Equivalent sieve diameter
Type of distribution	Mass(volume)

1.5.2. Microscopy

The main features of the microscopy method are summarized in Table 14.

Table 14: Features of microscopy method.

Principle	Analysis of images
Size range	depends on magnification
Type of diameter	Often area based. but depends on choice
Type of distribution	Number

1.5.3. Sedimentation

Interaction between particles and fluid

- Settling of a single sphere under a gravitational force

  Consider a spherical particle of diameter x and density ρ_p settling freely in a fluid of density ρ_f and viscosity μ_f due to the gravity force. Here it is assumed that the particles is a rigid sphere and there is no multiparticle and wall effects.

  The forces of gravity F_g, buoyancy F_b and drag F_d act on the particle. The drag force is the resistive force exerted on the particle by fluid if a difference in velocity exists between a particle and fluid surrounding it. The drag force acting upwards is

$$F_d = C_D \cdot A_D \cdot \frac{\rho_f v^2}{2}$$

  where C_D is the drag coefficient, A_D is the projected particle area, $A_D = \pi x^2/4$, and v is the relative velocity. If fluid is stagnant, $v = v_p$, where v_p is the particle velocity.

The gravity force acting downwards is

$$F_g = m_p \cdot g = \rho_p \cdot \left(\frac{\pi x^3}{6}\right) \cdot g,$$

where m_p is the mass of the particle.

The buoyancy force acting upwards equals the weight of the fluid displaced

$$F_b = m_f \cdot g = \rho_f \cdot \left(\frac{\pi x^3}{6}\right) \cdot g$$

where m_f is the mass of fluid displaced.

The acceleration force F_a is

$$F_a = m_p \cdot \frac{dv_p}{dt} = \rho_p \cdot \left(\frac{\pi x^3}{6}\right) \cdot \frac{dv_p}{dt},$$

The resulting force balance is

$$\rho_p \cdot \left(\frac{\pi x^3}{6}\right) \cdot \frac{dv_p}{dt} = \rho_p \cdot \left(\frac{\pi x^3}{6}\right) \cdot g - \rho_f \cdot \left(\frac{\pi x^3}{6}\right) \cdot g - C_D \cdot A_D \cdot \frac{\rho_f v_p^2}{2} \tag{1.49}$$

Rewriting Eq. (1.49) in terms of particle acceleration yields

$$\frac{dv_p}{dt} = \frac{\rho_p - \rho_f}{\rho_p} \cdot g - \frac{3\rho_f}{4\rho_p} \cdot C_D \cdot \frac{v_p^2}{x} \tag{1.50}$$

Small particles quickly reach a constant ***terminal*** velocity v_{St} derived from Eq. (1.50) by equating $dv/dt = 0$ as

$$v_{St} = \sqrt{\frac{4(\rho_p - \rho_f)gx}{3\rho_f C_D}} \tag{1.51}$$

The drag coefficient is a function of a particle Reynolds number, $Re = \frac{\rho_f v_p x}{\mu}$. In the laminar flow region, for $Re \to 0$ the drag coefficient is $C_D = 24/Re$. Then, the drag force is $F_D = 3\pi x \mu v_p$.

Finally, the relationship between the particle diameter and its Stokes velocity is

$$x = \sqrt{\frac{18\mu v_{St}}{(\rho_p - \rho_f)g}} \tag{1.52}$$

where v_{St} is the particle terminal velocity in the laminar flow region.

- Settling of a single sphere under a centrifugal force

  The force balance for a spherical particle settling in a centrifugal field in the laminar flow region is

$$\left(\frac{\pi d_{St}^3}{6}\right)\cdot(\rho_p-\rho_f)\cdot\frac{d^2r}{dt^2}=\left(\frac{\pi d_{St}^3}{6}\right)\cdot(\rho_p-\rho_f)\cdot w^2r-3\pi\mu d_{St}\frac{dr}{dt}, \tag{1.53}$$

  where r is distance from the axis to the particle, dr/dt is the outward velocity of the particle, d_{St} is the Stokes diameter of the particle and w is the speed of rotation in radians per second. At the terminal velocity $d^2r/dt^2=0$, and the velocity is a function of radius as

$$\frac{dr}{dt}=\frac{(\rho_p-\rho_f)d_{St}^2w^2}{18\mu}\cdot r \tag{1.54}$$

  Rewriting Eq. (1.54) in integral form as

$$\int_{r_s}^{r}\frac{dr}{r}=\int_0^t\frac{(\rho_p-\rho_f)d_{St}^2w^2}{18\mu}dt$$

  and integrating yields

$$\ln\left(\frac{r}{r_s}\right)=\left(\frac{(\rho_p-\rho_f)d_{St}^2w^2}{18\mu}\right)t$$

  where t is the time for a particle of Stokes diameter d_{St} to settle from the surface of the liquid at radius r_s to measurement radius r.

  Finally, the Stokes diameter in the centrifugal field is

$$d_{St}=\sqrt{\frac{18\mu\ln(r/r_s)}{(\rho_p-\rho_f)w^2t}}, \tag{1.55}$$

The main features of the sedimentation method are summarized in Table 15.

Table 15: Features of sedimentation method.

Principle	Particle dispersed in non-aqueous and aqueous media in gravitational or centrifugal field
Size range	Gravity: $300-10\mu$m, Centrifugal: 10μm - 1 nm
Type of diameter	Stokes
Type of distribution	Volume

1.5.4. Electrozone sensing

The schematic illustration of electrical sensing zone device is shown in Fig. 20 and the main features of the method are summarized in Table 16 .

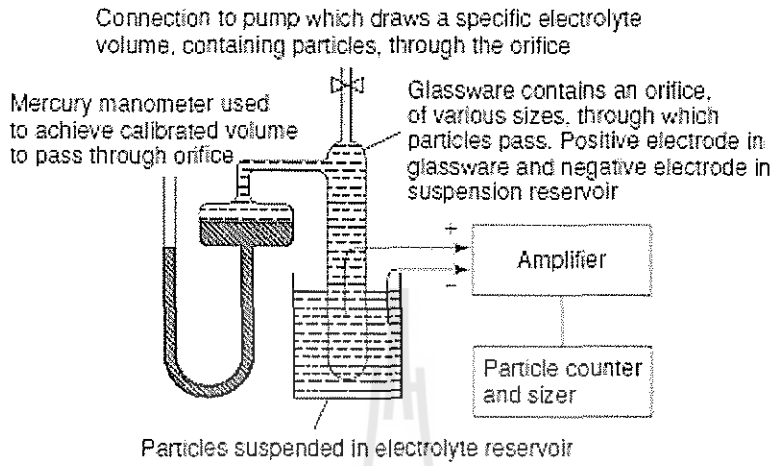

Figure 20: Illustration of electrical sensing zone measurement.

Table 16: Features of electrical sensing zone method.

Principle	Particle dispersed in electrolyte pass through orifice
Size range	from 1000μm to 0.5μm
Type of diameter	Volume equivalent
Type of distribution	Number

1.5.5. Laser diffraction

The schematic illustration of laser light scattering device is shown in Fig. 21 and the main features of the method are summarized in Table 17 .

Table 17: Features of laser light scattering method.

Principle	Model-based distribution calculation from angular pattern of scattered light intensity
Size range	from 3000μm to 0.1μm
Type of diameter	Equivalent light scatter diameter
Type of distribution	Volume

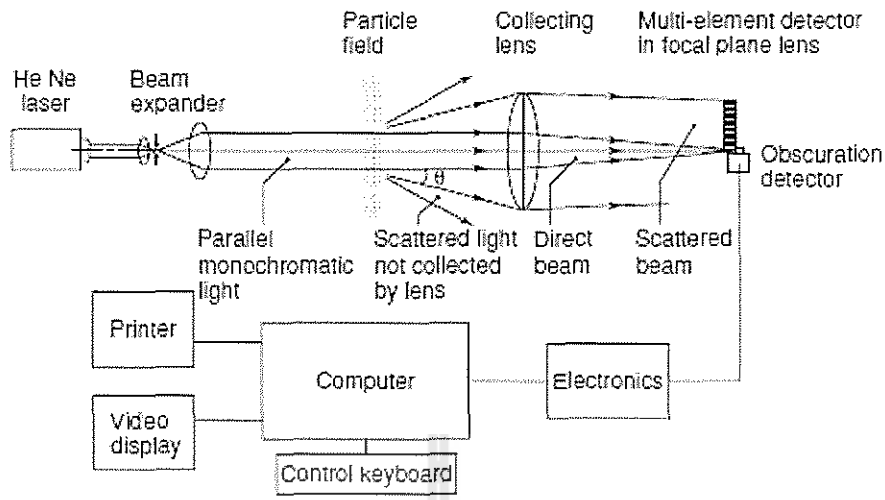

Figure 21: Illustration of laser light scattering measurement.

2. Particle shape

The shape of a particle can be characterized on various scales, such as macro, meso and microscales [7, 2].

- Macroscale: the 3D form of particle, for example the ratio of main three dimensions
- Mesoscale: the roundness and angularity of particle outline
- Microscale: the smoothness of particle surface

The qualitative and quantitative descriptions of particle shape on macroscale level are frequently based on the following definition of the thickness, breadth and length:

1. Thickness (T) is the minimum distance between two parallel planes which are tangential to opposite surfaces of the particle with one plane being the plane of maximum stability
2. Breadth (B) is the maximum distance between two parallel planes which are perpendicular to the planes defining the thickness and are tangential to opposite sides of particle
3. Length (L) is the distance between two parallel plane which are perpendicular to the planes defining thickness and breadth and are tangential to opposite sides of the particle.

Figure 22 illustrates the definition of thickness, breadth and length.

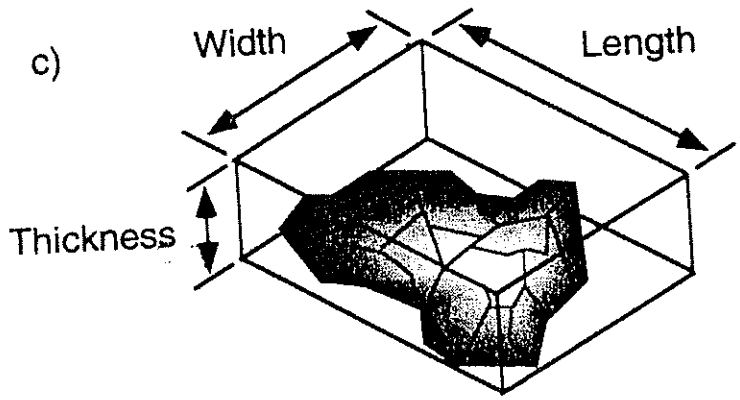

Figure 22: Illustration of thickness, width and length of particle.

The qualitative description of particle shape is based on visual observation and classification by comparison with standard samples. Frequently used definitions are summarized bellow and are illustrated in Fig. 23.

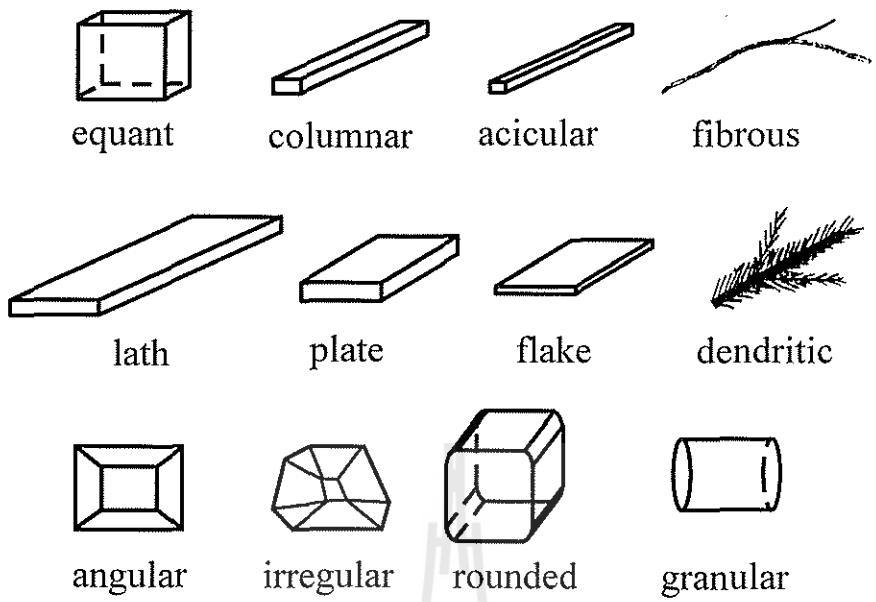

Figure 23: Qualitative description of particle shapes.

Equant	particle with regular shape of similar length, breadth and thickness (L:B:T=1:1:1), including cubes and spheres
Columnar	long, thin particle (L:B:T=(3-10): 1: 1)
Acicular	slender, needle-shape particle of similar breadth and thickness, which are much smaller than length (L:B:T=(10-100): 1: 1)
Fibrous	threadlike particle, which has a very large length/diameter ratio (L:B:T=(>100): 1: 1)
Lath	long, thin and blade-like particle (L:B:T=(10-50):(2-5): 1)
Plate	flat particle of similar length and breadth but with greater thickness than flake (L:B:T= 1: 1:(0.1-0.6))
Flake	thin, flat particle of similar length and breadth (L:B:T= 1: 1:(<0.1))
Dendritic	particle shape of pine tree structure
Angular	particle shape showing sharp edges or having approximately polyhedral shape
Irregular	particle of about equal dimensions lacking any symmetry
Rounded	particle of any shape, usually having similar length, breadth and thickness, with rounded edges
Granular	particle shape is irregular but has about equal dimensions $(\mathrm{L} : \mathrm{B} : \mathrm{T} = \sim 1 : \sim 1 : (0.5 - 2))$

Some quantitative descriptors are summarized below.

- Heywood ratios
  - Elongation ratio $n = L/B$
  - Flakiness ratio $m = B/T$
- Hausner shape descriptors
  - Elongation factor = a/b
  - Bulkiness = $\dfrac{A}{a \times b}$
  - Surface factor = $\dfrac{C^2}{12.6A}$

  where A is the projected area of a particle, C is the actual perimeter of the particle, a and b are the length of the sides of the minimum area embracing rectangle
- Wadell shape factor
  - Sphericity $\psi_{\mathrm{W}} = \dfrac{\text{Surface area of a sphere having the same volume as the particle}}{\text{Surface area of the particle}}$

    $$\psi_{\mathrm{W}} = \left(\frac{d_v}{d_s}\right)^2$$

  - Coefficient of angularity = $\dfrac{1}{\text{sphericity}}$
- Circularity

  Circularity = $\dfrac{4\pi \times A}{P^2} = \dfrac{d_a}{d_c}$,

  where A is the projected area of particle outline, P is the perimeter of particle, d_a is the diameter of circle having a same projected area as the particle in stable orientation, d_c is the diameter of circle having a same perimeter as the projected outline of the particle.

  Circularity is equal to 1 for a circle and circularity decreases for non-spherical particles.

2.1. Particle shape characterization using Fourier analysis of particle outline in radial coordinates

$$R(\theta) = a_0 + \sum_{j=1}^{\infty} \{a_j \cos(j\theta) + b_j \sin(j\theta)\} = R_{r,av} + \sum_{j=1}^{\infty} A_j \cos\{(j\theta) - \alpha_j\}$$

$$a_j = \int R(\theta) \cos(j\theta)\, d\theta/\pi$$

$$b_j = \int R(\theta) \sin(j\theta)\, d\theta/\pi$$

$$A_j = \sqrt{(a_j{}^2 + b_j{}^2)}$$

$$\alpha_j = \tan^{-1}(b_j/a_j)$$

$$R_{r,av} = \frac{1}{2\pi}\int_0^{2\pi} R(\theta)d\theta = C/2\pi = a_0,$$

where C is the perimeter.

$$S = \frac{1}{2}\int_0^{2\pi} R(\theta)^2 d\theta = \pi\left\{a_0{}^2 + \frac{1}{2}\sum_{j=1}^{\infty}\left(a_j{}^2 + b_j{}^2\right)\right\} = \pi\left[R_{r,av}{}^2 + \frac{1}{2}\sum_{j=1}^{\infty} A_j{}^2\right]$$

2.2. Particle shape characterization using Fourier analysis of particle outline in rectangular coordinates

A set of coordinate points is sampled along the particle outline $(Pd_x(n), Pd_y(n), n = 0, \cdots, N-1)$ of the perimeter corresponding to every incremental step angle θ_d. Assuming that the particle perimeter, L, corresponds to 2π, the step angle become

$$\theta_{d,i} = \frac{2\pi j}{N}, j = 0, 1, \cdots, N-1, 0 \leq \theta_{d,i} < 2\pi \tag{2.1}$$

Here $Pd_x(0), Pd_y(0)$ are the coordinates of the starting point on particle outline.

Then, the Fourier transformations of functions $x(\theta_d)$ and $y(\theta_d)$ can be independently written as

$$x(\theta_{d,i}) = \frac{a_x(0)}{2} + \sum_{j=1}^{M}\{a_x(j)\cos(j\theta_{d,i}) + b_x(j)\sin(j\theta_{d,i})\} \tag{2.2}$$

$$y(\theta_{d,i}) = \frac{a_y(0)}{2} + \sum_{j=1}^{M}\{a_y(j)\cos(j\theta_{d,i}) + b_y(j)\sin(j\theta_{d,i})\} \tag{2.3}$$

The Fourier coefficients for the j-th harmonic of the x function are

$$a_x(j) = \frac{2}{N}\sum_{i=0}^{N-1} P_{d,x}(i)\cos\left(\frac{2\pi ij}{N}\right)$$

$$b_x(j) = \frac{2}{N}\sum_{i=0}^{N-1} P_{d,x}(i)\sin\left(\frac{2\pi ij}{N}\right)$$

and y function

$$a_y(j) = \frac{2}{N}\sum_{i=0}^{N-1} P_{d,y}(i)\cos\left(\frac{2\pi ij}{N}\right)$$

$$b_y(j) = \frac{2}{N}\sum_{i=0}^{N-1} P_{d,y}(i)\sin\left(\frac{2\pi ij}{N}\right)$$

Using only the first harmonic, the ellipse approximated the particle outline is given with coordinates

$$x(\theta_{d,i}) = a_x(1)\cos(\theta_{d,i}) + b_x(1)\sin(\theta_{d,i})$$

$$y(\theta_{d,i}) = a_y(1)\cos(\theta_{d,i}) + b_y(1)\sin(\theta_{d,i})$$

$$\frac{X^2}{(BC-AD)^2/(C^2+D^2)} + \frac{Y^2}{(BC-AD)^2/(A^2+B^2)} = 1$$

$$\begin{aligned} A &= a_x(1)\cos\beta + a_y(1)\sin\beta \\ B &= b_x(1)\cos\beta + b_y(1)\sin\beta \\ C &= -a_x(1)\sin\beta + a_y(1)\cos\beta \\ D &= -b_x(1)\sin\beta + b_y(1)\cos\beta \end{aligned}$$

$$\beta = -\frac{1}{2}\tan^{-1}\left\{\frac{2(a_x(1)a_y(1)+b_x(1)b_y(1))}{a_y(1)^2+b_y(1)^2-a_x(1)^2-b_x(1)^2}\right\}$$

$$r_{el,l} = \sqrt{\frac{(BC-AD)^2}{C^2+D^2}}$$

$$r_{el,s} = \sqrt{\frac{(BC-AD)^2}{A^2+B^2}}$$

The shape index is defined as

$$K_{ael} = \frac{r_{el,s}}{r_{el,l}} \tag{2.4}$$

The coefficient of variation of distance from centroid of particle outline is

$$C_{v,rs} = \frac{\sqrt{\frac{1}{N}\sum\left(R(\theta_{el}) - r_{el}\right)^2}}{r_c} \tag{2.5}$$

where $R(\theta_{el})$ is the radius of outline point, $R(\theta_{el}) = \sqrt{{P_{d,x}}^2 + {P_{d,y}}^2}$, and r_{el} is the radius of equivalent ellipse.

$$r_{el} = \sqrt{\frac{r_{el,l}^2 r_{el,s}^2}{r_{el,l}^2 - (r_{el,l}^2 - r_{el,s}^2)\cos^2\theta_{el}}}$$

The radius of equivalent circle to ellipse perimeter is

$$r_c = \frac{2r_{el,l}}{\pi}\int_0^{\frac{\pi}{2}} \sqrt{1 - \left(1 - \frac{r_{el,s}^2}{r_{el,l}^2}\right)\sin^2\theta_{el}}\, d\theta_{el} \tag{2.6}$$

3. Particle and powder bulk densities

3.1. Particle density

Particle density, ρ_p is defined as the total mass of the particle divided by its total volume. Depending on the definition of the particle total volume, the following densities are used [8]

- True particle density, $\rho_{p,t}$

  The particle total volume excludes both open and closed pores as shown in Fig. 24.

  This is the density of the solid material from which the particle is made.

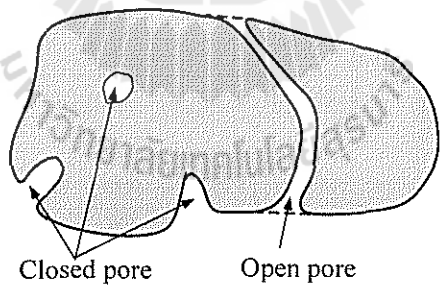

Figure 24: Illustration of density definitions.

- Apparent particle density, $\rho_{p,a}$

  The particle total volume excludes open pores but includes closed pores.

  The apparent particle density is usually measured by the fluid displacement method.

  – Liquid pyknometry

The calibrated 50 ml bottle shown in Fig. (25) is used for measurements. The measurement procedure is as follows

(a) Weight empty bottle, m_0

(b) Weight bottle filled with liquid, m_l

(c) Fill about 1/3 of empty bottle with particles and weight, m_s

(d) Add liquid up to almost full

(e) Remove bubbles by evacuation, ultrasound or boiling

(f) Top up liquid and weight, m_{sl}

The apparent density can be calculated as

$$\rho_{p,a} = \frac{\text{Mass of particles}}{\text{Volume total of particles}} = \frac{m_s - m_0}{V_{\text{empty bottle}} - V_{\text{liquid added in a bottle with particles}}}$$

$$\rho_{p,a} = \frac{m_s - m_0}{\frac{m_l - m_0}{\rho_l} - \frac{m_{sl} - m_s}{\rho_l}}$$

$$\rho_{p,a} = \frac{(m_s - m_0)\rho_l}{(m_l - m_0) - (m_{sl} - m_s)}$$

– Gas pyknometry

The schematics of the gas pyknometer is shown in Fig. 26.

At ambient pressure P_a the state of the system is described as

$$P_a V_C = nRT_a, \tag{3.1}$$

where n is the number of gas moles occupying volume V_C at P_a.

When a sample of volume V_p is placed in the sample cell, Eq. (3.1) can be rewritten as

$$P_a(V_C - V_p) = n_1 RT_a, \tag{3.2}$$

where n_1 is the number of gas moles in the sample cell at P_a.

When the system is pressurized to P_2, it is described by

$$P_2(V_C - V_p) = n_2 RT_a, \tag{3.3}$$

where n_2 is the number of gas moles in the sample cell at P_2.

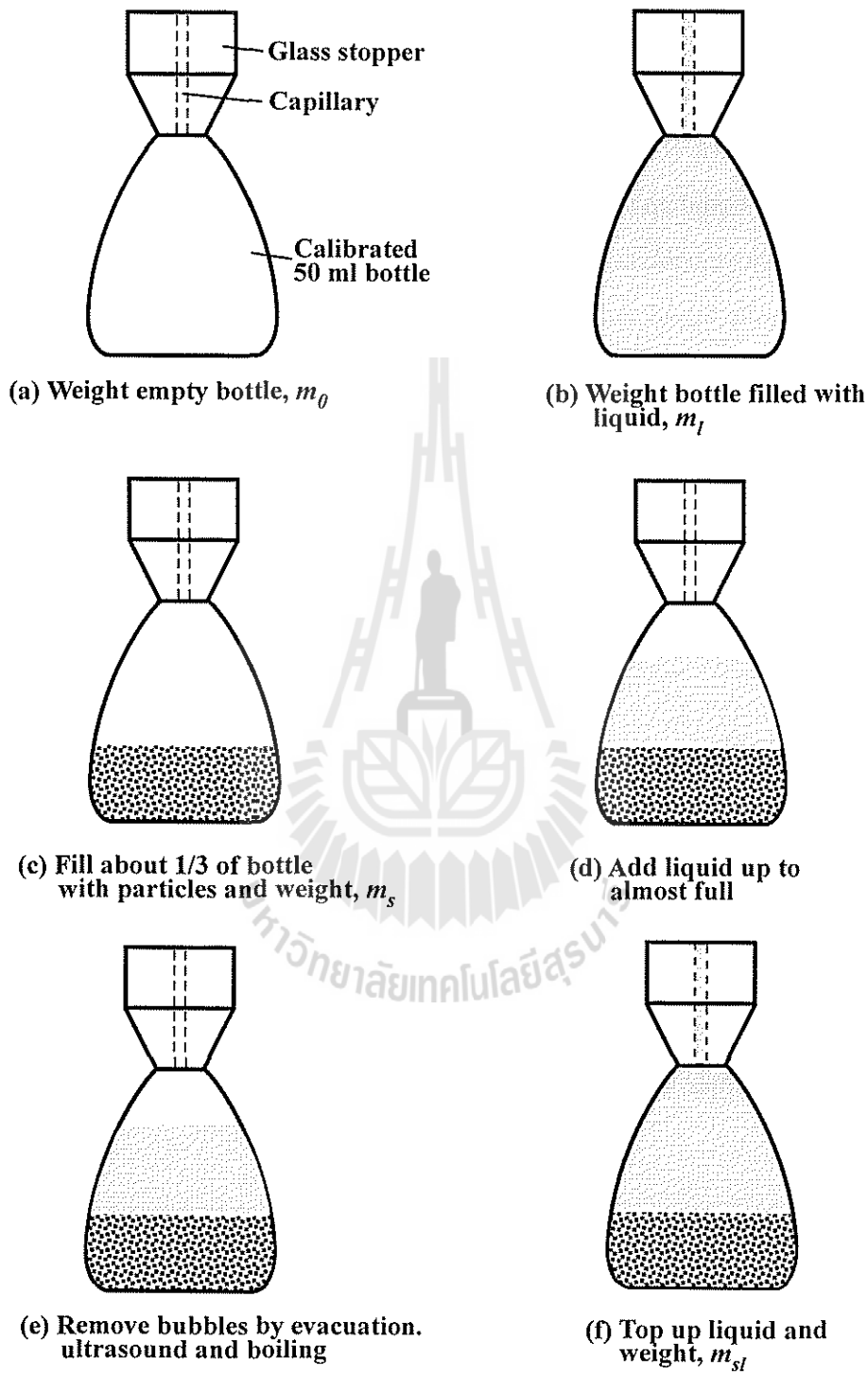

Figure 25: Procedure of measurement of apparent particle density with liquid pyknometer.

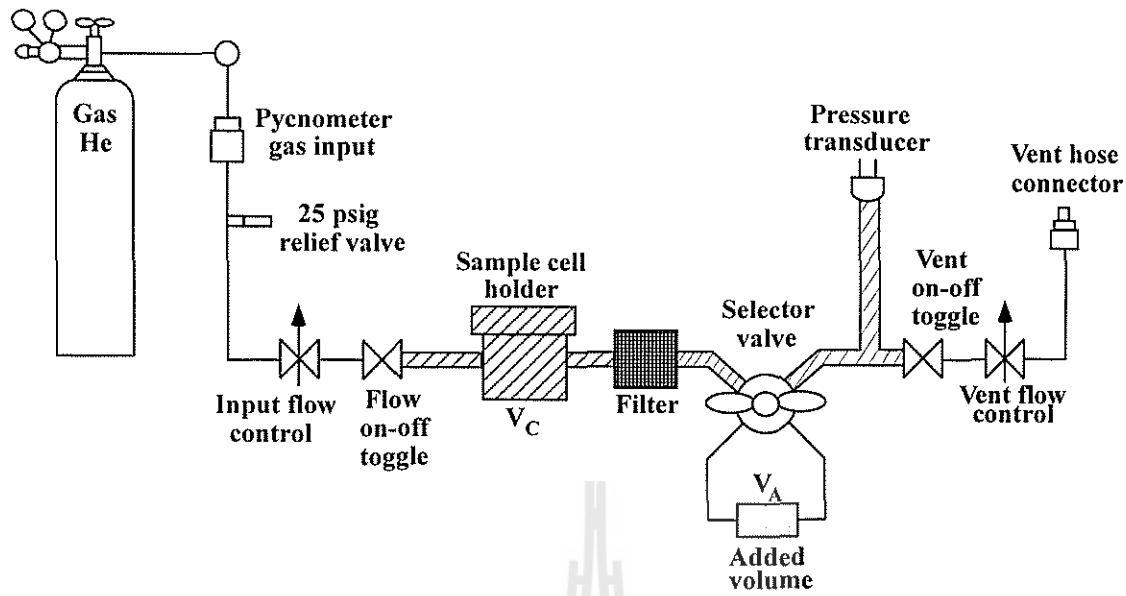

Figure 26: Schematics of gas pyknometer.

After switching the selector valve, the volume V_A is added to the system and the pressure decreases to P_1. Then,

$$P_1(V_C - V_p + V_A) = n_2 RT_a + n_A RT_a, \tag{3.4}$$

where n_A is the number of gas moles in the added volume at P_a.

Substituting $P_a V_A$ for $n_A RT_a$ into Eq. (3.4) and combining with Eq. (3.3) results in

$$P_1(V_C - V_p + V_A) = P_2(V_C - V_p) + P_a V_A \tag{3.5}$$

Simplifying Eq. (3.5) yields

$$V_p(P_1 - P_2) = V_C(P_1 - P_2) + V_A(P_1 - P_a)$$

Solving the above equation for V_p results in

$$V_p = V_C + V_A \frac{P_1 - P_a}{P_1 - P_2} \tag{3.6}$$

Assuming $P_a = 0$, Eq. (3.6) becomes

$$V_p = V_C + V_A \frac{P_1}{P_1 - P_2} = V_C + \frac{V_A}{1 - \frac{P_2}{P_1}} \tag{3.7}$$

To measure V_A and V_c, two experiments are carried out with empty sample cell

$$V_p = 0 = V_C + \frac{V_A}{1 - \frac{P_2}{P_1}} \tag{3.8}$$

and with calibrated spheres of known volume,V_{cal}, in the sample cell

$$V_p = V_{cal} = V_C + \frac{V_A}{1 - \frac{P_2'}{P_1'}} \tag{3.9}$$

From Eq. (3.8)

$$V_C = \frac{V_A}{\frac{P_2}{P_1} - 1} \tag{3.10}$$

Combining Eq. (3.10) with Eq. (3.9) results in

$$V_{cal} = V_A \left(\frac{1}{\frac{P_2}{P_1} - 1} - \frac{1}{\frac{P_2'}{P_1'} - 1} \right)$$

and V_A can be evaluated as

$$V_A = \frac{V_{cal}}{\left(\frac{1}{\frac{P_2}{P_1} - 1} - \frac{1}{\frac{P_2'}{P_1'} - 1} \right)} \tag{3.11}$$

Substitution of Eq. (3.11) into Eq. (3.10) gives

$$V_C = \frac{V_{cal}}{\frac{1}{\frac{P_2}{P_1}-1} - \frac{1}{\frac{P_2'}{P_1'}-1}} \cdot \frac{1}{\frac{P_2}{P_1}-1} = \frac{V_{cal}}{\left(1 - \frac{\frac{P_2}{P_1}-1}{\frac{P_2'}{P_1'}-1}\right)}$$

$$= \frac{V_{cal}}{\frac{P_2'}{P_1'} - \frac{P_2}{P_1}} \cdot \left(\frac{P_2'}{P_1'} - 1\right) = V_{cal} \frac{\frac{P_2' - P_1'}{P_1'}}{\frac{P_2'P_1 - P_2P_1'}{P_1'P_1}} = V_{cal} \frac{(P_2' - P_1')P_1'P_1}{P_1'(P_2'P_1 - P_2P_1')}$$

Finally, V_C is

$$V_C = V_{cal} \frac{P_1 (P_2' - P_1')}{(P_2'P_1 - P_2P_1')} \tag{3.12}$$

- Effective particle density, $\rho_{p,e}$

  The particle total volume includes both open and closed pores.

  - Caking end point method
  - Bed voidage method
  - Bed pressure drop method

    This method is based on measurement of bed pressure drop as a function of gas velocity at two different voidages. The gas flow is assumed to be laminar.

    The bed is first fluidized and then gently settled to get a maximum voidage. The pressure drop is measured for at least four different velocities.

    The bed is then tapped to reach voidage as low as possible and the measurements repeated.

3.2. Powder bulk density

The powder bulk density, ρ_b, is defined as

$$\rho_b = \rho_p(1 - \epsilon) + \rho_a\epsilon, \tag{3.13}$$

where ρ_p is the particle density, ϵ is the bed voidage and ρ_a is the air density. As the air density is small comparative to the particle density, the second term on the right-hand side of Eq. (3.13) can be neglected and the powder bulk density becomes

$$\rho_b = \rho_p(1 - \epsilon) \tag{3.14}$$

There are various definitions of the powder bulk density depending on the state of compaction of powder.

- Aerated powder bulk density, $\rho_{b,a}$

  The aerated bulk density is defined as the bulk density after the powder has been aerated. It corresponds to the most loosely packed bed. Figure 27 illustrates the equipment for measurement of aerated powder density.

  The powder is poured through the vibrating sieve and allowed to fall a fixed height (25 cm) through the stationary chute into the cylindrical cup to fill it in 20 to 30 seconds.

- Poured powder bulk density, $\rho_{b,p}$

- Tapped powder bulk density, $\rho_{b,t}$

  The tapped density is a powder bulk density attained after mechanically tapping a container with the powder sample.

  The volume of the powder sample of known weight is measured until further changes is not observed.

  The mechanical tapping is achieved by raising the cylinder and allowing it drop a specified distance (3 mm) under its own mass using a cam at a rate of 250 taps per minute.

- Compacted powder bulk density, $\rho_{b,c}$

3.3. Flow properties from powder bulk densities

The Hausner ratio is defined as the ratio of tap density to aerated powder bulk density [9].

$$HR = \frac{\rho_{b,t}}{\rho_{b,a}} \tag{3.15}$$

The powder flowability can be characterized by the Hausner ratio as summarized in Table 18 .

Table 18: Hausner flow ratio (HR) of free flowing and cohesive powder.

HR<1.28	free flowing
1.28<HR<1.57	intermediate flowability
HR>1.57	cohesive

References

[1] Introduction to particle technology, Ed. Rhodes M., John Wiley & Sons, Second ed., 2008.

[2] Allen T. Particle size measurement. Vol. I. Powder sampling and particle size measurement, Kluwer, 1999.

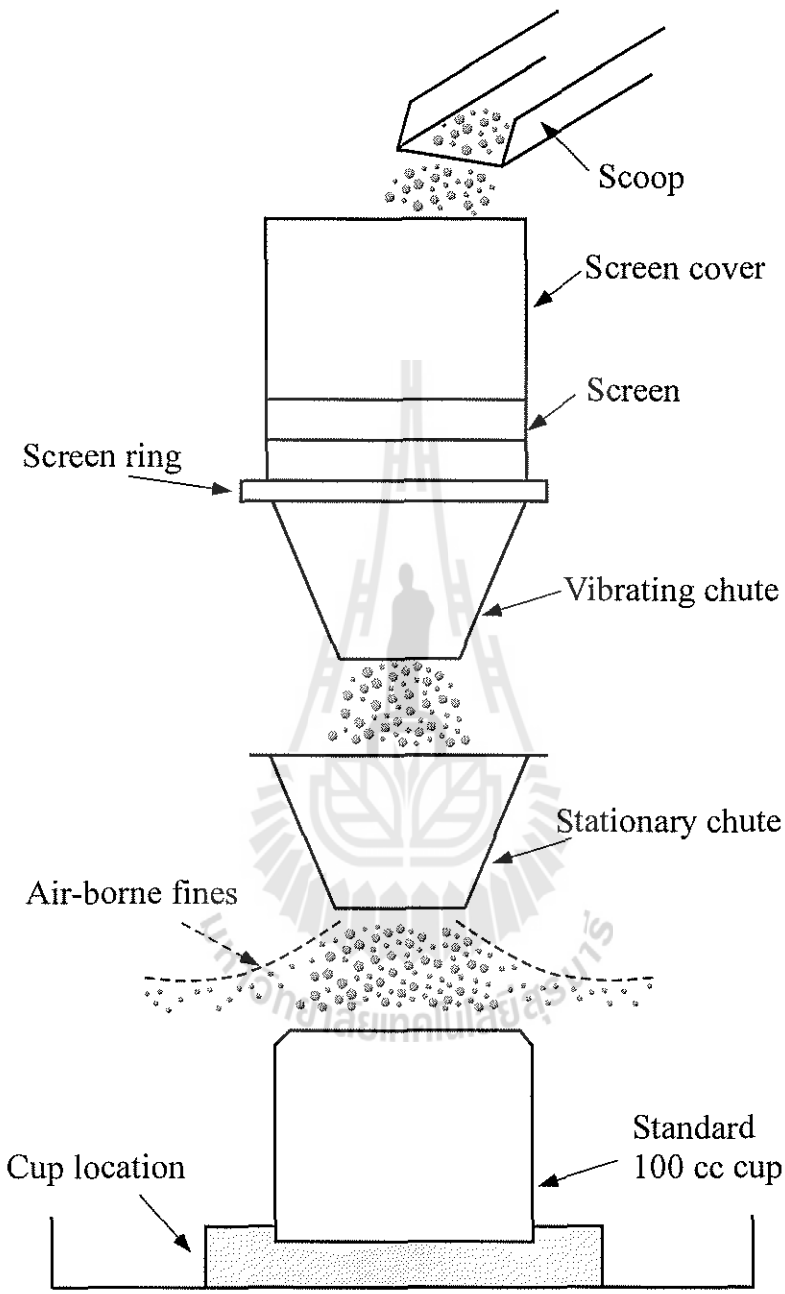

Figure 27: Schematic illustration of equipment for measurement of aerated gas density.

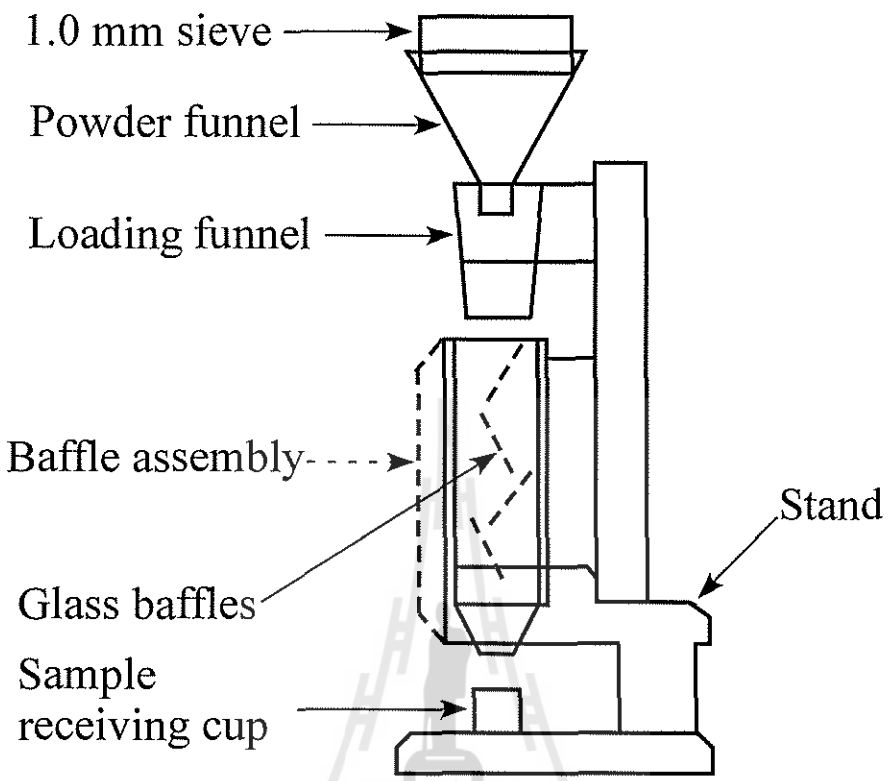

Figure 28: Schematic illustration of equipment for measurement of poured gas density.

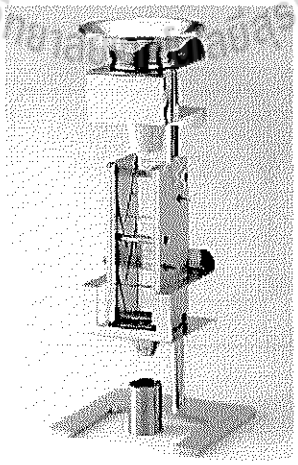

Figure 29: Equipment for measurement of poured gas density using Scott volumetric method.

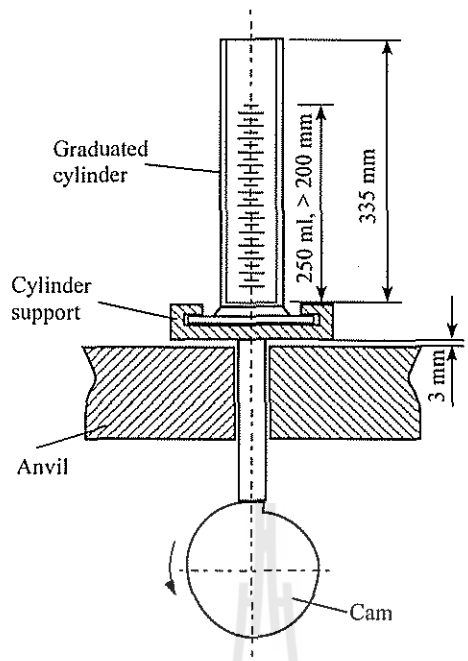

Figure 30: Equipment for measurement of tapped gas density.

[3] Washington C. Particle size analysis in pharmaceutics and other industries, Ellis Horwood, 1992.

[4] Hinds W.G. Aerosol technology, John Wiley & Sons, Second ed., 1999.

[5] Peleg, M. and M.D. Normand, "Simulation of size reduction and enlargement processes by a modified version of the beta distribution function," AICHE J., 32, 1928-1930 (1986).

[6] Merkus H.G. Particle size measurements, Springer, 2009.

[7] Characterization of bulk solids, Ed. McGlinchey D., Blackwell, 2005.

[8] Svarovsky L. Powder testing guide, Elsevier, 1987.

[9] Bulk solids handling, Ed. McGlinchey D.,, Blackwell, 2008.

Part II.
Fluid-Solid Separation

4. Efficiency of Particle Separation

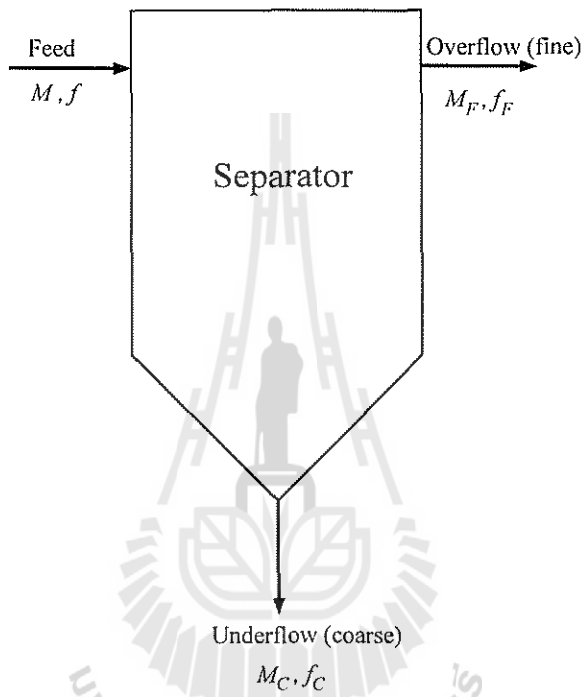

Figure 31: Notation of efficiency of particle separation.

The total mass balance of separator, assuming no accumulation of material in the equipment, is

$$M = M_C + M_F, \tag{4.1}$$

where M is the mass flow rate of the feed [kg · s^{-1}], M_C is the mass flow rate of the coarse material in the underflow [kg · s^{-1}] and M_F is the mass flow rate of the fine material in the overflow [kg · s^{-1}].

The total separation efficiency, E_T, is defined as

$$E_T = \frac{M_C}{M} = 1 - \frac{M_F}{M}. \tag{4.2}$$

The mass balance for any size fraction present in the feed, assuming no change in particle

size of the solids inside the separator, i.e. no agglomeration or comminution, is

$$M_{x_1 \sim x_2} = M_{C_{x_1 \sim x_2}} + M_{F_{x_1 \sim x_2}}. \tag{4.3}$$

The mass balance for each particle size x present in the feed is

$$M_x = M_{C_x} + M_{F_x} \tag{4.4}$$

or using the frequency distribution of particle sizes $f(x)$

$$Mf(x)dx = M_C f_C(x)dx + M_F f_F(x)dx \tag{4.5}$$

or using the cumulative distribution of particle sizes $F(x)$

$$MdF(x) = M_C dF_C(x) + M_F dF_F(x) \tag{4.6}$$

The grade efficiency of separation of size x is defined as

$$G(x) = \frac{M_{C_X}}{M_x} = \frac{M_C f_C(x)}{Mf(x)} \tag{4.7}$$

From Eq. (4.2) it follows that

$$M_C = E_T M \text{ and } M_F = (1 - E_T)M \tag{4.8}$$

Introduce Eq. (4.8) into Eq. (4.5)

$$Mf(x) = E_T M f_C(x) + (1 - E_T)M f_F(x) \tag{4.9}$$

The relationships between particle size distributions of the feed, the coarse and fine products are

$$f(x) = E_T f_C(x) + (1 - E_T) f_F(x) \tag{4.10}$$

$$F(x_2) - F(x_1) = E_T(F_C(x_2) - F_C(x_1)) + (1 - E_T)(F_F(x_2) - F_F(x_1)) \tag{4.11}$$

$$F(x) = E_T F_C(x) + (1 - E_T) F_F(x) \tag{4.12}$$

Equation (4.12) can be rewritten as

$$E_T = \frac{F(x) - F_F(x)}{F_C(x) - F_F(x)} \tag{4.13}$$

Using Eq. (4.8), we can rewrite Eq. (4.7) as

$$G(x) = E_T \frac{dF_C}{dF(x)} = E_T \frac{f_C(x)}{f(x)} \tag{4.14}$$

The grade efficiency can be obtained from the size distribution of the feed $F(x)$ and the fine product $F_F(x)$ or from the fine and coarse products by using the following relationships

$$G(x) = 1 - (1 - E_T) \frac{dF_F(x)}{dF(x)} \tag{4.15}$$

and

$$\frac{1}{G(x)} = 1 + \left(\frac{1}{E_T} - 1 \right) \frac{dF_F(x)}{dF_C(x)} \tag{4.16}$$

Calculation of grade efficiency for the two processes in series

The flowchart of processes is illustrated in Fig. 32.

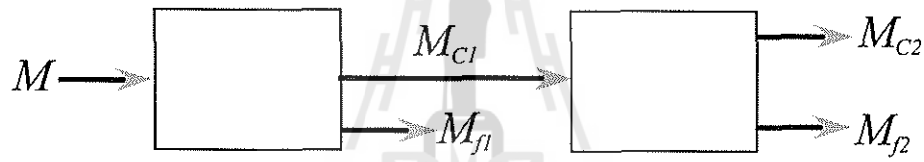

Figure 32: Illustration of grade efficiency for two processes in series.

The amount of product in the feed stream for the second separator is

$$M_{C1,x} = G_1(x) \cdot M_x$$

The amount of the course product of the size x in the second separator is

$$M_{C2,x} = G_2(x) \cdot M_{C1,x} = G_2(x) \cdot G_1(x) \cdot M_x$$

$$M_{F2,x} = (1 - G_2(x)) \cdot G_1(x) \cdot M_x$$

As $G < 1$, then $M_{C2,x} < M_{C1,x}$. Therefore, the more separation steps in the process, the smaller the yield of desired product.

The typical grade efficiency curve is illustrated in Fig. 33. The grade efficiency curve is the partition probability curve, i.e. the probability with which any particular size in the feed will separate or leave with fluid.

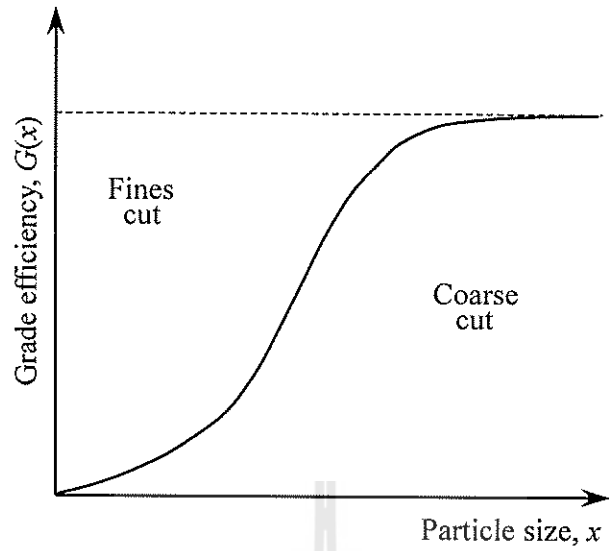

Figure 33: Typical grade efficiency curve.

Comparison of grade efficiency curves for two filters, A and B, is shown in Fig. 34. Filter A is $\sim$ 99% efficient at removing 1 μm particles. Filter B is only $\sim$ 50% efficient at removing 1 μm particles, but it is $\sim$ 99% efficient at removing 10 μm particles.

For an unsteady process such as filtration, the grade efficiency changes with time, as shown in Fig. 35.

4.1. Cut size and sharpness of cut

Cut size (or the equiprobable size x_{50}) is the size corresponding to 50% probability, i.e. the particle size for which 50% of the particles exit the separation process in the coarse product stream and 50% exit in the fines product stream, as shown in Fig. 36.

Limit of separation is the size x_{max} of the largest particles remaining in the overflow after the separation (maximum particle size that would have a chance to escape). The grade efficiency is 100% for all x larger then x_{max}.

Sharpness of cut can be defined as

- A ratio of particle sizes specified at two efficiencies, typically at 20% and 80%

$$I_{80/20} = \frac{x_{80}}{x_{20}} > 1 \tag{4.17}$$

$$I_{20/80} = \frac{x_{20}}{x_{80}} < 1 \tag{4.18}$$

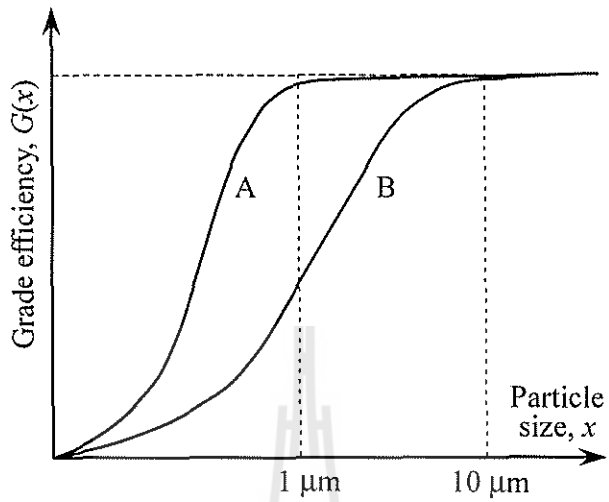

Figure 34: Comparison of grade efficiency curves for two filters.

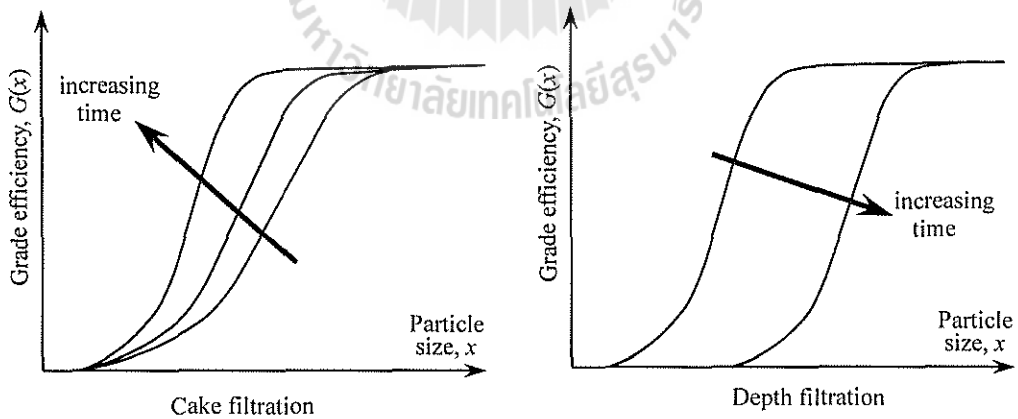

Figure 35: Grade efficiency curves for unsteady processes.

- A slope of the grade efficiency curve

$$I_x = \frac{dG(x)}{dx} \tag{4.19}$$

Figure 36 illustrates various definitions of the sharpness of cut.

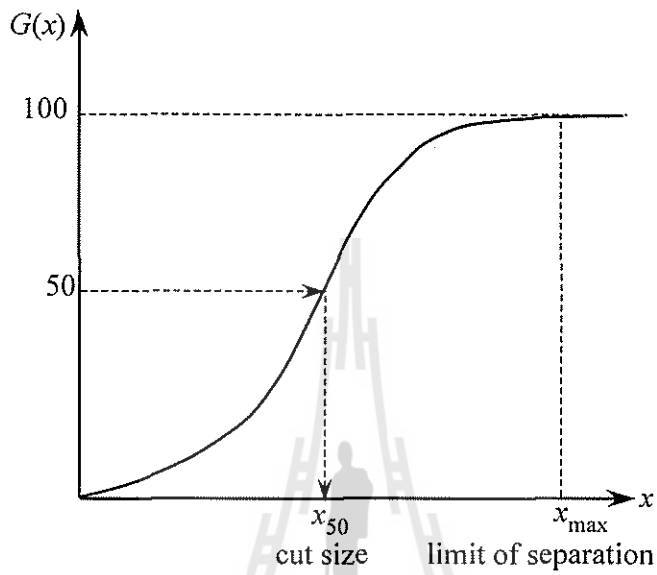

Figure 36: Illustration of sharpness of cut.

Determination of the total efficiency from the grade efficiency and the size distribution of the feed

From Eq. (10)

$$G(x)dF = E_T dF_C$$

The size distribution of the feed material, $dF(x)/dx$ must be known

Integration of above equation in the size range 0 x_{max} gives

$$\int_0^1 G(x)dF = E_T \int_0^1 dF_C$$

since E_T is constant for a given application.

From the definition of the particles size distribution

$$\int_0^1 dF_C = 1$$

Therefore,

$$E_T = \int_0^1 G(x)dF$$

5. Centrifuge Separators

Centrifuge separators, or cyclones, are widely used in industry to separate particles from gas. A cyclone is a device that spins gas stream into a vortex to remove particles by centrifugal force.

Cyclones are simple and inexpensive to make, relatively economical to operate, and are adaptable to a wide range of operating conditions. Cyclones can be made to withstand extreme temperatures and pressures, can accommodate high dust loadings, and can handle large gas flows.

Typical applications are found in mining and metallurgical operations, the cement and plastics industries, pulp and paper mill operations, chemical and pharmaceutical processes, petroleum production (cat-cracking cyclones), and combustion operations (fly ash collection). Typical performance of conventional and high-efficiency cyclones is shown in Table 19.

Table 19: Cyclone Collection Efficiency.

Particle size (μm)	Efficiency (% by wt.)	
	Conventional cyclone (%)	High-efficiency cyclone (%)
<5	-	50-80
5-20	50-80	80-90
15-20	80-95	90-99
>40	95-99	95-99

In the conventional cyclone, as illustrated in Fig. 37, dirty gas tangentially enters the cyclone and is forced into a constrained vortex in the cylindrical part of the cyclone. Particles tend to move outward across the gas stream due to the centrifugal force. They may reach the outer cyclone wall where it is carried by gravity and assisted by the downward movement of the outer vortex and/or secondary eddies, toward the dust outlet at the bottom of the cyclone. The flow vortex is reversed in the conical part and the cleaned gas then passes up through the center of the cyclone (inner vortex) and out of the collector.

Consider a particle of diameter x and density ρ_p rotating with tangential velocity $v_{t,p}$. Figure 38 shows the forces acting on a particle at radial position r. The tangential velocities of gas and small particle are assumed to be equal, $v_{t,p} = v_{t,g} = v_t$. The particle moves radially outward with velocity $v_{r,p}$.

Here we assume that

- particles are dispersed and there is no interaction effects

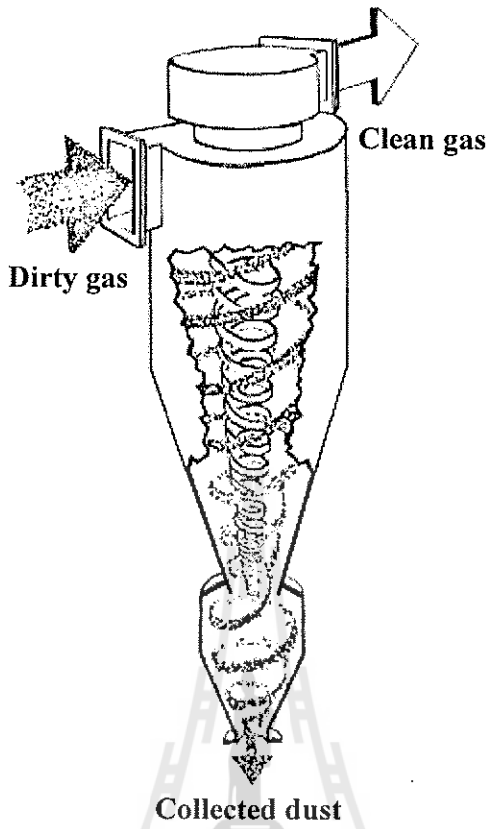

Figure 37: Illustration of a conventional cyclone.

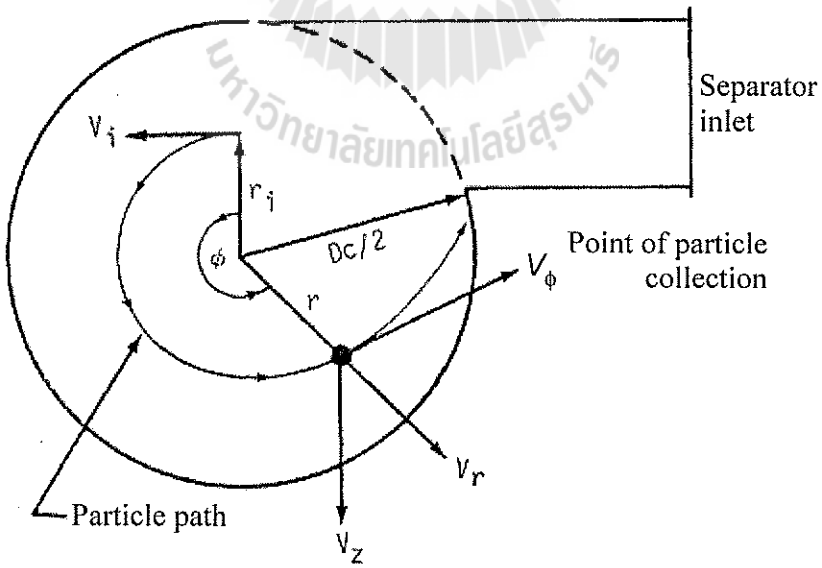

Figure 38: Illustration of forces on a particle in a cyclone.

- particles are not influence on the gas velocity field
- particles are spherical
- separation is taking place when the particle reaches the outer wall of cyclone and particle reentrainment is not considered
- the influences of gas turbulence, Brownian forces and wall effects on the particle are neglected

The centrifugal force, F_c, acting on a particle is given as

$$F_c = \left(\frac{\pi x^3}{6}\right)\rho_p \frac{v_{t,p}^2}{r}$$

The drag force, F_d, acting on a particle as it moves outward is described by Stokes law as

$$F_d = 3\pi\mu x(v_{r,f} - v_{r,p})$$

The buoyancy force, F_b, is

$$F_b = \left(\frac{\pi x^3}{6}\right)\rho \frac{v_t^2}{r}$$

A force balance on the particle in the radial direction is

- in the radial direction

$$m_p \frac{dv_{r,p}}{dt} = \left(\frac{\pi x^3}{6}\right)\rho_p \frac{dv_{r,p}}{dt} = -3\pi\mu x(v_{r,f} - v_{r,p}) \tag{5.1}$$

- in the tangential direction

$$m_p \frac{dv_{\theta,p}}{dt} = \left(\frac{\pi x^3}{6}\right)\rho_p \frac{dv_{\theta,p}}{dt} = 3\pi\mu x(v_{\theta,f} - v_{\theta,p}) \tag{5.2}$$

- in the vertical direction

$$m_p \frac{dv_{z,p}}{dt} = (\rho - \rho_p)\left(\frac{\pi x^3}{6} + 3\pi\mu x(v_{z,f} - v_{z,p})\right) \tag{5.3}$$

Here, $v_r = dr/dt$, $v_r = r \cdot w = rd\theta/dt$ and $v_z = dz/dt$, where w is the particle angular velocity.

References

[1] Theodore L., Buonicore A.J. Industrial Air Pollution Control Equipment for Particulates, CRC Press, 1976.

[2] Fayed M.E. (ed.) Handbook of powder science and technology, 2 ed., Chapman, 1997.

Part III.
Stresses in Bulk Solids

6. Introduction

The state of stress of a bulk solid under the load is described using the continuum or discrete approaches. In the case of continuum approach, the forces are considered on the boundaries of a bulk volume element which is much larger than a particle. In contrast, the forces on the individual particles of the bulk solids are taking into account in the discrete analysis [1-4].

7. Analysis of stresses

In continuum mechanics, stress is a measure of average internal force per unit area of a surface on which internal forces acts. The dimension of stress is that of pressure, i.e. $Pa = N/m^2$.

The concept of the stress is illustrated by considering an elementary cuboid with edges parallel to the co-ordinate directions, as shown in Fig. 39. The faces of such cuboid are named according to the directions of their normals. The force acting on the x-face ($dydz$ plane) is denoted by F_x. This force can be resolved into components in the three co-ordinate directions, such as F_{xx}, F_{xy} and F_{xz}. Here, the force component F_{xx} acts normal to the x-face, and force components F_{xy} and F_{xz} act parallel to the x-face in directions of y and z axis, correspondingly.

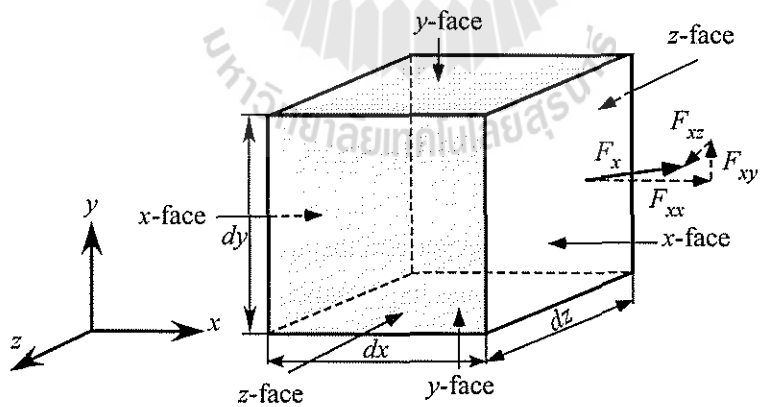

Figure 39: Definition of forces acting on the face of elementary cuboid.

Then, the normal stress can be defined as

$$\sigma_{xx} = F_{xx}/A_x, \tag{7.1}$$

and the shear stresses are

$$\tau_{xy} = F_{xy}/A_x,\ \tau_{xz} = F_{xz}/A_x, \tag{7.2}$$

where A_x is the area of the x-face, $A_x = dy \cdot dz$.

The stress components in a rectangular co-ordinate system are as follows

$$\begin{pmatrix} \sigma_{xx} & \tau_{xy} & \tau_{xz} \\ \tau_{yx} & \sigma_{yy} & \tau_{yz} \\ \tau_{zx} & \tau_{zy} & \sigma_{zz} \end{pmatrix}$$

The diagonal elements of this matrix are the normal stresses $\sigma_{ij}, i = j$, and all other elements are the shear stresses τ_{ij}. In this formulation, the first subscript refers to the face on which the stress acts and the second subscript to the direction in which the associated force acts. The second subscript for normal stresses is often omitted, i.e. $\sigma_x = \sigma_{xx}$.

7.1. Two-dimensional analysis of stresses

Sign notation for granular materials:

- the compressive stress is taken as positive
- the shear stress is taken as positive when acting on the element in an anticlockwise direction

The directions of the positive stresses are shown in Fig. 40.

The stresses acting on a plane inclined at angle θ anticlockwise from the x-face are illustrated in Fig. 41.

This plane will form a wedge-shaped element having faces parallel to the x and y coordinates and a face tilted to the x axis, as shown in Fig. 42(a). The stresses and forces acting on the element are illustrated in Fig. 42(b).

Take the element depth normal to the paper and the area of the hypotenuse plane to be unity, $h = 1$ and $A = h \cdot l = 1$. Therefore, the hypotenuse is of unit length, $l = 1$. The area of the x-face will be $h \cdot (l \cos(\theta)) = 1 \cdot 1 \cdot \cos(\theta) = \cos(\theta)$ and the the area of the y-face will be $h \cdot (l \sin(\theta)) = 1 \cdot 1 \cdot \sin(\theta) = \sin(\theta)$. Thus the forces on the x-face are $\sigma_{xx} \cos(\theta)$ and $\tau_{xy} \cos(\theta)$ and those on the y-face are $\sigma_{yy} sin\theta$ and $\tau_{xy} \sin\theta$, as shown in Fig. 42(c).

Assuming static equilibrium conditions, the force balance in the direction of σ is

$$\sigma + \tau_{xy} \cos(\theta) \sin(\theta) = \sigma_{yy} \sin(\theta) \sin(\theta) + \tau_{yx} \sin(\theta) \cos(\theta) + \sigma_{xx} \cos(\theta) \cos(\theta) \tag{7.3}$$

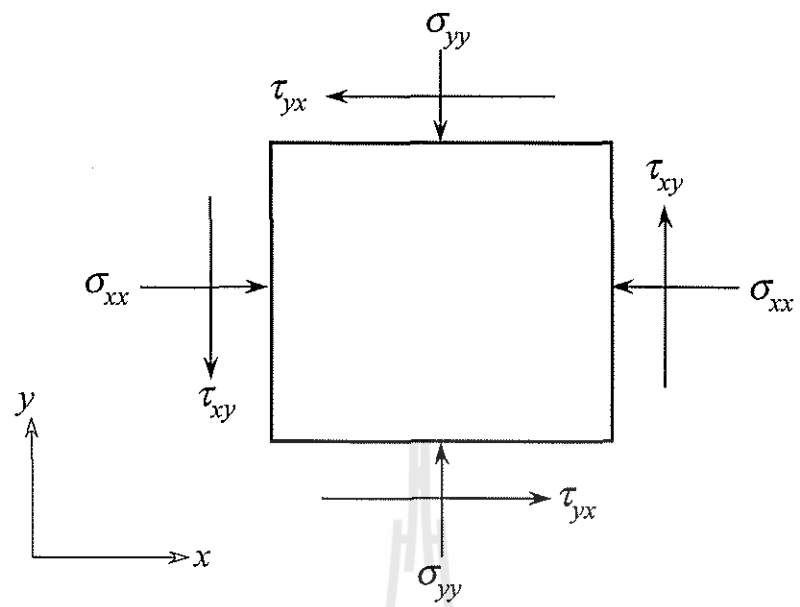

Figure 40: Definition of two-dimensional stresses.

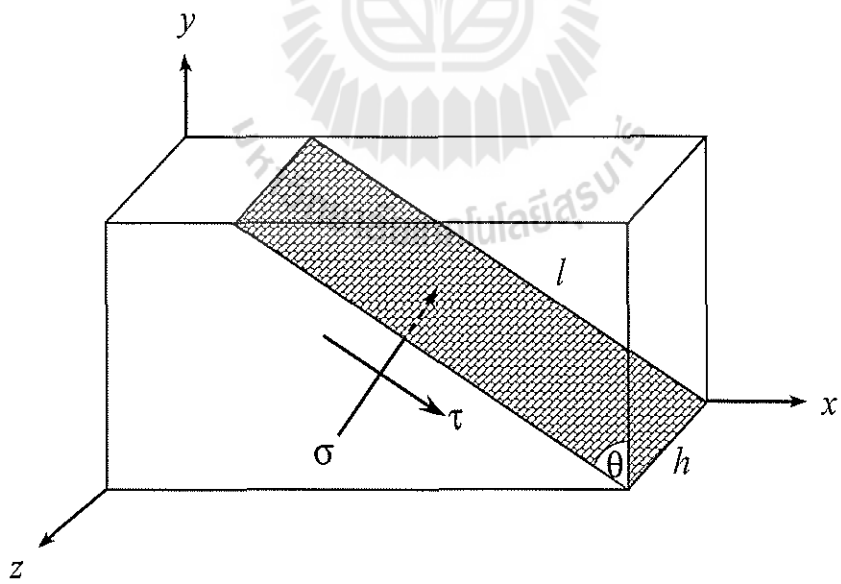

Figure 41: Stresses acting on a plane inclined at angle θ from the x-face.

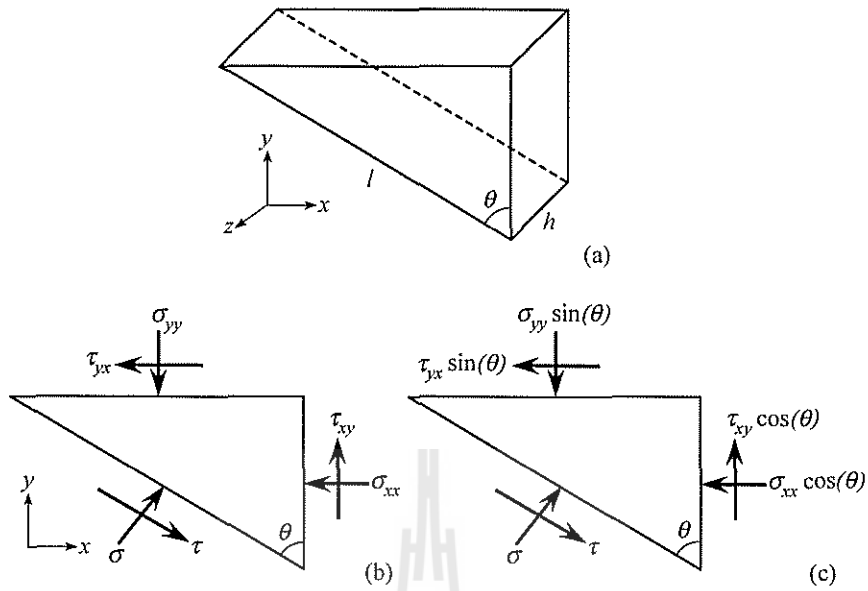

Figure 42: Stresses and forces acting on a wedge-shaped element.

The force balance in the direction of τ is

$$\tau + \sigma_{yy} \sin(\theta) \cos(\theta) = \tau_{yx} \sin(\theta) \sin(\theta) + \tau_{xy} \cos(\theta) \cos(\theta) + \sigma_{xx} \cos(\theta) \sin(\theta) \quad (7.4)$$

Figure 43 illustrates the derivation of force balances in σ and τ directions.

Taking moments about the axis normal to the paper we find that, for stability,

$$\tau_{xy} = -\tau_{yx} \quad (7.5)$$

The following trigonometric relationships will be used in further derivation

$$\cos(2\theta) = 1 - 2\sin^2(\theta) = 2\cos^2(\theta) - 1 \quad (7.6)$$

and

$$\sin(2\theta) = 2\sin(\theta)\cos(\theta) \quad (7.7)$$

With minor rearrangement, Eq. (7.3) can be written as

$$\sigma = \sigma_{yy} \sin^2(\theta) + \sigma_{xx} \cos^2(\theta) + \tau_{yx} \sin(\theta) \cos(\theta) - \tau_{xy} \cos(\theta) \sin(\theta) \quad (7.8)$$

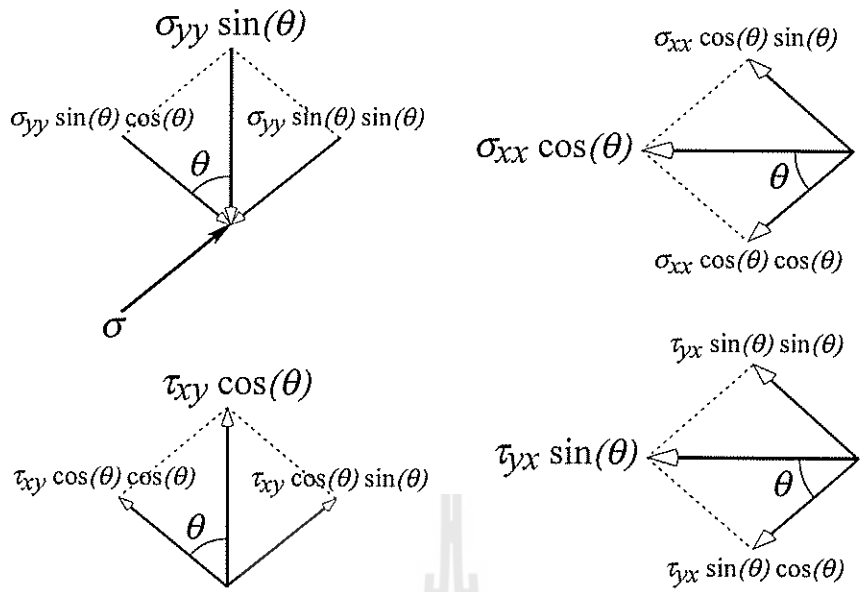

Figure 43: Derivation of force balances.

Substitution of Eq. (7.5) into Eq. (7.8) results in

$$\sigma = \sigma_{yy} \sin^2(\theta) + \sigma_{xx} \cos^2(\theta) - \tau_{xy} \sin(\theta) \cos(\theta) - \tau_{xy} \cos(\theta) \sin(\theta) \tag{7.9}$$

Using Eq. (7.7) yields

$$\sigma = \sigma_{yy} \sin^2(\theta) + \sigma_{xx} \cos^2(\theta) - \tau_{xy} \sin(2\theta) \tag{7.10}$$

Expansion of Eq. (7.10) gives

$$\begin{aligned}
\sigma &= \sigma_{yy} \sin^2(\theta) + \sigma_{xx} \cos^2(\theta) - \tau_{xy} \sin(2\theta) + \frac{1}{2}\sigma_{yy} - \frac{1}{2}\sigma_{yy} + \frac{1}{2}\sigma_{xx} - \frac{1}{2}\sigma_{xx} \\
&= \frac{1}{2}\sigma_{yy}(2\sin^2(\theta) - 1) + \frac{1}{2}\sigma_{xx}(2\cos^2(\theta) - 1) - \tau_{xy} \sin(2\theta) + \frac{1}{2}\sigma_{yy} + \frac{1}{2}\sigma_{xx} \\
&= -\frac{1}{2}\sigma_{yy}(1 - 2\sin^2(\theta)) + \frac{1}{2}\sigma_{xx}(2\cos^2(\theta) - 1) - \tau_{xy} \sin(2\theta) + \frac{1}{2}(\sigma_{yy} + \sigma_{xx})
\end{aligned}$$

Using Eq. (7.6) results in

$$\sigma = -\frac{1}{2}\sigma_{yy} \cos(2\theta) + \frac{1}{2}\sigma_{xx} \cos(2\theta) - \tau_{xy} \sin(2\theta) + \frac{1}{2}(\sigma_{yy} + \sigma_{xx})$$

and finally

$$\boxed{\sigma = \frac{1}{2}(\sigma_{xx} - \sigma_{yy}) \cos(2\theta) + \frac{1}{2}(\sigma_{yy} + \sigma_{xx}) - \tau_{xy} \sin(2\theta)} \tag{7.11}$$

Equation (7.4) can be rearranged as

$$\tau = \tau_{yx}\sin^2(\theta) + \tau_{xy}\cos^2(\theta) + \sigma_{xx}\cos(\theta)\sin(\theta) - \sigma_{yy}\sin(\theta)\cos(\theta) \tag{7.12}$$

Using Eq. (7.7), Eq. (7.12) is written as

$$\tau = \tau_{yx}\sin^2(\theta) + \tau_{xy}\cos^2(\theta) + \frac{1}{2}(\sigma_{xx} - \sigma_{yy})\sin(2\theta) \tag{7.13}$$

Expansion of Eq. (7.13) gives

$$\tau = \frac{1}{2}(\sigma_{xx} - \sigma_{yy})\sin(2\theta) + \tau_{yx}\sin^2(\theta) + \tau_{xy}\cos^2(\theta) + \frac{1}{2}\tau_{yx} - \frac{1}{2}\tau_{yx} + \frac{1}{2}\tau_{xy} - \frac{1}{2}\tau_{xy}$$

Using Eqs. (7.5) and (7.6) results in

$$\begin{aligned}\tau &= \frac{1}{2}(\sigma_{xx} - \sigma_{yy})\sin(2\theta) + \frac{1}{2}\tau_{yx}(2\sin^2(\theta) - 1) + \frac{1}{2}\tau_{xy}(2\cos^2(\theta) - 1) + \frac{1}{2}\tau_{yx} + \frac{1}{2}\tau_{xy} \\ &= \frac{1}{2}(\sigma_{xx} - \sigma_{yy})\sin(2\theta) + \frac{1}{2}\tau_{xy}(1 - 2\sin^2(\theta)) + \frac{1}{2}\tau_{xy}(2\cos^2(\theta) - 1) - \frac{1}{2}\tau_{xy} + \frac{1}{2}\tau_{xy} \\ &= \frac{1}{2}(\sigma_{xx} - \sigma_{yy})\sin(2\theta) + \frac{1}{2}\tau_{xy}\cos(2\theta) + \frac{1}{2}\tau_{xy}\cos(2\theta) - \frac{1}{2}\tau_{xy} + \frac{1}{2}\tau_{xy}\end{aligned}$$

and finally

$$\boxed{\tau = \frac{1}{2}(\sigma_{xx} - \sigma_{yy})\sin(2\theta) + \tau_{xy}\cos(2\theta)} \tag{7.14}$$

Introducing the following notation:

$$p = \frac{1}{2}(\sigma_{xx} + \sigma_{yy}) \tag{7.15}$$

$$R^2 = \left(\frac{\sigma_{xx} - \sigma_{yy}}{2}\right)^2 + \tau_{xy}^2 \tag{7.16}$$

$$\tan(2\lambda) = \frac{2\tau_{xy}}{(\sigma_{xx} - \sigma_{yy})} \tag{7.17}$$

Eq. (7.14) can be rearranged as

$$\begin{aligned}\tau^2 &= \left(\frac{(\sigma_{xx} - \sigma_{yy})}{2}\sin(2\theta) + \tau_{xy}\cos(2\theta)\right)^2 \\ &= \left(\frac{\sigma_{xx} - \sigma_{yy}}{2}\right)^2\sin^2(2\theta) + 2\left(\frac{\sigma_{xx} - \sigma_{yy}}{2}\right)\sin(2\theta)\tau_{xy}\cos(2\theta) + \tau_{xy}^2\cos^2(2\theta) \\ &= \tau_{xy}^2\left[\left(\frac{\sigma_{xx} - \sigma_{yy}}{2\tau_{xy}}\right)^2\sin^2(2\theta) + 2\left(\frac{\sigma_{xx} - \sigma_{yy}}{2\tau_{xy}}\right)\sin(2\theta)\cos(2\theta) + \cos^2(2\theta)\right]\end{aligned}$$

or

$$\tau^2 = \tau_{xy}^2 \left(\frac{\sigma_{xx} - \sigma_{yy}}{2\tau_{xy}} \right)^2 \cdot \left[\sin^2(2\theta) + 2\sin(2\theta)\cos(2\theta) \left(\frac{2\tau_{xy}}{\sigma_{xx} - \sigma_{yy}} \right) + \cos^2(2\theta) \left(\frac{2\tau_{xy}}{\sigma_{xx} - \sigma_{yy}} \right)^2 \right] \tag{7.18}$$

Using Eq. (7.17), the first term of the right hand side of Eq. (7.18) can be written as

$$\begin{aligned} \tau_{xy}^2 \left(\frac{\sigma_{xx} - \sigma_{yy}}{2\tau_{xy}} \right)^2 &= \tau_{xy}^2 \frac{1}{\tan^2(2\lambda)} \\ &= \tau_{xy}^2 \frac{1}{\sin^2(2\lambda)} \cos^2(2\lambda) \end{aligned} \tag{7.19}$$

Then, we can transform the trigonometric relation

$$1 = \sin^2(2\lambda) + \cos^2(2\lambda)$$

as

$$\frac{1}{\sin^2(2\lambda)} = 1 + \frac{\cos^2(2\lambda)}{\sin^2(2\lambda)} = 1 + \frac{1}{\tan^2(2\lambda)}$$

and using Eq. (7.17)

$$\frac{1}{\sin^2(2\lambda)} = 1 + \left(\frac{\sigma_{xx} - \sigma_{yy}}{2\tau_{xy}} \right)^2 \tag{7.20}$$

Substitution of Eq. (7.20) into Eq. (7.19) results in

$$\begin{aligned} \tau_{xy}^2 \left(\frac{\sigma_{xx} - \sigma_{yy}}{2\tau_{xy}} \right)^2 &= \tau_{xy}^2 \left[1 + \left(\frac{\sigma_{xx} - \sigma_{yy}}{2\tau_{xy}} \right)^2 + 1 \right] \cos^2(2\lambda) \\ &= \left[\tau_{xy}^2 + \tau_{xy}^2 \left(\frac{\sigma_{xx} - \sigma_{yy}}{2\tau_{xy}} \right)^2 \right] \cos^2(2\lambda) \\ &= \left[\tau_{xy}^2 + \left(\frac{\sigma_{xx} - \sigma_{yy}}{2\tau_{xy}} \right)^2 \right] \cos^2(2\lambda) \end{aligned}$$

Using the notation for R^2 by Eq. (7.16), Eq. (7.19) can be reformulated as

$$\tau_{xy}^2 \left(\frac{\sigma_{xx} - \sigma_{yy}}{2\tau_{xy}} \right)^2 = R^2 \cos^2(2\lambda) \tag{7.21}$$

Substitution of Eq. (7.21) into Eq. (7.18) yields

$$\tau^2 = R^2 \cos^2(2\lambda) \cdot \left[\sin^2(2\theta) + 2\sin(2\theta)\cos(2\theta) \left(\frac{2\tau_{xy}}{\sigma_{xx} - \sigma_{yy}} \right) + \cos^2(2\theta) \left(\frac{2\tau_{xy}}{\sigma_{xx} - \sigma_{yy}} \right)^2 \right]$$

$$= R^2 \cdot \left[\cos^2(2\lambda)\sin^2(2\theta) + 2\sin(2\theta)\cos(2\theta) \left(\frac{2\tau_{xy}}{\sigma_{xx} - \sigma_{yy}} \right) \cos^2(2\lambda) + \right.$$

$$\left. \cos^2(2\theta) \left(\frac{2\tau_{xy}}{\sigma_{xx} - \sigma_{yy}} \right)^2 \cos^2(2\lambda) \right]$$

Further simplification by introducing $\tan(2\lambda)$ by Eq. (7.17) gives

$$\tau^2 = R^2 \cdot \left[\cos^2(2\lambda)\sin^2(2\theta) + 2\sin(2\theta)\cos(2\theta) \left(\frac{\sin(2\lambda)}{\cos(2\lambda)} \right) \cos^2(2\lambda) + \right.$$

$$\left. \cos^2(2\theta) \left(\frac{\sin^2(2\lambda)}{\cos^2(2\lambda)} \right)^2 \cos^2(2\lambda) \right]$$

$$= R^2 \cdot \left[\cos^2(2\lambda)\sin^2(2\theta) + 2\sin(2\theta)\cos(2\theta)\sin(2\lambda)\cos(2\lambda) + \right.$$

$$\left. \cos^2(2\theta) \left(\frac{\sin^2(2\lambda)}{\cos^2(2\lambda)} \right)^2 \cos^2(2\lambda) \right]$$

$$= R^2 \cdot \left[\cos^2(2\lambda)\sin^2(2\theta) + \sin(2\lambda)\cos(2\theta) \right]^2$$

Therefore,

$$\tau = R\left(\cos^2(2\lambda)\sin^2(2\theta) + \sin(2\lambda)\cos(2\theta) \right)$$

and using the trigonometric relationship

$$\sin(x+y) = \sin(x)\cos(y) + \cos(x)\sin(y)$$

we can finally write

$$\boxed{\tau = R\sin(2\theta + 2\lambda)} \tag{7.22}$$

Substitution of Eq. (7.15) into Eq. (7.11) gives

$$\sigma = p + \left[\frac{1}{2}(\sigma_{xx} - \sigma_{yy})\cos(2\theta) - \tau_{xy}\sin(2\theta) \right] \tag{7.23}$$

The second term of the right hand side of Eq. (7.23) can be transformed as

$$\left[\frac{\sigma_{xx}-\sigma_{yy}}{2}\cos(2\theta)-\tau_{xy}\sin(2\theta)\right]^2=$$
$$=\left(\frac{\sigma_{xx}-\sigma_{yy}}{2}\right)^2\cos^2(2\theta)-2\left(\frac{\sigma_{xx}-\sigma_{yy}}{2}\right)\tau_{xy}\cos(2\theta)\sin(2\theta)+\tau_{xy}^2\sin^2(2\theta)$$
$$=\tau_{xy}^2\left(\frac{\sigma_{xx}-\sigma_{yy}}{2\tau_{xy}}\right)^2\cos^2(2\theta)-2\tau_{xy}^2\left(\frac{\sigma_{xx}-\sigma_{yy}}{2\tau_{xy}}\right)\cos(2\theta)\sin(2\theta)+\tau_{xy}^2\sin^2(2\theta)$$
$$=\tau_{xy}^2\left(\frac{\sigma_{xx}-\sigma_{yy}}{2\tau_{xy}}\right)^2\left[\cos^2(2\theta)-2\sin(2\theta)\cos(2\theta)\left(\frac{2\tau_{xy}}{\sigma_{xx}-\sigma_{yy}}\right)+\right.$$
$$\left.\sin^2(2\theta)\left(\frac{2\tau_{xy}}{\sigma_{xx}-\sigma_{yy}}\right)^2\right]$$

Using Eqs. (7.21) and (7.17) one can obtain

$$\left[\frac{\sigma_{xx}-\sigma_{yy}}{2}\cos(2\theta)-\tau_{xy}\sin(2\theta)\right]^2=$$
$$=R^2\cos^2(2\lambda)\left[\cos^2(2\theta)-2\sin(2\theta)\cos(2\theta)\left(\frac{2\tau_{xy}}{\sigma_{xx}-\sigma_{yy}}\right)+\sin^2(2\theta)\left(\frac{2\tau_{xy}}{\sigma_{xx}-\sigma_{yy}}\right)^2\right]$$
$$=R^2\left[\cos^2(2\lambda)\cos^2(2\theta)-2\sin(2\theta)\cos(2\theta)\cos^2(2\lambda)\left(\frac{\sin(2\lambda)}{\cos(2\lambda)}\right)+\right.$$
$$\left.\sin^2(2\theta)\cos^2(2\lambda)\left(\frac{\sin(2\lambda)}{\cos(2\lambda)}\right)^2\right]$$
$$=R^2\left[\cos^2(2\lambda)\cos^2(2\theta)-2\cos(2\lambda)\cos(2\theta)\sin(2\theta)\sin(2\lambda)+\sin^2(2\theta)\sin^2(2\lambda)\right]$$
$$=R^2\left[\cos(2\lambda)\cos(2\theta)-\sin(2\theta)\sin(2\lambda)\right]^2$$

Using the trigonometric relationship

$$\cos(x+y)=\cos(x)\cos(y)-\sin(x)\sin(y)$$

we can write

$$\left[\frac{\sigma_{xx}-\sigma_{yy}}{2}\cos(2\theta)-\tau_{xy}\sin(2\theta)\right]^2=R^2\left(\cos(2\theta+2\lambda)\right)^2$$

Therefore, Eq. (7.23) becomes

$$\boxed{\sigma = p + R^2 \left(\cos\left(2\theta + 2\lambda\right)\right)^2} \tag{7.24}$$

Equations (7.22) and (7.24) define a Mohr's circle on (σ, τ) axes with a center at the point $(p, 0)$ and a radius R, as shown in Fig. 44. Every point on the circle represents the combination of σ and τ on some plane, for example stresses (σ_{xx}, τ_{xy}) on the x-plane and (σ_{yy}, τ_{yx}) on the y-plane are marked by the points X and Y, respectively. The stresses on a plane inclined at θ anticlockwise from the x-plane are given by the end of the radius inclined at 2θ anticlockwise from the radius to the point X. In particular, the stresses on the y-plane, for which $\theta = 90°$ are therefore given by the other end of the diameter from the point X. Therefore, the following relationship should be kept, $\tau_{xy} = -\tau_{yx}$. The stresses on the u-plane (σ_{uu}, τ_{uv}) are given by the point U. The radius to the point U is inclined at angle 2θ to the radius to point X. Thus, we rotate Mohr's circle in the same direction as we rotate our axes but through twice the angle.

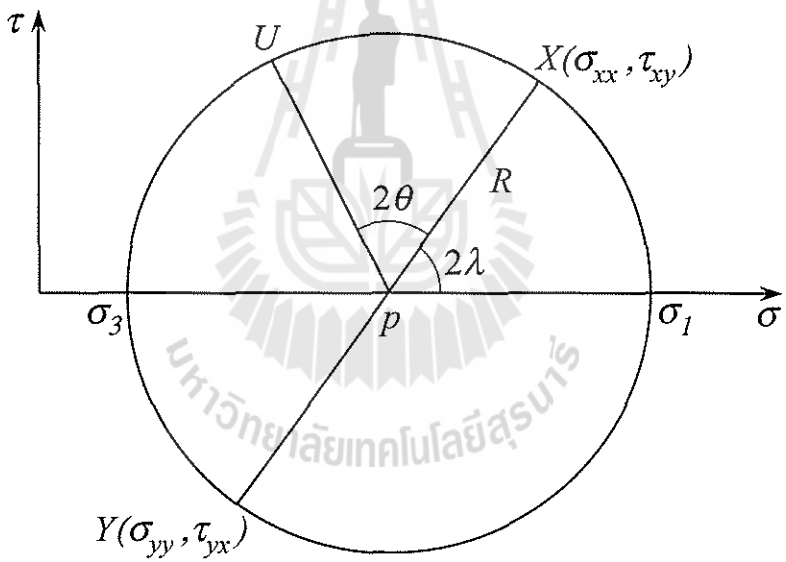

Figure 44: Mohr's circle for stresses.

The principal planes are the planes on which the shear stress is zero. The corresponding stresses σ_1 and σ_3 are called the major and minor principal stresses. From Fig. 44 it can be seen that the major principal plane lies at an angle λ clockwise from the x-plane and the minor principal plane lies at an angle $90 - \lambda$ anticlockwise from the x-plane. Since the principal planes lies at opposite ends of a diameter, they are at right-angles to each other.

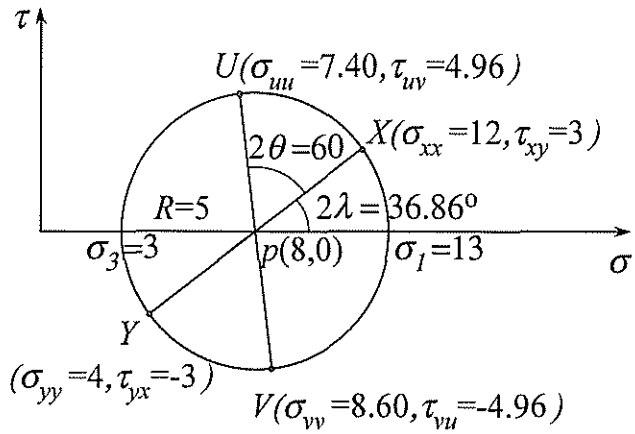

Figure 45: Example of the use of Mohr's circle.

An example of the use of Mohr's circle is illustrated in Fig. 45. Let us consider a situation in which $\sigma_{xx} = 12$ kN m^{-2}, $\sigma_{yy} = 4$ kN m^{-2} and $\tau_{xy} = 3$ kN m^{-2}.We can identify the points X and Y since they have coordinates (12,3) and (4,-3) and plot them on a Mohr's diagram. Using Eqs. (7.15) and (7.16), the center and the radius of the circle can be calculated as $p(8, 0)$ and $R = 5$ kN m^{-2}. Thus the principal stresses are $\sigma_1 = 13$ kN m^{-2} and $\sigma_3 = 3$ kN m^{-2}. Also using Eq. (7.17), we found that $\tan(2\lambda)$ is $3/4$ or an angle λ is 18.43°. Thus the major principal stress acts in a direction inclined at 18.43° clockwise from the x-axis. If we need to find the stresses on a plane at 30° anticlockwise from the x-plane, we can construct the radius at $2 \times 30° = 60°$ anticlockwise from the radius to point X. The coordinates of the end of this radius, (σ_{uu}, τ_{uv}) are

$$\sigma_{uu} = p + R\cos(2\theta + 2\lambda) = 8 + 5\cos(60 + 36.86) = 7.40 \text{ kN m}^{-2}$$
$$\tau_{uv} = R\sin(2\theta + 2\lambda) = 4.96 \text{ kN m}^{-2}$$

and the stresses on the perpendicular plane are

$$\sigma_{uu} = 8 + 5\cos(60 + 36.86 + 180) = 8.60 \text{ kN m}^{-2}$$
$$\tau_{vu} = 5\sin(36.86 + 60 + 180) = -4.96 \text{ kN m}^{-2}.$$

8. Flow properties of bulk solids

The flow properties of bulk solids depend on particle size distribution, particle shape, chemical composition of the particles, moisture, temperature, etc. [2].

"Flowing" means that a bulk solid is deformed plastically due to the loads acting on it, e.g. failure of a previously consolidated bulk solid sample. The magnitude of the load necessary for flow is a measure of flowability.

Consider a uniaxial compression test shown in Fig. 46. A hollow cylinder of cross-sectional area A is filled with a fine-grained bulk solids. An internal wall of the cylinder is assumed to be frictionless.

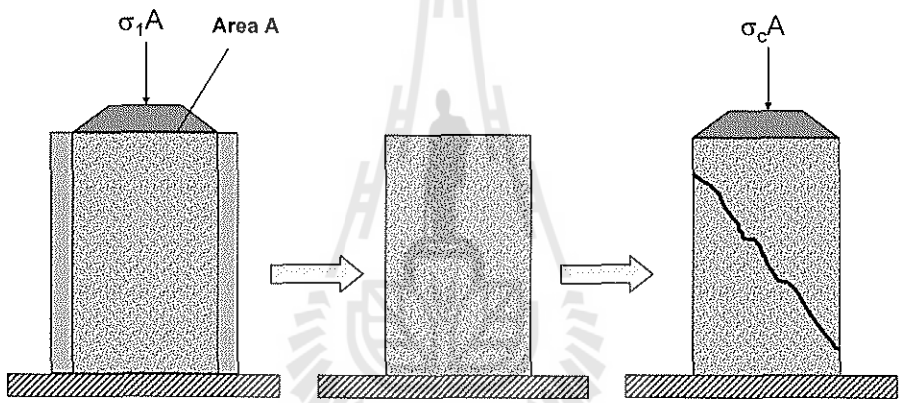

Figure 46: Uniaxial compression test.

The bulk solid is loaded by the stress σ_1 in the vertical direction and compressed. This stress is called *consolidation* or *major principal stress*. The more the volume of the bulk solid is reduced, the more compressible the bulk solid. In addition to the increase in bulk density, the strength of the bulk solid specimen will also increase. Hence, the bulk solid is both consolidated and compressed through the effect of the consolidation stress.

After consolidation, the bulk solid specimen is relieved of the consolidation stress and the hollow cylinder is removed. If subsequently the consolidated cylindrical bulk solid specimen is loaded with an increasing vertical compressive stress, the specimen will break (fail) at a

certain stress. The stress causing failure is called *compressive strength*, *cohesive strength*, or *unconfined yield strength*, f_c or σ_c.

In bulk solids technology one calls the failure "incipient flow", because at failure the consolidated bulk solid specimen starts to flow. Thereby the bulk solid dilates somewhat in the region of the surface of the fracture, since the distances between individual particles increase. Therefore, incipient flow is plastic deformation with decrease of bulk density. Since the bulk solid fails only at a sufficiently large vertical stress, which is equal to its compressive strength, there must exist a material specific yield limit for the bulk solid. Only when this yield limit is reached does the bulk solid start to flow. The yield limits of many solid materials (e.g. metals) are listed in tables. However, the yield limit of a bulk solid is dependent also on its stress history, i.e., previous consolidation: The greater the consolidation stress, σ_1, the greater are bulk density, ρ_b, and unconfined yield strength, f_c.

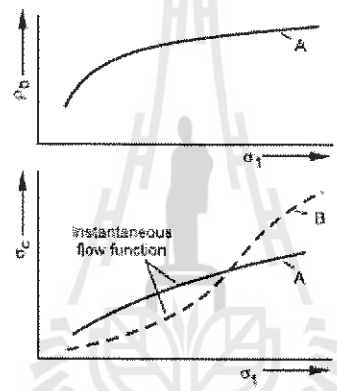

Figure 47: Influence of consolidation stress, σ_1, on bulk density, ρ_b, and unconfined yield strength, f_c.

A plot of f_c against σ_1 is the flow function (FF) for the powder, or *instantaneous flow function* to emphasize that the strength is measured directly after consolidation.

Some bulk solids increase in strength if they are stored for a period of time at rest under a compressive stress. This effect is called *time consolidation* or *caking*. Time consolidation is the result of the increase of interparticle adhesive forces with time based on different mechanisms. The instantaneous and time flow functions are shown in Fig. 48.

FF<1	not flowing
1<FF<2	very cohesive
2<FF<4	cohesive
4<FF<10	easy-flowing
10<FF	free-flowing

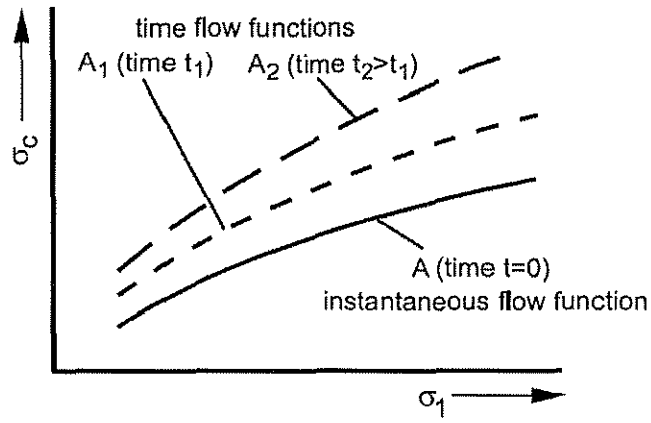

Figure 48: Instantaneous and time flow functions.

Flowability of a bulk solids can be characterized numerically by the ratio $ff_c = \frac{\sigma_1}{f_c}$. The larger ff_c, the better a bulk solid flows, as shown in Fig. 49. This figure illustrates that the larger value of flowability of bulk solid A is obtained at a greater consolidation stress though an unconfined yield also increases.

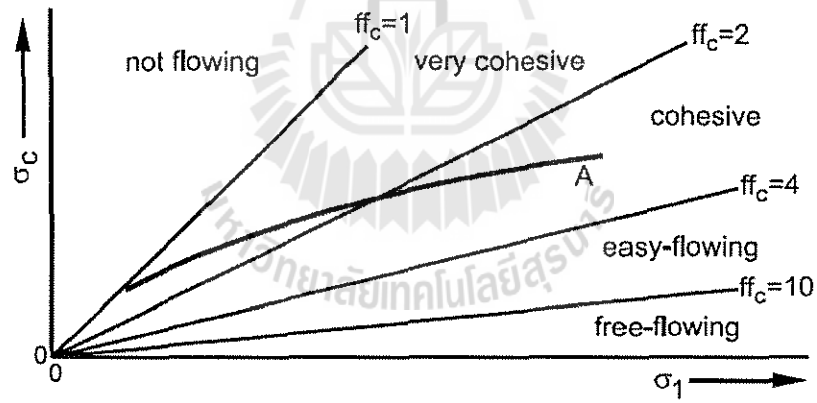

Figure 49: Instantaneous flow functions and lines of constant flowability.

The instantaneous flow function and time flow functions from Fig. 48 are shown in Fig. 50 along with the boundaries of the ranges, which follow from the classification of flowability as outlined above. It can be seen that flowabilities measured at identical consolidation stress, but after different consolidation periods, decrease with increasing consolidation time, t. The decrease of flowability with consolidation period is shown in Fig. 50.b.

From the dependence of flowability, ff_c, on consolidation stress, σ_1, it follows that one can compare the flow behavior of several bulk solids quantitatively using ff_c only if all measure-

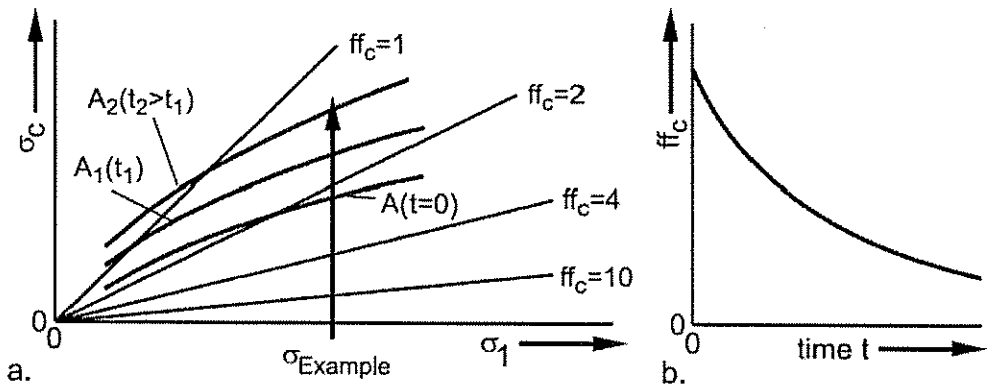

Figure 50: Influence of storage period on flowability.

ments have been performed at identical consolidation stresses. In addition, the time consolidation of different bulk solids can be compared only at identical consolidation stress and identical consolidation time. Therefore, besides the ff_c value, one must provide the consolidation stress and the consolidation period values used. The consolidation stress and the consolidation period selected for testing should reflect, as much as possible, the actual process conditions in which the problem occurs (e.g. stress and storage period for storage in bags on pallets, stress near the outlet opening of a silo, etc.).

With many applications the bulk solid flows by gravity, e.g. when flowing out from a bin or silo. Two bulk solids with the same flowability value, ff_c, but a different bulk density, ρ_b, will flow differently because a larger gravitational force acts on the bulk solid with the larger bulk density. This means, for all applications utilizing gravity flow of bulk solids (e.g. flow out of a silo), that flow of a bulk solid with greater bulk density is supported by a greater force. Because of the greater force of gravity at equal flowability the strength of the bulk solid with the greater bulk density can be overcome more easily.

Sometimes one finds very strong differences between the bulk densities of samples to be compared, particularly with very fine-grained products. Here bulk density must be considered in order to reach conclusions about flowability under gravity flow. It might be useful then to consider the dimensionless product of flowability, ff_c, and bulk density, ρ_b, which is called the *density-weighed flowability*:

$$ff_\rho = ff_c \cdot \frac{\rho_b}{\rho_w} \tag{8.1}$$

with $\rho_w = 1000\text{kg/m}^3$ (liquid water at 0 deg C, 1 bar).

9. Design of storage vessel for bulk materials

9.1. Introduction

The design of storage vessel for reliable discharge of bulk materials is based largely on work of Jenike [3, 4].

- Consideration in designing for mass-flow vessel
  1. the hopper walls should be steep enough to ensure that particles slide along the walls
  2. the discharge orifice should be large enough to prevent the formation of cohesive arches
- Consideration in designing for funnel-flow vessel
  1. the discharge orifice should be large enough to prevent the formation of cohesive arches and piping

The two basic causes for the formation of a stable arch at the outlet are by mechanical interlocking of large ($d_p > 3000\mu$) free-flowing particles or by the cohesive bulk strength of fine grains (Figure 3.2). Mechanical arching may be avoided by having an outlet size that is several times larger than the particle size. Cohesive arching is more common in industrial silos, and its prevention in a given situation requires detailed information on material bulk and frictional properties and the type of flow prevailing in the silo.

9.2. Flow patterns

Two primary flow patterns can develop when a bulk solid discharges from a bin: mass flow and funnel flow. The mass flow is defined as a flow pattern in which all of the material is in motion during withdrawal but not necessarily at the same velocity at a given height across the cross section, as shown in Fig. 51.

Funnel flow, also called core flow, is defined as a flow pattern in which some material is stationary while the rest is moving, as illustrated in Fig. 52.

Rotter (2005) further refined the definition of funnel flow into pipe flow and mixed flow. The distinction between the two is whether or not the flow channel intersects any portion of the walls of the bin (usually in the cylinder section). If there is no intersection (pipe flow), the flow channel walls may be vertical (parallel pipe flow), converging from top to bottom (taper pipe flow), vertical along the sidewall of the bin (eccentric parallel pipe flow) or converging along the sidewalls of the bin (eccentric taper pipe flow) (see Fig. 53).

If the flow channel intersects the cylinder wall (mixed flow), the converging flow channel may be symmetric about the centreline of the bin (concentric mixed flow), fully eccentric if

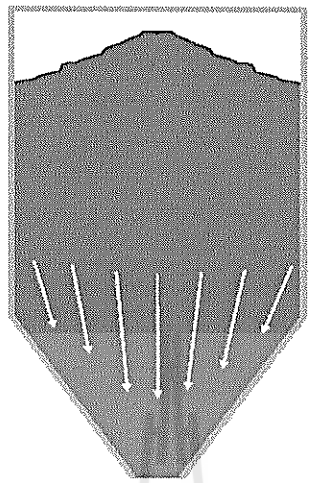

Figure 51: Illustration of mass flow pattern.

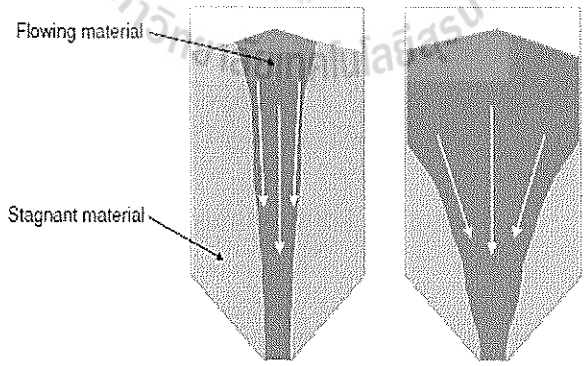

Figure 52: Illustration of funnel flow pattern.

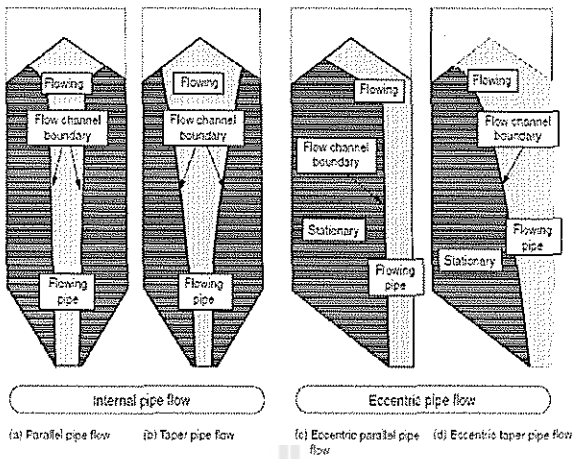

Figure 53: Forms of pipe flow.

the hopper opening is to one side of the vessel (fully eccentric mixed flow), or intersecting the cylinder walls at varying elevations because of a partially eccentric outlet (partially eccentric mixed flow) (see Fig. 54).

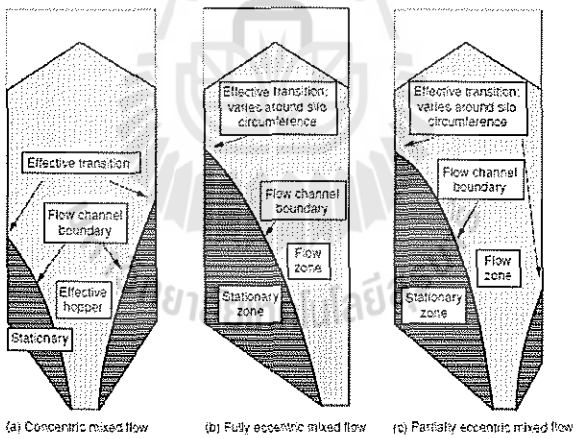

Figure 54: Forms of mixed flow.

A third flow pattern, expanded flow, is a combination of funnel flow and mass flow (see Fig. 55). Usually this is achieved by placing a small mass flow hopper below a funnel flow hopper. The mass flow hopper section expands the flow channel from the outlet up to the top cross section of the mass flow hopper.

Problems with hoppers

- Ratholing

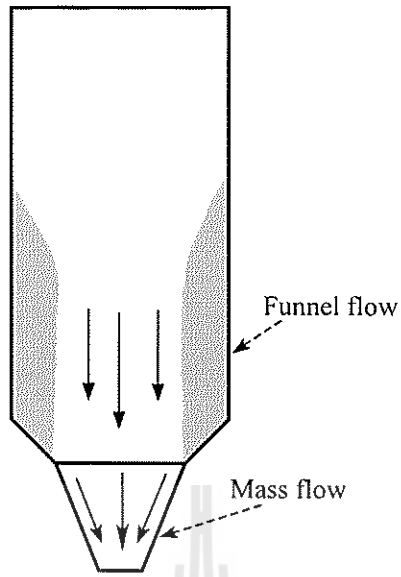

Figure 55: Forms of mixed flow.

- Arching
- Insufficient flow
- Flushing

9.3. Mass-flow silos:flow/no flow criterion

- The pressure acting in the bulk solid and the cohesive strength of the powder
- Unconfined yield strength of cohesive materials
- Flow function (FF) for the powder

9.4. Stresses in a vertical bunker

The method of differential slices developed by Janssen [3] is widely used for calculation of stresses in a vertical bunker. Consider the stress distribution in the bunker containing cohesionless particles as shown in Fig. 56.

A cylindrical coordinate system with an origin at the center of the flat top surface is utilized to formulate the force balance on a slice element of the thickness dz at depth z below the top surface. Assuming an uniform vertical stress σ_V across any horizontal plane, the force balance on the slice can be written as

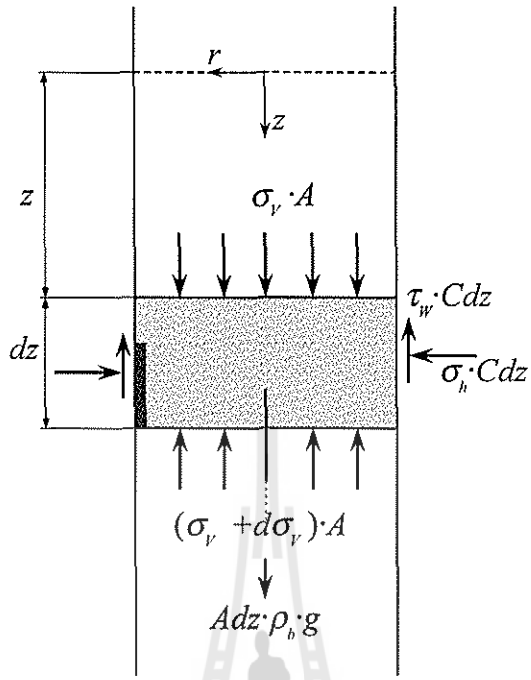

Figure 56: Illustration of a model of pressure distribution in a bunker.

{downward force on the top surface $= A \cdot \sigma_V$} +
{weight of particles within the slice $= Adz \cdot \rho_b g$} −
{upward force on the base surface $= A \cdot (\sigma_V + d\sigma_V)$} −
{upward force on the slice side due to the wall shear stress $= \tau_W \cdot Cdz$} $= 0$

$$A \cdot \sigma_V + Adz \cdot \rho_b g - A \cdot (\sigma_V + d\sigma_V) - \tau_W \cdot Cdz = 0, \tag{9.1}$$

where A is the cross-sectional area of the bunker, C is the bunker circumference, $\sigma_V + d\sigma_V$ is the vertical solids pressure at the base surface, ρ_b is the bulk density, τ_W is the shear (tangential) stress at the wall due to the friction between particles and the vessel wall and g is the acceleration due to gravity.

The lateral stress ratio K, i.e. the ratio of the horizontal to the vertical solids stresses is assumed to be constant everywhere in the slice and is independent of the stress value

$$K = \frac{\sigma_h}{\sigma_V}, \tag{9.2}$$

where σ_h is the normal (horizontal) stress at the wall.

The wall friction is

$$\mu_W = \tan(\varphi_W) = \frac{\tau_W}{\sigma_h}, \tag{9.3}$$

where μ_W is the particle-wall friction coefficient and φ_W is the particle-wall friction angle. Using Eqs. (9.2) and (9.3) and expanding Eq. (9.1) results in

$$\frac{d\sigma_V}{dz} + \frac{\mu_W KC}{A} \cdot \sigma_V = \rho_b g. \tag{9.4}$$

Equation (9.4) is a linear first-order differential equation in a standard form provided that the bulk density is constant. To solve this equation, it should be multiplied by an integrating factor $\exp\left(\int \frac{\mu_W KC}{A} dz\right) = \exp\left(\frac{\mu_W KC}{A} z\right)$. The general solution is

$$\sigma_V \cdot \exp\left(\frac{\mu_W KC}{A} z\right) = \int \exp\left(\frac{\mu_W KC}{A} z\right) \rho_b g dz + C_1, \tag{9.5}$$

where C_1 is the integration constant.

Integration of the right-hand side of Eq. (9.5) results in

$$\sigma_V \cdot \exp\left(\frac{\mu_W KC}{A} z\right) = \rho_b g \exp\left(\frac{\mu_W KC}{A} z\right) \frac{A}{\mu_W KC} + C_1. \tag{9.6}$$

The integration constant C_1 is determined from the boundary conditions. Assuming that the top surface of material is open to the atmosphere, the normal stress on it may be taken to be zero:

$$\sigma_V = 0 \text{ at } z = 0 \tag{9.7}$$

Therefore, the integration constant is

$$C_1 = -\frac{\rho_b g A}{\mu_W KC}. \tag{9.8}$$

Substituting Eq.(9.8) into Eq. (9.6) and using Eqs. (9.2) and (9.3), the variations of stresses with bed depth are described as

$$\sigma_V = \frac{\rho_b g A}{\mu_W KC}\left[1 - \exp\left(-\frac{\mu_W KC}{A} z\right)\right] \tag{9.9}$$

$$\sigma_h = K\sigma_V = \frac{\rho_b g A}{\mu_W C}\left[1 - \exp\left(-\frac{\mu_W KC}{A} z\right)\right] \tag{9.10}$$

$$\tau_W = \mu_W \sigma_h = \frac{\rho_b g A}{C}\left[1 - \exp\left(-\frac{\mu_W KC}{A} z\right)\right] \tag{9.11}$$

For large values of z, $z \to \infty$, all three stresses tend exponentially to asymptotic values

$$\sigma_{V,\infty} = \frac{\rho_b g A}{\mu_W K C};\ \sigma_{h,\infty} = \frac{\rho_b g A}{\mu_W C};\ \tau_{W,\infty} = \frac{\rho_b g A}{C} \tag{9.12}$$

For cylindrical bunker, $A = \pi D^2/4, C = \pi D$ and $A/C = D/4$. Thus, at great depth the stress normal to the wall, σ_h, depends only on the bunker diameter, coefficient of wall friction, bulk density and does not depend on the depth. The maximum possible stress is proportional to the bunker diameter. The pressure on the smooth wall of large diameter bunker will be high. All stresses vary linearly with the solid bulk density. The load on the bottom of the bunker is only a small fraction of the total weight of the particles, as the most weight is supported by the side walls.

The rate of approach to the asymptotic value is governed by the term $\exp(-z/z_c)$, where z_c is the characteristic depth or the Janssen reference depth, $z_c = \dfrac{A}{C\mu_W K}$. Therefore, z_c is the depth over which the departure from the asymptote decreases by a factor of e. The stresses will reach 90% of their final values at a depth of about $2.5z_c$.

The asymptotic value of the stress normal to the wall, $\sigma_{h,\infty}$ does not depend on K, conforming that Jansenn's theory is correct for sufficiently deep beds even if the initial assumption of constant K is not true. At great depth, conditions are stable and the stresses are constant. Therefore, the weight of particles within the slice is equilibrated by the force due to the wall shear stress.

At shallow depth as $z \to 0$, the exponential term in Eqs. (9.9),(9.10) and (9.11) may be related to

$$\exp\left(-\frac{\mu_W K C}{A} z\right) = 1 - \frac{\mu_W K C}{A} z \tag{9.13}$$

Substitution of Eq. (9.13) in Eq. (9.9) results in

$$\sigma_{V,0} = \rho_b g z \tag{9.14}$$

which is the hydrostatic pressure. Eqs. (9.10) and (9.11) become

$$\sigma_{h,0} = K\rho_b g z;\ \tau_{W,0} = \mu_W K \rho_b g z. \tag{9.15}$$

Using the definitions of asymptotic stresses and characteristic depth, Eqs. (9.9) - (9.11) can be rewritten as

$$\sigma_V = \sigma_{V,\infty}\left[1 - \exp\left(-\frac{z}{z_c}\right)\right] \tag{9.16}$$

$$\sigma_h = \sigma_{h,\infty}\left[1 - \exp\left(-\frac{z}{z_c}\right)\right] \tag{9.17}$$

$$\tau_W = \tau_{W,\infty}\left[1 - \exp\left(-\frac{z}{z_c}\right)\right] \tag{9.18}$$

The typical pattern of the stress normal to the wall calculated by Eq. (9.17) is illustrated in Fig. 57.

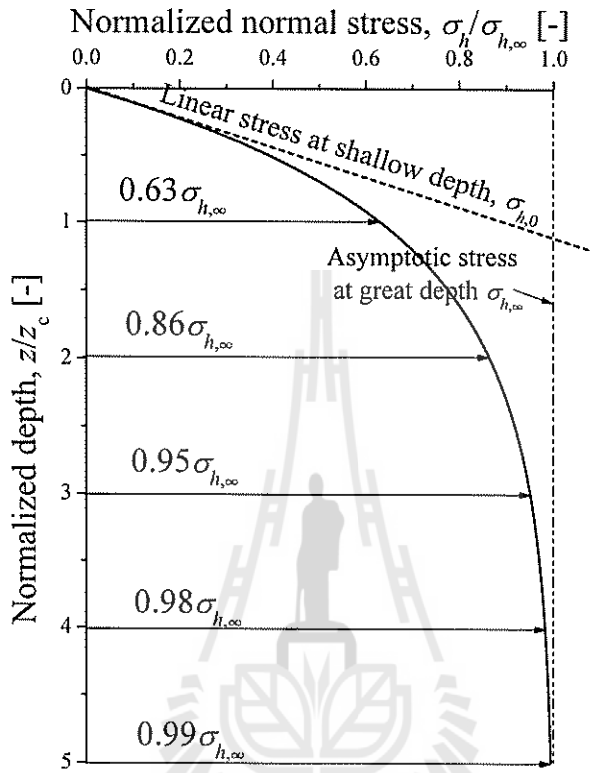

Figure 57: Illustration of stress pattern in a bunker.

9.5. Stress distribution in a hopper

Consider the pressure distribution in a conical hopper of half-angle α containing a cohesionless particles as shown in Fig. 58. The cylindrical coordinates (r, h) are used in this case with distance h measured vertically upward from the apex of the hopper.

Assuming an uniform vertical stress σ_V across any horizontal plane, the force balance in a vertical direction on a cylindrical slice of thickness dh at distance h from the apex can be written as

$$\{\text{upward force on the base surface} = \sigma_V \cdot \pi r^2\} +$$
$$\left\{\text{upward force on the slice side due to the normal force at the wall} =\right.$$

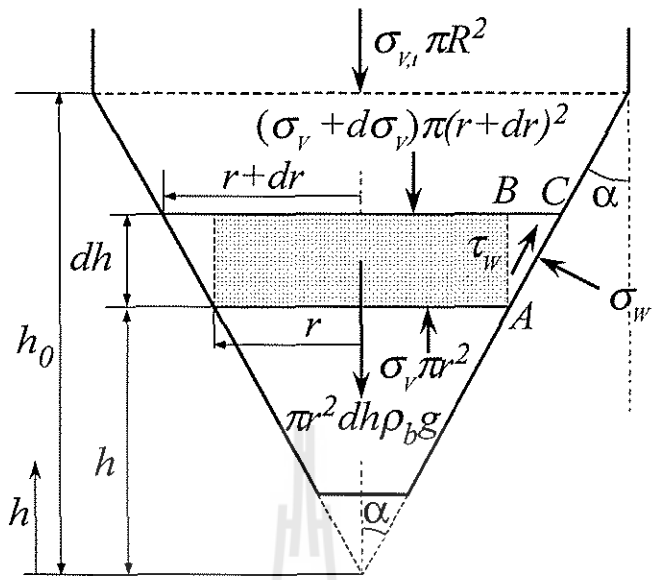

Figure 58: Illustration of a model of stress distribution in a conical hopper.

$$\sigma_W \sin(\alpha) \cdot \left[2\pi r \left(\frac{dh}{\cos(\alpha)}\right)\right]\Big\} +$$

$\Big\{$upward force on the slice side due to the wall shear stress $=$

$$\tau_W \cos(\alpha) \cdot \left[2\pi r \left(\frac{dh}{\cos(\alpha)}\right)\right]\Big\} -$$

$\{$downward force on the top surface $= (\sigma_V + d\sigma_V) \cdot \pi(r+dr)^2\} -$

$\{$weight of particles within the slice $= \pi r^2 dh \cdot \rho_b g\} \quad = 0$

Here the weight of particles in the wedge ABC is neglected as its contribution to the powder weight in the slice becomes small when $dh \to 0$.

$$\sigma_V \cdot \pi r^2 + \sigma_W \sin(\alpha) \cdot \left[2\pi r \left(\frac{dh}{\cos(\alpha)}\right)\right] + \tau_W \cos(\alpha) \cdot \left[2\pi r \left(\frac{dh}{\cos(\alpha)}\right)\right] - (\sigma_V + d\sigma_V) \cdot \pi(r+dr)^2 - \pi r^2 dh \cdot \rho_b g = 0 \tag{9.19}$$

Expanding the forth term in Eq.(9.19) and ignoring higher-order terms such as dr^2, $d\sigma_V dr$ and $d\sigma_V dr^2$ results in

$$\begin{aligned}(\sigma_V + d\sigma_V) \cdot \pi(r+dr)^2 &= (\sigma_V + d\sigma_V) \cdot \pi(r^2 + 2rdr + dr^2) = \\ \sigma_V \pi r^2 + \sigma_V \pi 2rdr + \cancel{\sigma_V \pi dr^2} + d\sigma_V \pi r^2 + \cancel{d\sigma_V \pi 2rdr} + \cancel{d\sigma_V \pi dr^2} &= \\ \sigma_V \pi r^2 + \sigma_V \pi 2rdr + d\sigma_V \pi r^2 &\end{aligned} \tag{9.20}$$

Substitution of Eq. (9.20) into Eq. (9.19) yields

$$\cancel{\sigma_V \pi r^2} + \sigma_W \sin(\alpha) \cdot \left[2\pi r \left(\frac{dh}{\cos(\alpha)}\right)\right] + \tau_W \cos(\alpha) \cdot \left[2\pi r \left(\frac{dh}{\cos(\alpha)}\right)\right]$$
$$-(\cancel{\sigma_V \pi r^2} + \sigma_V \pi 2r dr + d\sigma_V \pi r^2) - \pi r^2 dh \cdot \rho_b g = 0$$

Dividing by πr^2, substituting $r = h\tan(\alpha)$ and rearranging results in

$$\sigma_W \frac{\sin(\alpha)}{\cos(\alpha)} \frac{2dh}{h\tan(\alpha)} + \tau_W \frac{2}{h\tan(\alpha)} dh - 2\sigma_V \frac{dh \cancel{\tan(\alpha)}}{h \cancel{\tan(\alpha)}} - d\sigma_V - dh\rho_b g = 0$$

Using $\tau_W = \sigma_W \cdot \tan(\varphi_W)$ yields

$$2\sigma_W \frac{dh}{h} + \sigma_W \frac{2dh}{h} \frac{\tan(\varphi_W)}{\tan(\alpha)} - 2\sigma_V \frac{dh}{h} - d\sigma_V - dh\rho_b g =$$
$$2\frac{dh}{h\tan(\alpha)} \sigma_W (\tan(\alpha) + \tan(\varphi_W)) - 2\sigma_V \frac{dh}{h} - d\sigma_V - dh\rho_b g = 0$$

Dividing by dh and multiplying by h results in

$$\frac{2\sigma_W}{\tan(\alpha)} (\tan(\alpha) + \tan(\varphi_W)) - 2\sigma_V - h\frac{d\sigma_V}{dh} - \rho_b g h = 0$$

Using the hopper stress ratio F defined as $F = \sigma_W / \sigma_V$ yields

$$\frac{2F\sigma_V}{\tan(\alpha)} (\tan(\alpha) + \tan(\varphi_W)) - 2\sigma_V - h\frac{d\sigma_V}{dh} - \rho_b g h = 0$$

Rearranging result in

$$h\frac{d\sigma_V}{dh} + \sigma_V \left[2 - 2F - 2F\frac{\tan(\varphi_W)}{\tan(\alpha)}\right] = -h\rho_b g$$

Finally, the ordinary differential equations is obtained as follows

$$\frac{d\sigma_V}{dh} - \frac{n}{h}\sigma_V = -h\rho_b g, \tag{9.21}$$

where $n = \left[2\left(F + F\frac{\tan(\varphi_W)}{\tan(\alpha)} - 1\right)\right]$.

The initial condition is

$$\sigma_V = \sigma_{V,t} \text{ at } h = h_0 \tag{9.22}$$

where $\sigma_{V,t}$ is the mean vertical stress in the solid at the transition of bunker to hopper parts.

Equation Eq. (9.21) is a linear first-order differential equation in a standard form. To solve

this equation, it should be multiplied by an integrating factor $\exp\left(\int \frac{-n}{h} dh\right) = \exp\left(-n \ln\left(h\right)\right) = h^{-n}$.

The general solution is

$$\sigma_V h^{-n} = \int h^{-n}(-\rho_b g) dh + C_2, \tag{9.23}$$

where C_2 is the integration constant. Integration of Eq. (9.23) yields

$$\sigma_V h^{-n} = -\rho_b g \frac{h^{-n+1}}{-n+1} + C_2 = \frac{\rho_b g}{n-1} h^{-n} h + C_2$$

Rearranging result in

$$\sigma_V = \frac{\rho_b g}{n-1} h + C_2 h^n \tag{9.24}$$

Integration constant C_2 is found by substitution the initial condition by Eq. (9.22) into Eq. (9.24)

$$C_2 = \frac{\sigma_{V,t} - \frac{\rho_b g}{n-1} h_0}{h_0^n}$$

Substitution of C_2 into Eq.(9.24) results in

$$\sigma_V = \frac{\rho_b g}{n-1} h + \left(\sigma_{V,t} - \frac{\rho_b g}{n-1} h_0\right) \left(\frac{h}{h_0}\right)^n$$

Therefore, the variation of the vertical stress with particle height in the conical hopper is described by the following equation

$$\sigma_V = \sigma_{V,t} \left(\frac{h}{h_0}\right)^n + \frac{\rho_b g h_0}{n-1} \left(\frac{h}{h_0} - \left(\frac{h}{h_0}\right)^n\right) \tag{9.25}$$

The distribution of the normal stress at the wall is

$$\sigma_W = F \left[\sigma_{V,t} \left(\frac{h}{h_0}\right)^n + \frac{\rho_b g h_0}{n-1} \left(\frac{h}{h_0} - \left(\frac{h}{h_0}\right)^n\right)\right] \tag{9.26}$$

The hopper stress ratio F is obtained from the Mohr circle representing the stress conditions at the wall as shown in Fig. 59. The major principal stress is in the direction shown by σ_1 and the major principal plane is at right angles to it. β is the angle between the wall and the major principal plane.

Assuming the switch from static to dynamic stress field occurs as soon as discharge is initiated, and that the material yields within itself as it passes through the converging channel, the stresses in the powder close to the wall are represented by a Mohr circle which just touches the powder yield locus OM. Further, as mass flow prevails, the material must be slipping at the wall

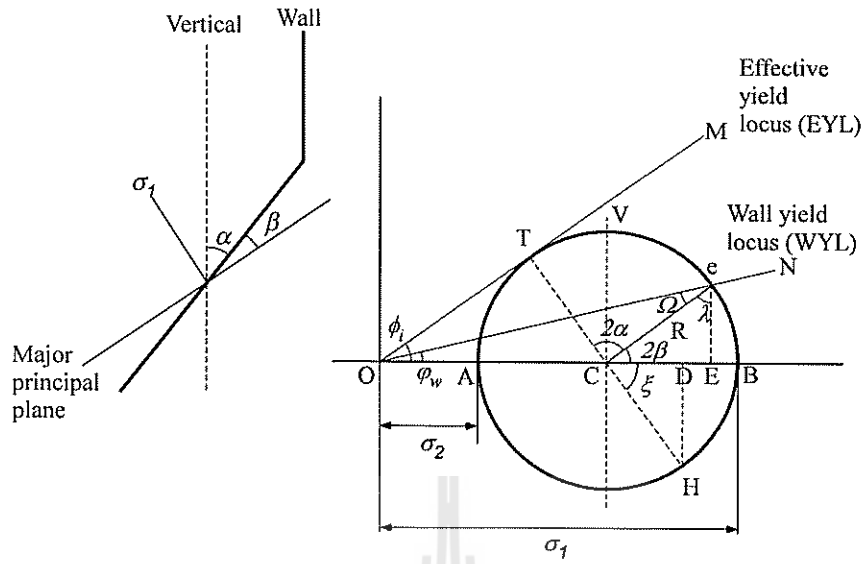

Figure 59: Stress conditions at hopper wall.

and therefore the wall stress are represented by a point on the wall yield locus ON. In the present case of a converging channel, this is given by point e. Thus, OE represents the magnitude of the normal wall stress σ_W.

On the Mohr circle, points H and V represent the horizontal and vertical directions, respectively. The magnitude of the vertical stress, σ_V is represented by OD.

From the geometry of the Mohr circle of radius R:

$$\mathrm{OD} = \mathrm{OC} + \mathrm{CD} = \frac{R}{\sin(\phi_i)} + R\cos(\xi) = \frac{R}{\sin(\phi_i)} - R\cos(2\beta + 2\alpha)$$

while

$$\mathrm{OE} = \mathrm{OC} + \mathrm{CE} = \frac{R}{\sin(\phi_i)} + R\cos(2\beta)$$

therefore

$$F = \frac{\sigma_W}{\sigma_V} = \frac{\mathrm{OE}}{\mathrm{OD}} = \frac{1 + \sin(\phi_i)\cos(2\beta)}{1 - \sin(\phi_i)\cos(2\alpha + 2\beta)} \tag{9.27}$$

An angle β can be expressed in terms of φ_W and ϕ_i by referring to the geometry of the Mohr circle and noting that

$$\varphi_W + \pi/2 + \Omega + \lambda = \pi \text{ and } 2\beta + \lambda + \pi/2 = \pi,$$

i.e.

$$2\beta = \varphi_w + \Omega.$$

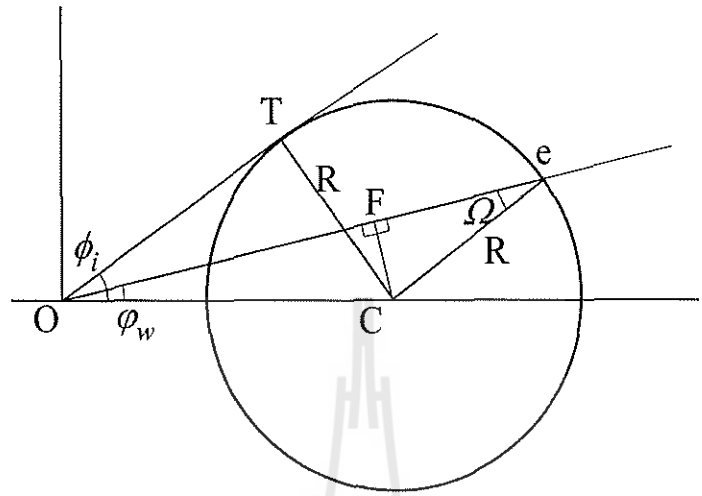

Figure 60: Illustration of derivation of hopper stress ratio.

Consider triangles OCT and OCe as shown in Fig. 60. From triangles OCF and CFC one can write

$$\sin(\varphi_w) = \frac{\mathrm{CF}}{\mathrm{OC}} \text{ and } \sin(\Omega) = \frac{\mathrm{CF}}{\mathrm{R}}.$$

Therefore,

$$\frac{\sin(\Omega)}{\sin(\varphi_w)} = \frac{\mathrm{OC}}{\mathrm{R}} \tag{9.28}$$

From triangle OCT

$$\sin(\phi_i) = \frac{\mathrm{R}}{\mathrm{OC}} \tag{9.29}$$

Combination of Eqs. (9.28) and (9.29) results in

$$\sin(\Omega) = \frac{\sin(\varphi_w)}{\sin(\phi_i)} \text{ and } \Omega = \sin^{-1}\left(\frac{\sin(\varphi_w)}{\sin(\phi_i)}\right) \tag{9.30}$$

Thus,

$$2\beta = \varphi_w + \sin^{-1}\left(\frac{\sin(\varphi_w)}{\sin(\phi_i)}\right) \tag{9.31}$$

Finally, one can use Eq. (9.27) together with Eq. (9.31) for calculation of F.

9.6. Discharge rate through a flat-bottomed hopper

9.6.1. Mono-sized particles

An empirical equation was proposed by Beverloo et al. (1961) for the prediction of the discharge rate of mono-sized particles through a circular orifice in a flat-bottomed cylindrical hopper.

$$W = C\rho_b\sqrt{g}(D_0 - kd_p)^{5/2}, \tag{9.32}$$

where W is the average solid discharge rate, C is the empirical discharge coefficient, k is the empirical shape coefficient, ρ_b is the powder bulk density, g is the gravitational acceleration, D_0 is the orifice diameter and d_p is the mean particle diameter. This equation is valid for particles larger 0.500 mm.

A modified form of the Beverloo equation was developed for particles less than 0.500 mm taking into account the pressure gradient generated by the self-entrained gas

$$W = C\rho_b\sqrt{g + \left(\frac{dP}{dz}\right)_0 \frac{1}{\rho_b}}(D_0 - kd_p)^{\frac{5}{2}}, \tag{9.33}$$

where the pressure gradient $(dP/dz)_0$ is evaluated by Ergun's equation as

$$\left(\frac{dP}{dz}\right)_0 = \left(\frac{150}{\rho_g U_{mf} d_p/(1-\epsilon_d)\mu_g} + 1.75\right)\frac{\rho_g U_{mf}^2}{d_p}\frac{1-\epsilon_d}{\epsilon_d^3} + \rho_g g, \tag{9.34}$$

The coefficient k is found to be independent of particle size and equal to 1.5 ± 0.1 for mono-sized spherical particles and in the range of $1 < k < 2$ for different particle shapes.

The value of discharge coefficient C was found to be dependent on the bulk powder density and is in the range of $0.55 < C < 0.65$ [Beverloo et al. (1961)]. Later, Huntington and Rooney (1971) argued that ρ_b depends also on the consolidation time requited to compact powder in a bed and proposed to use the ratio of mass flow rate to volumetric flow rate instead of ρ_b. They found a range of modified discharge coefficient as $0.575 < C' < 0.590$.

9.6.2. Binary mixtures

Tuzun et al. (1990) proposed a modified form of the Beverloo equation to predict the discharge rate of fine binary mixture

$$W = C'\rho_p(1-\epsilon_d)\sqrt{g + \left(\frac{dP}{dz}\right)_0 \frac{1}{\rho_p(1-\epsilon_d)}}(D_0 - Z'(d_{\text{eff}}))^{\frac{5}{2}}, \tag{9.35}$$

where $C' = 0.58$, ρ_p is the solid mass density of the mixture, ϵ_d is the flowing void fraction and Z' is the empty annulus width,

$$Z'(d_{\text{eff}}) = 2.1939 d_{\text{VM}} - 0.0009, \tag{9.36}$$

where the volume-moment mean diameter, d_{VM}, is calculated as

$$d_{\text{VM}} = \frac{\sum X_{ni} d_i^4}{X_{ni} d_i^3} \tag{9.37}$$

9.7. Discharge rate through a conical hopper

9.7.1. Polydisperse mixtures

- Fine particles

$$W = 0.58 \rho_b \sqrt{g + \left(\frac{dP}{dz}\right)_0 \frac{1}{\rho_b}} (D_0 - 1.5 d_{50})^{\frac{5}{2}} \tag{9.38}$$

or Eq (9.35) and

$$Z'(d_{\text{eff}}) = 2.1939 d_{\text{VM}} - 0.00053, \tag{9.39}$$

- Coarse particles Eq. (9.38) or Eq (9.35) and Eq (9.36)

References

[1] Seville J.P.K., Tuzun U., Clift R., Processing of particulate solids, Chapman & Hall, 1997.

[2] Schulze D. Powders and bulk solids, Springer, 2008.

[3] McGlinchey D. ed., Bulk solids handling, Blackwell, 2008.

[4] Shamlou P.A. Handling of bulk solids, Butterworths, 1988.